EPITAXIAL GROWTH OF $YBa_2Cu_3O_{7-x}$ (110) THIN FILMS ON $SrTiO_3$ (110) SUBSTRATES

($YBa_2Cu_3O_{7-x}$ (110)薄膜在$SrTiO_3$ (110)基板上的外延生長)

---

by

Tang Yeung Shun

(鄧楊順)

A Thesis Submitted in Partial Fulfillment
of the Requirements for the Degree of
Master of Philosophy in Physics

The Chinese University of Hong Kong

June 1993

ACKNOWLEDGEMENT

I wish to express my sincere gratitude to Dr. H.K.Wong, my supervisor, for awakening me this topic which has drawn the whole of my interest.

I am specially indebted to Mr. W.S.Au and Mr. W.K.Chao for their technical assistance and the setup of pulsed laser deposition. Special thanks should be given to Mr. S.H.Ling for his assistance in performing x-ray diffraction experiments, enlightening suggestions and discussions.

ABSTRACT

YBCO thin films have been grown on $SrTiO_3$(110) substrates by pulsed laser deposition. The orientation of the film depends on the substrate temperature. The films grown at 525°C have a (110) orientation. At higher substrate temperatures (≥ 650°C), the films have a mixture of (103) and (013) orientations. The structure of the films was characterized by various x-ray diffraction techniques. ϕ scan of (102) diffraction was used to distinguish the three orientations — (110), (103) and (013). After corrected for the defocusing and absorption effects, the intensities of the (102) diffraction peaks from the three phases were used to find the percentage of the (110) phase in the samples. The transition temperatures of the films were measured by four point method. The (110) oriented film shows no transition to superconducting state down to 12 K. This is likely due to an oxygen disordering but not the oxygen deficiency. However, a superconducting (110) oriented film was fabricated by a modified bilayer process — a thin layer of YBCO film was grown at 525°C first and then the substrate temperature was increased to 650°C without interrupting the film growth. The resistance of the film produced drops to zero at 81.8 K.

CONTENT

CHAPTER 1

INTRODUCTION

After the discovery of the high transition temperature (T_c) superconductors by Bednorz and Muller[1], a huge amount of research activities has been concentrated on this exciting field. The Y-Ba-Cu-O system contains compounds with T_c higher than the boiling point of liquid nitrogen (77 K) and thus has promising applications in electronic devices. However it is well known that bulk $YBa_2Cu_3O_{7-x}$ (YBCO) has high T_c (> 90 K) , but relatively small critical current density (j_c) (Table 1.1) because of the weak-link behavior of grain boundaries[5,6]. Many research groups had fabricated thin YBCO films with high j_c (Table 1.1) . This reflects that YBCO samples with extremely clean grain boundaries can be grown in thin film form[7]. Moreover, due to the highly anisotropic crystal structure of YBCO (Fig.1.1), its properties

Table 1.1 Some typical j_c values of YBCO at 77 K and zero magnetic field.

YBCO sample	j_c (A/cm^2)	Ref.
as-sintered bulk sample	~ 5×10^2	[2]
melt-texture grown bulk sample	~ 1.7×10^4	[2]
c-axis film on $SrTiO_3$ (100)	> 10^6	[3]
c-axis film on $LaAlO_3$ (100)	> 2×10^6	[4]

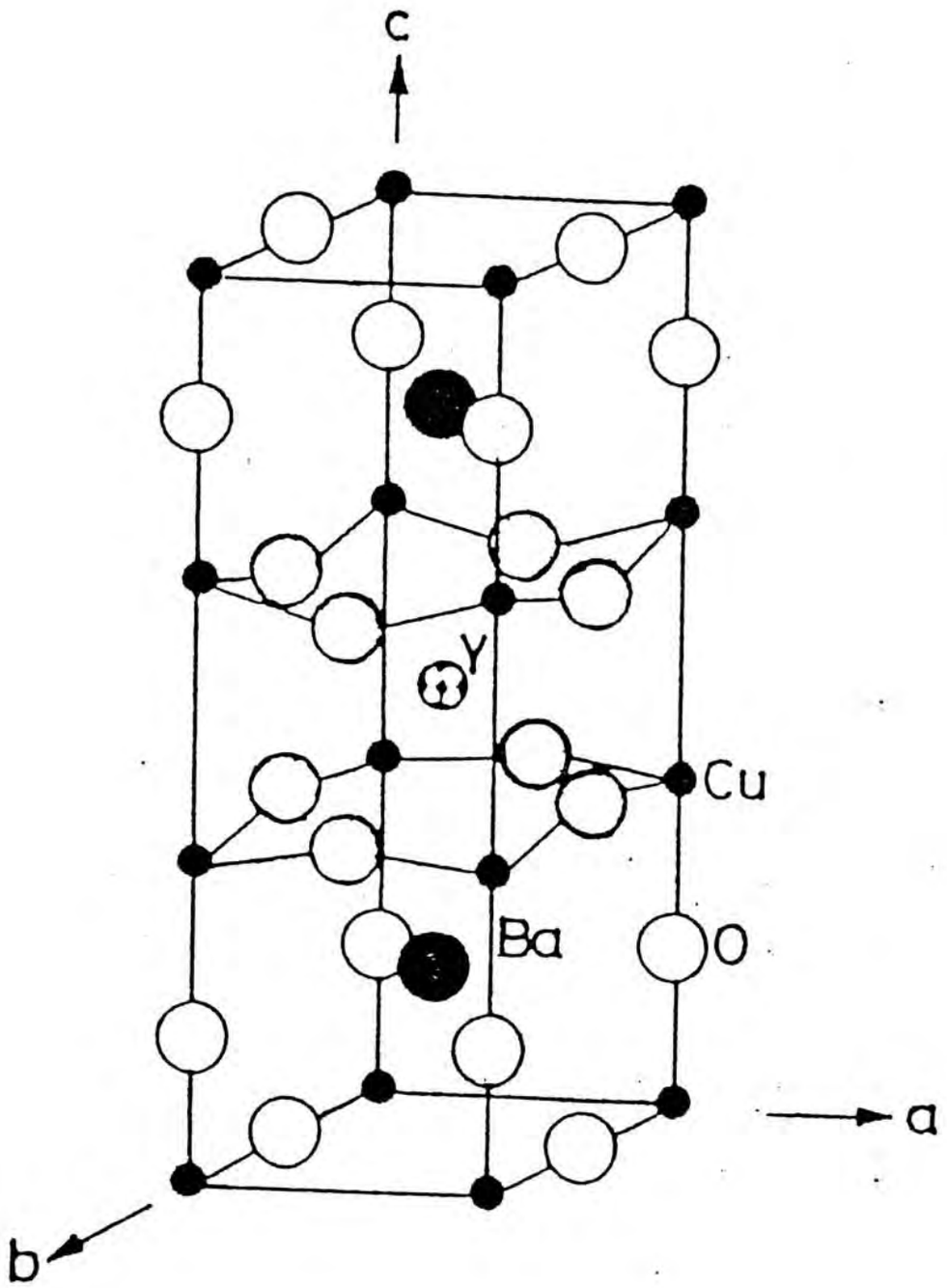

Fig. 1.1 the crystal structure of $YBa_2Cu_3O_7$.

are highly anisotropic. It is best to grow high quality YBCO films with desired orientation and examine its properties along different crystallographic directions.

High quality c-axis oriented films (with the c axis of YBCO perpendicular to the plane of substrate surface and also called (001) films) were grown epitaxially on a variety of substrates such as $SrTiO_3$(STO) (100) [8,9], MgO (100) [10,11], Y-ZrO_2 (100) [12] and $LaAlO_3$ (100) [13] by sputtering[9,11,12,13], laser ablation[8,10] or evaporation[3]. Because the lattice constants of YBCO are very close (a ≃ 3.82 Å and b ≃ 3.89 Å) , there are always 90° twinning in a-b domains in the c-axis films. This allows transport measurements on a-b plane only but not along the c-axis. Recently a-axis films were grown on substrates with (100) surface at a lower substrate temperature[14,15,16]. A-axis films are remarkable because they have a larger coherence length perpendicular to the film plane (coherence lengths: ξ_{ab} ≃ 15 Å in the a-b plane, ξ_c ≃ 2 Å along the c axis). This longer coherence length makes them more attractive than the c-axis films for the fabrication of planar Josephson junctions where current flows perpendicularly to the films. However, owing to the similar lattice constants of b and c/3 (c ≃ 11.68 Å) , the a-axis films can have their c-axis aligned along the [010] and [001] directions of the substrate. This makes them not possible for the investigation of the anisotropy of YBCO.

Several research groups had claimed successful fabrication of YBCO (110) films on STO (110) substrates and measured the

anisotropic electrical properties along the c-axis and [1$\bar{1}$0] direction[17,18,19]. STO (110) has a rectangular crystal surface (3.905 Å × 5.523 Å). This forces the c-axis of YBCO to lie along the STO [001] on the substrate plane and thus creates a (110) film with structural and electrical anisotropy along the surface. However, the c-axis can also lie along the [100] or [010] direction of the substrate, both pointing 45° to the substrate plane. This results in (103) or (013) film. Fig.1.2 shows these three possible orientations of YBCO on STO (110) substrate. Owing to $a \simeq b \simeq c/3$, the spacings between (110), (103) and (013) planes differ only a little and thus x-ray diffraction (XRD) gives similar two-theta values for these three crystal planes. It is difficult to resolve the diffraction peaks of STO (110) and YBCO (013), and YBCO (110) and YBCO (103). Moreover, the x-ray beam contains a small fraction of Cu $K\alpha_2$ line that also complicates the distinction. The d spacings and 2θ values are given in Table 1.2. Hence, when using XRD, great care is necessary in discriminating the orientation of YBCO films on (110) substrate surface.

Wang et al.[21] reported that highly oriented YBCO (110) films were grown on STO (110). But they characterized their films only by one XRD θ-2θ scan without considering the mixing of (013) and (110) orientations. Terashima et al.[22] reported the growth of (110) and (103) films at substrate temperatures around 530°C and 630°C respectively by activated evaporation. These different orientations were successfully explained by considering the lattice misfit of YBCO and STO at different temperatures. The orientation as determined only by the reflection high-energy

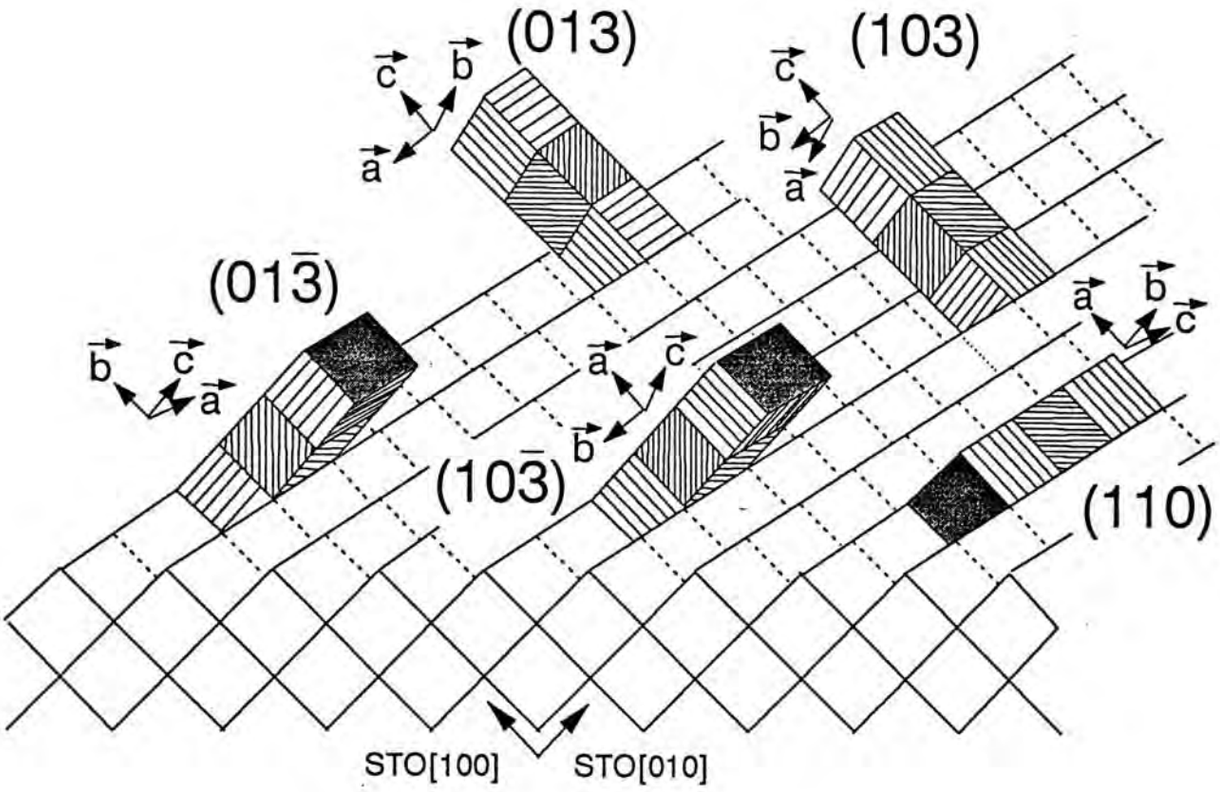

Fig.1.2 Possible epitaxial orientations of YBCO on STO(110) substrate.

Table 1.2 d spacings and XRD 2θ values of STO (hh0), and some crystal planes of possible orientations of YBCO.

Lattice constant of STO = 3.905 Å.

Lattice constants of YBCO [20] : a = 3.8185 Å , b = 3.8856 Å and c = 11.6804 Å.

	d spacings (Å)	x-rays	2θ
YBCO (013)	2.750	Cu $K\alpha_1$	32.538°
YBCO (110)	2.725		32.842°
YBCO (103)	2.725		32.842°
YBCO (026)	1.3751		68.134°
YBCO (220)	1.3635		68.797°
YBCO (206)	1.3619		68.888°
STO (110)	2.761		32.40°
		Cu $K\alpha_2$	32.48°
STO (220)	1.381	Cu $K\alpha_1$	67.82°
		Cu $K\alpha_2$	68.08°

electron diffraction (RHEED) pattern. But the (013) orientation had not yet been mentioned. Similar situation is found in the paper of Habermeier et al.[23] in which Raman scattering was used to discriminate the (103) and (110) orientations. However, no discussion on the occurrence of (013) orientation was reported. Zheng et al.[18] distinguish (110) and (103) orientations by XRD off-axis scans. Their samples were tilted ~ 10.2°, and (225) and (108) peaks were observed in order to find out the ratio of the amount of (110) phase in the samples. They reported the relationship of substrate temperature and percentage of (110) grains in the films prepared by pulsed laser deposition. But no effort on finding (013) grains had been reported. Wu et al.[24] reported high quality (110) films grown by inverted cylindrical magnetron sputtering. The XRD ϕ scans of (108) peak were performed to discriminate the (110) and (103) orientations. Also no experimental evidence was given to the non-existence of the (013) grains.

Linker et al.[25] observed (026) peak in XRD θ-2θ scan of (110) films prepared by hollow-cathode magnetron sputtering. The structure of the samples were only examined by XRD θ-2θ scans. They concluded that (110) film was obtained because no peaks other than the (110) and (220) peaks occurred. Obviously this sample may be (103) oriented and further experiments should be done to distinguish them. Eom et al.[26] fabricated (103)/(013) films by off-axis sputtering and measured the anisotropic transport properties. The structure was analyzed by XRD off-axis scans of (102) peak.

Table 1.3 lists these published results and the methods of structural analysis. In this thesis, we will give a detailed and systematic study on the structural properties of YBCO films on STO (110) at different substrate temperatures. The transport properties and the surface morphology of the films will also be presented.

Table 1.3 Epitaxial growth of "YBCO (110)" on STO (110).

Ref.	Technique	Substrate Temperature	Structural Analysis*
[18]	Pulsed laser deposition	580°C	Off-axis XRD
[21]	Electron beam multilayer deposition	450°C post-annealing	Normal XRD θ-2θ scan
[22]	Activated Evaporation	530°C	RHEED
[23]	Pulsed laser deposition	663°C increased to 720°C	Normal XRD θ-2θ scan Raman scattering Ellipsometry
[24]	Inverted magnetron sputtering	705°C	Off -axis XRD
[25]	hollow-cathode magnetron sputtering	700°C	Normal XRD θ-2θ scan

* Off-axis XRD : diffraction vector is not parallel to the substrate normal direction.

* Normal XRD : diffraction vector is parallel to the substrate normal direction.

CHAPTER 2

PREPARATION OF THIN FILMS

To deposit YBCO thin films, we used the standard pulsed laser deposition technique. [See articles in MRS Bulletin 17, (2) 1992.] Fig.2.1 is a schematic diagram showing the thin film deposition process. Films were deposited in a small stainless steel chamber. An ArF excimer laser (Questek, Model 2320, wavelength 193 nm, FWHM 12 ns) was used for the ablation. The pulsed laser beam was focused by a MgF_2 lens (focal length = 200 mm, from Oriel Corporation) onto the surface of a YBCO pellet (from Superconductive Components, Inc., 99.9% purity, 95% density, 1" diameter) at an angle of about 45° from the normal of target surface, to give a spot size of about 1 mm × 4 mm. The pulse energy used was 150 mJ and hence producing an energy fluence of about 3.7 J/cm^2. The target was mounted on a stainless steel target holder by silver paste. During deposition, the target was rotated by a stepper motor, through a rotary feedthrough, at a rate of about 0.3 revolution per second to give continuously a fresh surface for ablation.

A substrate holder, which was a stainless steel plate, was placed opposite and parallel to the target surface and heated resistively by a kanthal wire. STO (110) substrates were mounted on the substrate holder by silver paste and kept at about 3.1 cm apart from the target. The temperature was measured by a chromel-alumel thermocouple which was mechanically clamped on the surface of the substrate holder. The temperature control and

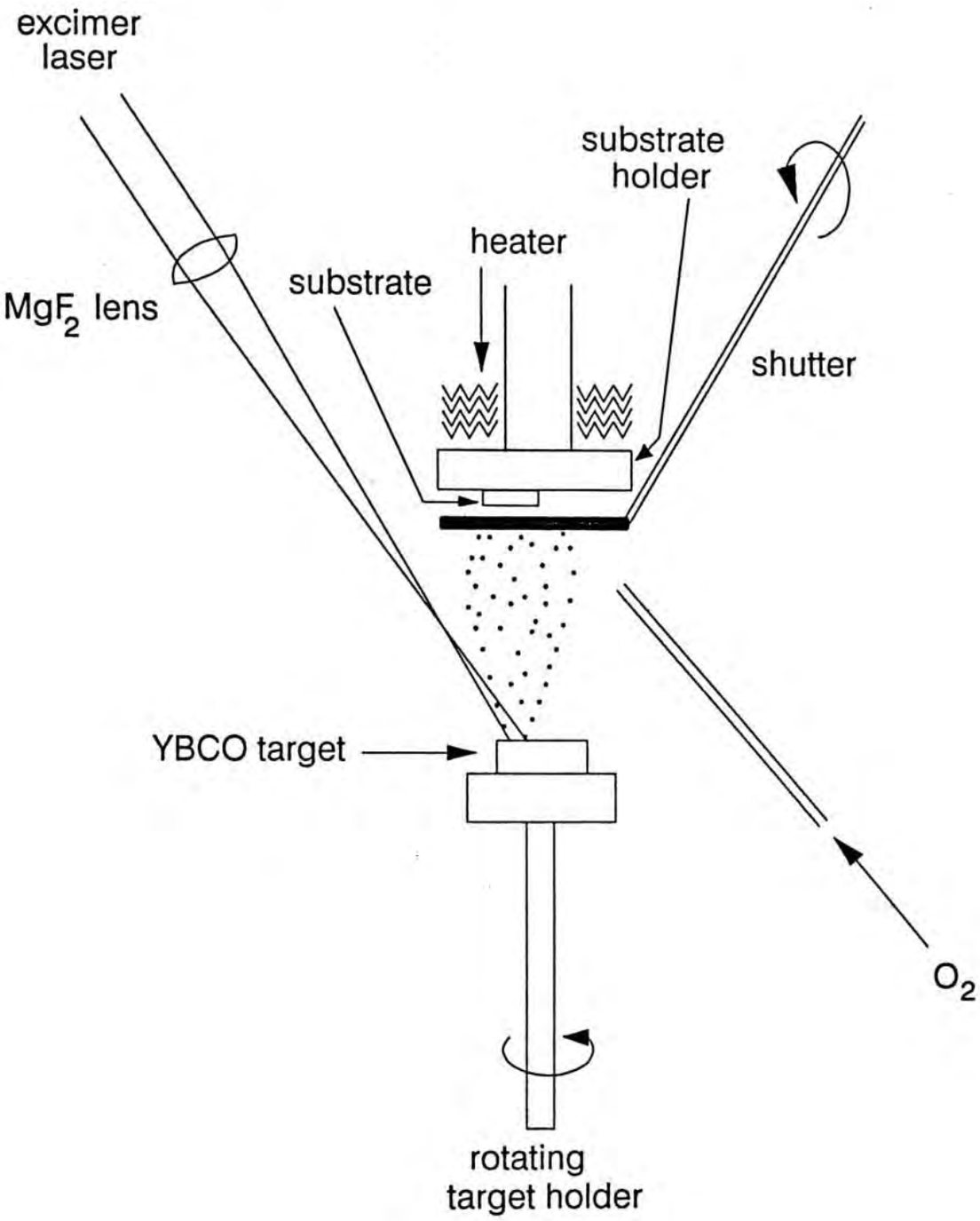

Fig. 2. 1 Schematic diagram of thin film deposition by laser ablation.

measurement was done by a digital temperature controller (DB series Digital Indicating Controller from Chino, Japan). The temperature measured was taken as the substrate temperature.

Before deposition, the substrate temperature was raised to the deposition temperature at a rate of 200°C per hour, and the chamber was evacuated to a pressure below 10^{-5} Torr by a diffusion pump buffered with a liquid-nitrogen trap and backed by a two-stage rotary pump. Then it was refilled with high purity (≥ 99.6%) oxygen gas to a pressure of 200 mTorr. During deposition, the pumping speed was reduced by adjusting a butterfly valve mounted between the cold trap and the diffusion pump. The chamber pressure was measured by a Baratron pressure gauge (MKS Instruments, Inc., Model 222C) and kept at 200 mTorr by adjusting the gas supply with a mass flow controller (Unit Instruments, Inc., Model UFC-1100). The fresh oxygen gas was directed towards the substrate by a copper nozzle.

There was a shutter in front of the substrate. After the YBCO target was ablated by the laser beam for about 30 s to remove the surface layer, the shutter was removed and then the deposition was started. The number of laser pulses for each deposition run was about 5,000 and the typical film thickness was about 2,000 Å. After the deposition, the chamber was immediately filled with oxygen to 1 atmospheric pressure. The heater current was switched off and the film was cooled to room temperature in about 1.5 hour.

A number of films were prepared at substrate temperatures

ranging from 500°C to 720°C. All other conditions were kept fixed.

CHAPTER 3

STRUCTURAL ANALYSIS

3.1 THE X-RAY DIFFRACTOMETER

The structures of our films were characterized by x-ray diffraction (XRD) at room temperature. Our XRD system is a computer-controlled 4-circle diffractometer with a Bragg-Brentano configuration. As illustrated by a schematic diagram in Fig.3.1, it is composed of a θ-2θ goniometer and an Eulerian cradle (Huber 424 and 511.1). Each circle has a step size of 0.001°. Our setup has a horizontal scattering plane, i.e. with vertical θ and 2θ axes. The χ axis always lies in the scattering plane. The χ angle is defined such that $\chi = 0^{\circ}$ when the ϕ axis is perpendicular to the scattering plane. The ϕ axis is always perpendicular to the χ axis.

The x-ray source is a sealed x-ray tube with a copper target operated at 40 kV and 20 mA. Cu Kα radiation is selected with a flat graphite crystal monochromator. The incident beam is formed using a 0.5 mm collimator. The diffracted beam passes through a set of receiving slits (1 mm horizontal, 2 mm vertical) and is detected by a NaI(Tl) scintillation counter.

Various XRD techniques have been used to determine the crystal quality and the texture of our films. These are summarized in Table 3.1 and will be presented in detail in the following sections.

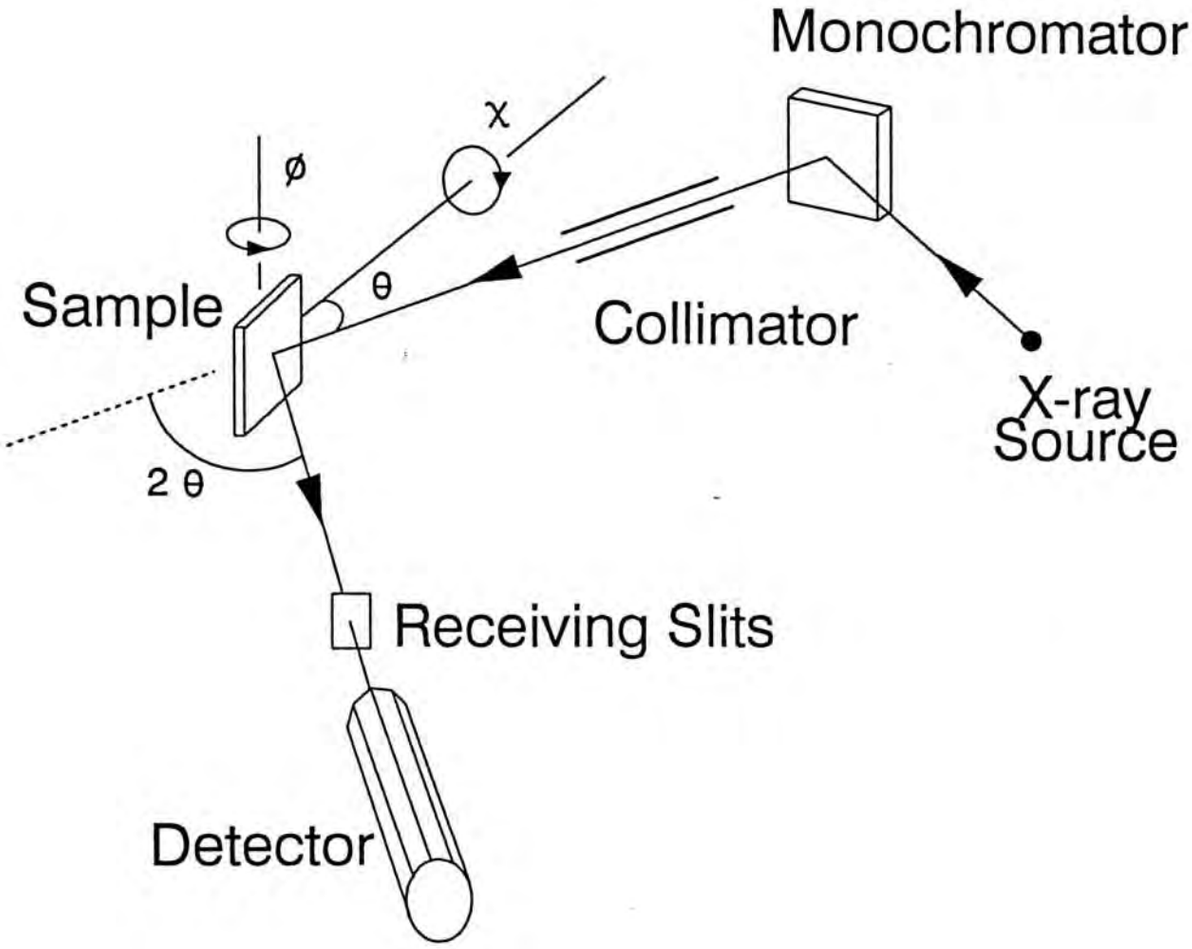

Fig. 3.1 X-ray diffraction setup.

Table 3.1 Various x-ray techniques for structural analysis. N is the normal of the substrate surface.

Technique		χ	Angles to be scanned	Sample mounting
Normal	θ-2θ	0°	$\theta/2\theta$	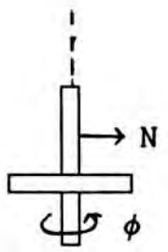
	rocking curve	0°	ϕ	
	pole-figure		ϕ , χ	
off-axis	θ-2θ	$\neq 0^\circ$	$\theta/2\theta$	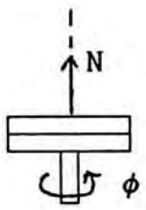
	ϕ-scan	$\neq 0^\circ$	ϕ	
GID	θ-2θ	$<1^\circ$	$\theta/2\theta$	
	ϕ-scan	$<1^\circ$	ϕ	

3.2 NORMAL θ-2θ SCAN

This is the most common method to explore the orientation of thin film samples. Only those crystal planes parallel (or nearly parallel) to the film surface are studied. Our samples were grown on STO (110) substrates. STO is cubic with lattice constant of 3.905 Å. All samples were aligned using the STO (110) diffraction peak. We first set the diffractometer to a $\theta/2\theta$ position with $2\theta = 32.40^\circ$ and then adjusted the angles ϕ and χ to maximize the count rate. Once the STO (110) peak was aligned, a θ-2θ scan was performed with 2θ varied from 5° to 70°.

Fig.3.2(a)-(f) show the diffraction patterns of some YBCO films which were grown on STO (110) substrates at different substrate temperatures. Note that the intensities are plotted on logarithmic scale. The diffraction peaks due to YBCO (hkℓ) planes are labeled as Y(hkℓ). The two strong peaks on the graphs are due to STO substrates. Our x-ray beam is contaminated by second harmonic component with wavelength = $\lambda/2$, λ is the Cu Kα wavelength. This part of x-rays can also contribute to the diffraction patterns. The two small peaks ($2\theta \simeq 16.4^\circ$, 49.6°) marked as $\lambda/2$ on the graphs are due to the $\lambda/2$ harmonic diffraction peaks of STO (110) and STO (330) respectively.

In addition to these substrate diffractions, the (110)/(103) and (220)/(206) diffraction peaks are clearly observed. The notation (110)/(103) is used because we cannot distinguish the two diffractions at this stage. The absence of other diffraction peaks of YBCO indicates that the films have single perovskite phase and

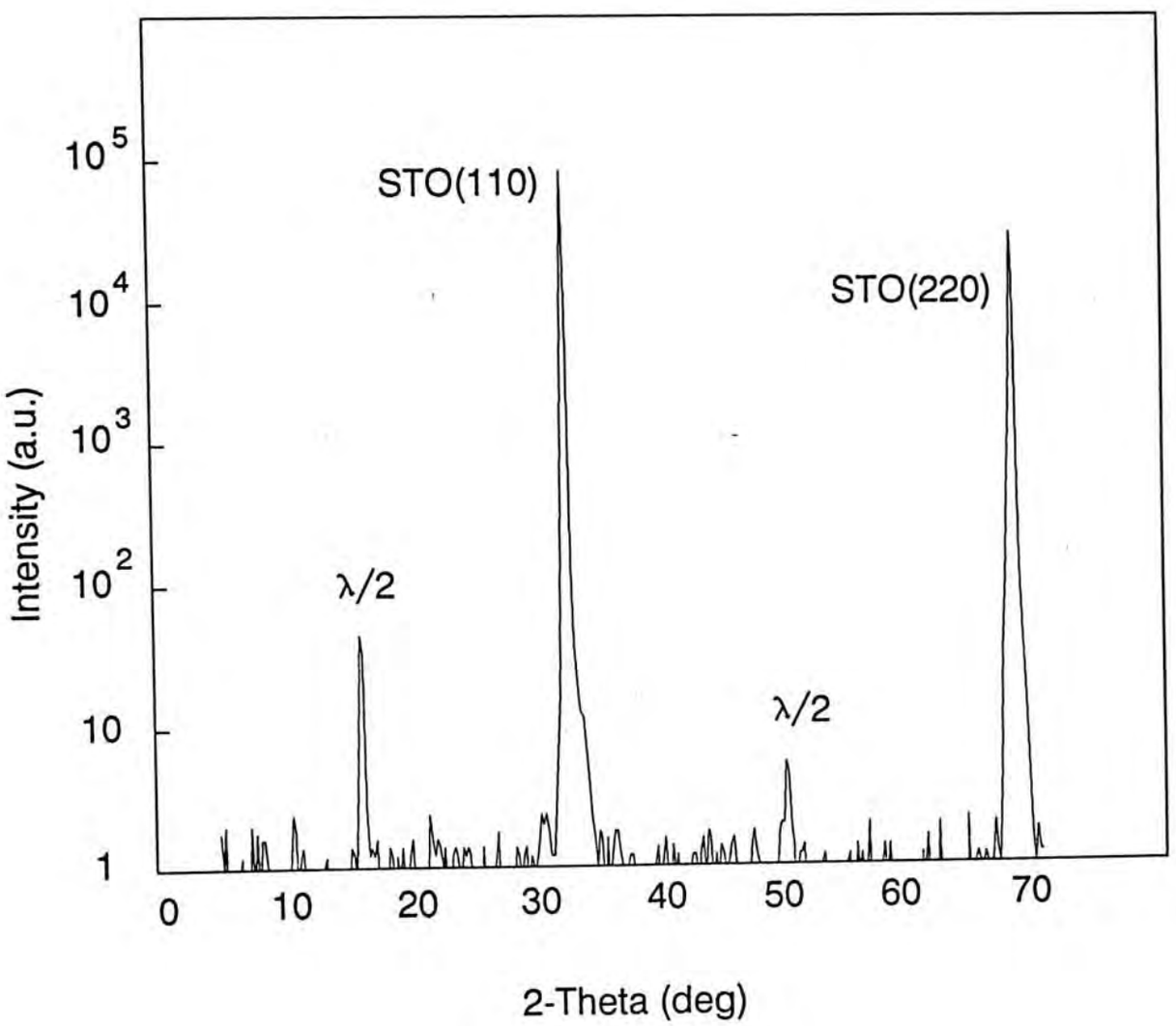

Fig.3.2(a) X-ray diffraction pattern of YBCO thin film grown at 500°C (sample 1).

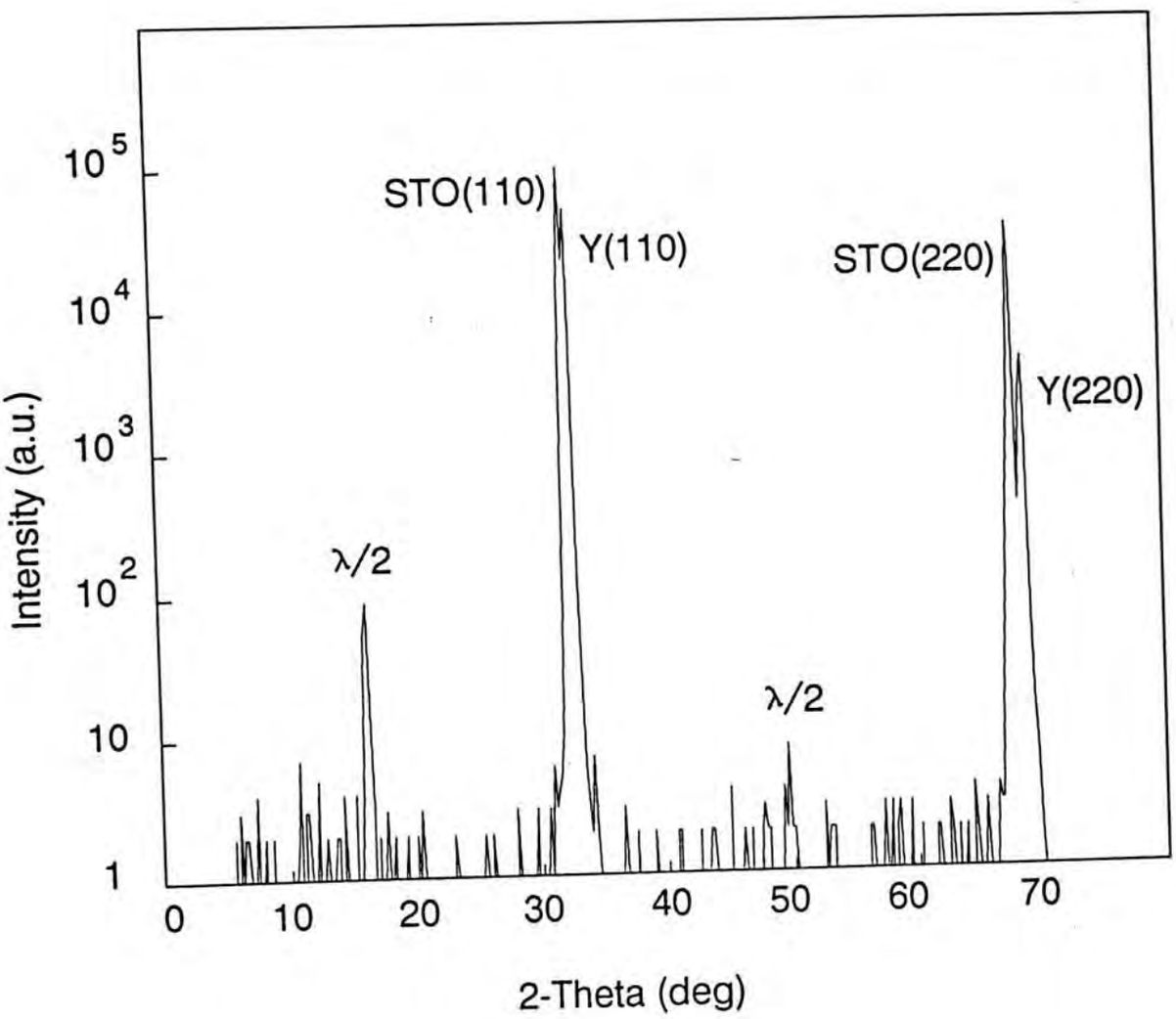

Fig. 3.2(b) X-ray diffraction pattern of YBCO thin film grown at 525°C (sample 2).

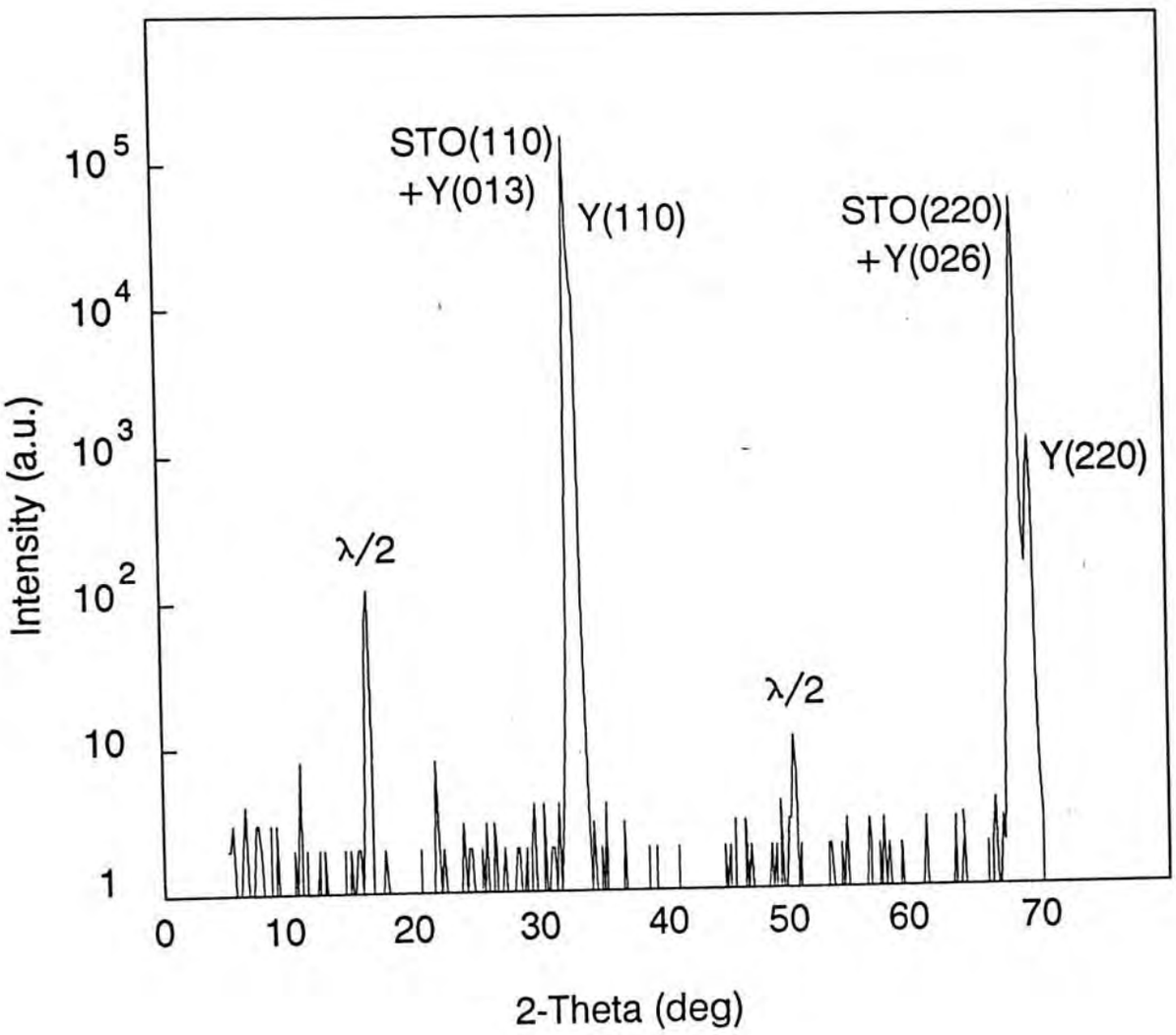

Fig.3.2(c) X-ray diffraction pattern of YBCO thin film grown at 550°C (sample 3).

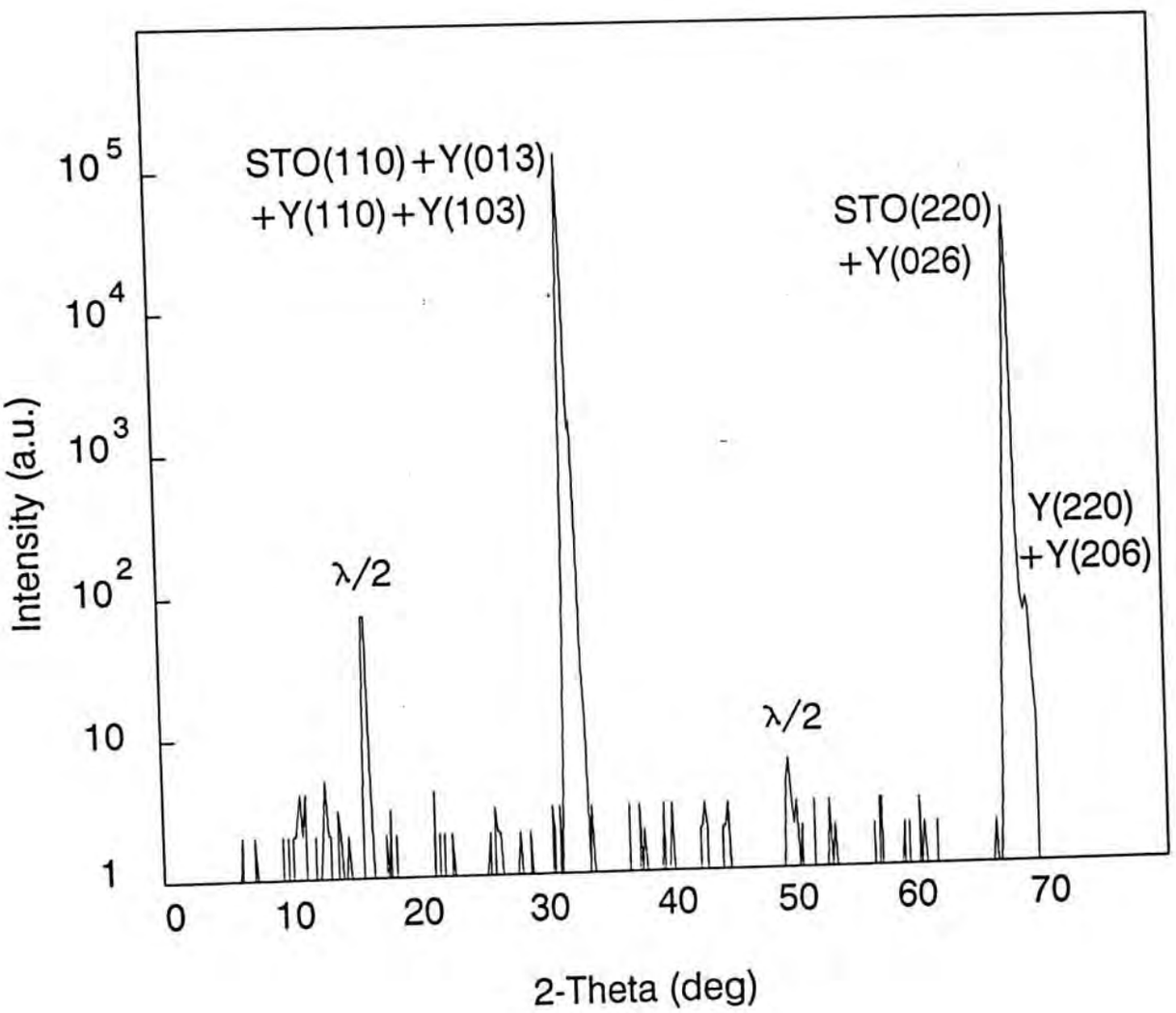

Fig.3.2(d) X-ray diffraction pattern of YBCO thin film grown at 600°C (sample 4).

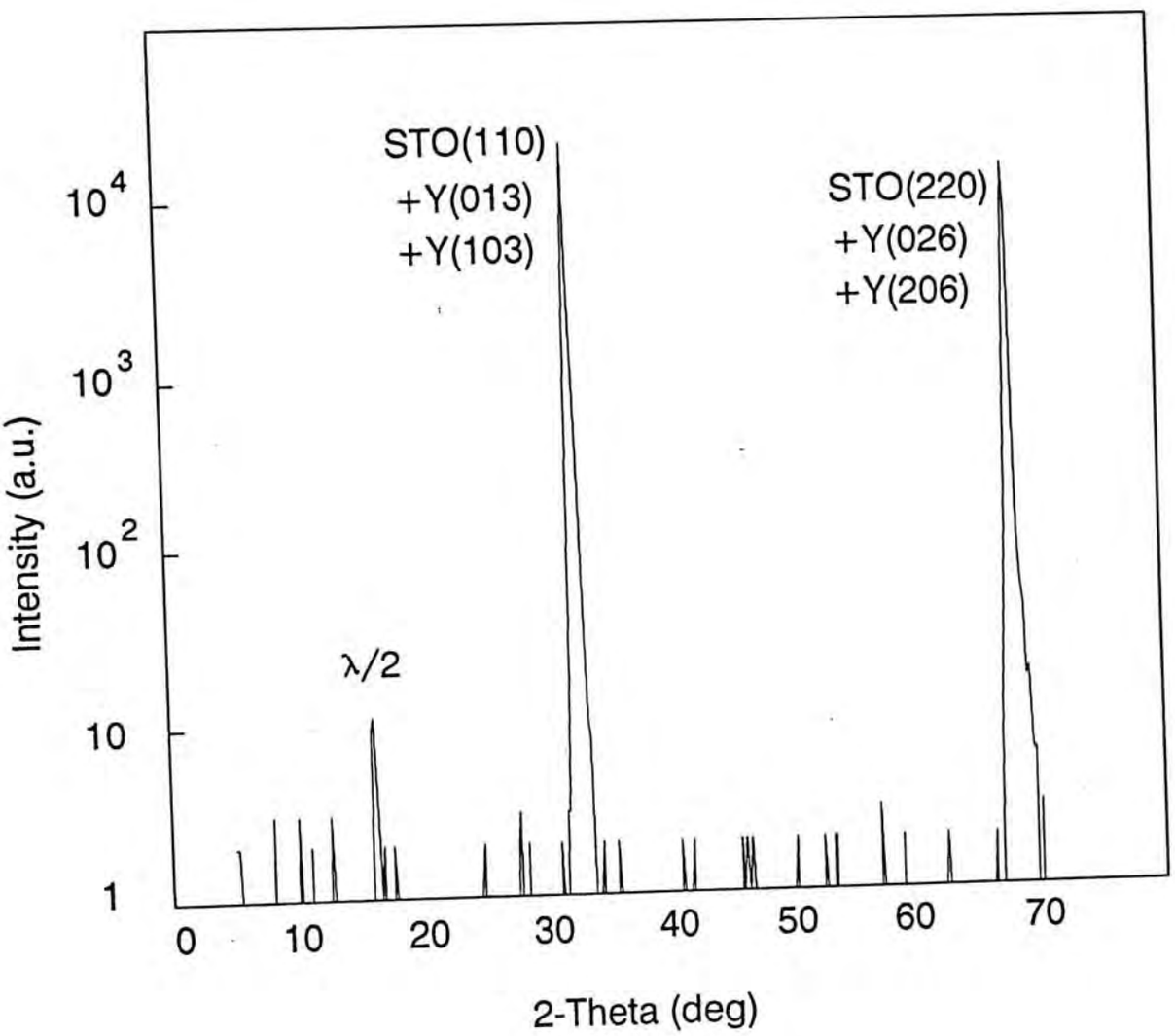

Fig.3.2(e) X-ray diffraction pattern of YBCO thin film grown at 650°C (sample 5).

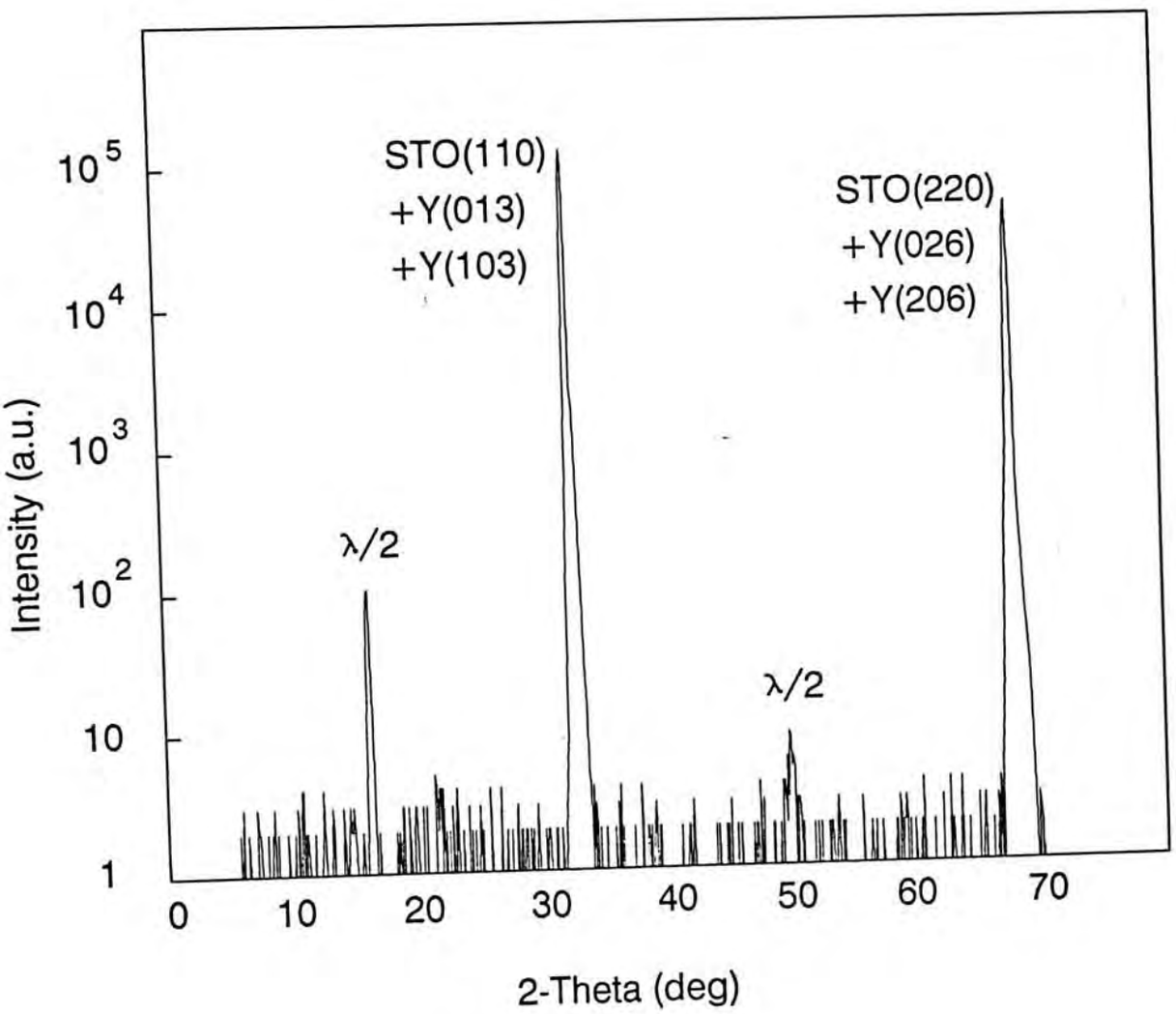

Fig.3.2(f) X-ray diffraction pattern of YBCO thin film grown at 720°C (sample 6).

of YBCO indicates that the films have single perovskite phase and contain grains with either (110), (103), (013), or a combination of these orientations. In Table 3.2 we summarize the structural properties of some YBCO films obtained as a result of the normal θ-2θ studies. Fig.3.2(a) shows only the substrate peaks. Together with other experiments to be discussed in the following sections, we conclude that the film grown at 500°C is amorphous. In Fig.3.2(b)-(d), the YBCO (220)/(206) peaks at $2\theta \cong 68.8^\circ$ are clearly observed. In Fig.3.2(e)-(f), no YBCO peaks distinguishable from the substrate peaks are observed. However, they were found to have (103)/(013) orientation by off-axis texture analysis (to be discussed in Section 3.5). The (103)/(013) peaks cannot be resolved from STO (110) peak using the conventional XRD system.

Finer θ-2θ scans were performed for a smaller 2θ range ($67^\circ \leq 2\theta \leq 70^\circ$) in order to display the peaks of STO (220), YBCO (220), YBCO (206) and YBCO (026). The 2θ values of these peaks were given in Table 1.2. Fig.3.3 shows the fine-scan pattern for the film grown at 525°C. The peaks correspond to STO (220) / YBCO (026) and YBCO (220) / YBCO (206) respectively. As we have discussed in chapter 1, these two pairs of peaks cannot be resolved with a conventional diffractometer. The peak marked by "S" ($2\theta \cong 68.08^\circ$) is due to the Cu $K\alpha_2$ x-rays (λ = 1.5443 Å). This was confirmed by performing a double crystal diffraction experiment in which no such splitting was observed for this sample. The same peak appears when the normal θ-2θ scan is performed with a bare substrate. (Linker et al.[25] also reported this kind of splitting of STO (110) crystal but no explanation had been given.) Such Cu $K\alpha_1/\alpha_2$

Table 3.2 Structural properties of YBCO films grown at different substrate temperatures.

Fig. 3.2		Substrate Temperature	Texture[a]	FWHM of rocking curve of (220)/(206)[b]
(a)	Sample 1[c]	500°C	amorphous	- - -
(b)	Sample 2	525°C	(110)	0.17°
(c)	Sample 3	550°C	(110) & (013)	0.40°
(d)	Sample 4	600°C	(110) & (103) & (013)	1.05° [d]
(e)	Sample 5	650°C	(103) & (013)	- - -
(f)	Sample 6	720°C	(103) & (013)	- - -

a: The texture analysis is given in Section 3.5.

b: Rocking curve analysis is given in Section 3.3.

c: Thickness of this film is about 400 Å.

d: FWHM of the (110)/(103) diffracted peak.

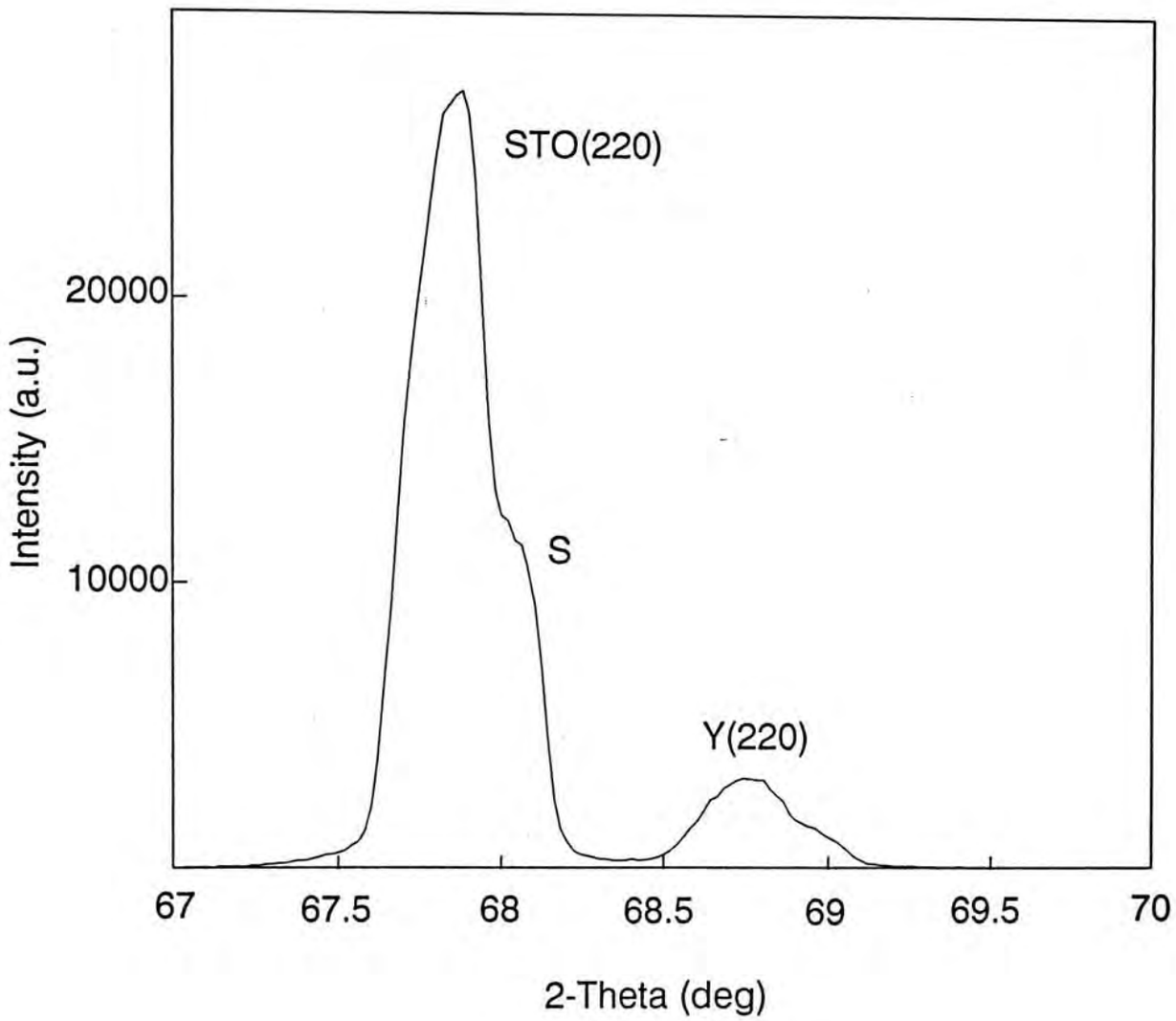

Fig. 3.3 Section of x-ray diffraction pattern of sample 2 showing splitting of STO (220) diffraction peak.

splitting can mask the YBCO (026) diffraction peak. Hence discrimination of (110), (103) and (013) orientations on STO (110) substrate cannot be done by a normal θ-2θ scan .

The intensity of the peak at $2\theta \simeq 68.8^{\circ}$ decreases with increasing substrate temperature. This peak may be associated with either YBCO (220) or YBCO (206). However, the structure factors of (206) and (220) diffractions differ dramatically. (The powder diffraction pattern of YBCO system is listed in Appendix A.) This implies that the peak at $2\theta \simeq 68.8^{\circ}$ is mainly due to (220) diffraction. The decrease in intensity reflects that the relative amount of (110) phase in the films decrease with increasing substrate temperature. This was also confirmed by texture analysis (to be discussed in Section 3.5).

3.3 ROCKING CURVE

Even with a well defined orientation, the thin film samples are actually made up of a number of tiny blocks called grains. For example, (110) film contains grains with (110) orientation. We will call them (110) grains. The orientation of these grains may vary slightly from each other. The extent of the disorientation in this mosaic structure can be determined by performing a rocking curve analysis. The experimental setup is the same as for the normal θ-2θ scan (Fig.3.1). But now the diffractometer is set at the $\theta/2\theta$ positions corresponding to the diffraction peak center in the normal θ-2θ scan. The sample is then rotated slightly by scanning ϕ angle and the corresponding intensity is recorded. The

curve of intensity against the rotation angle ϕ is called the rocking curve. As the crystal is rotated, each grain of a mosaic crystal in the irradiated area comes into the reflecting position. Therefore the full width at half maximum (FWHM) of a rocking curve is a direct measure of the degree of disorientation of a mosaic crystal.

For each film, we obtained the rocking curve for YBCO (110)/(103) or YBCO (220)/(206) diffraction. Table 3.2 shows the FWHM of these rocking curves. To determine the instrumental resolution, we also measured the rocking curve of a typical STO substrate. Such experiment was performed at the second harmonic peak of STO (110). The average FWHM of substrate was found to be 0.11°. In most cases, the FWHM of an oriented film decreases with increasing substrate temperature because higher substrate temperature results in better crystallinity. But as seen in Table 3.2, the FWHM of our films increases with substrate temperature from 0.17° at 525°C to 1.05° at 600°C. It was found by texture analysis (Section 3.5) that in this temperature range, as substrate temperature was increased, the orientation of YBCO films changed from pure (110) orientation to a mixed orientation with (110), (103) and (013) grains. Since we examined the rocking curve of the (110)/(103) or (220)/(206) diffraction peak, it is natural that the films with a mixed (110), (103) and (013) orientation have a larger FWHM than that of a pure (110) film.

3.4 POLE FIGURE

A figure that records the pole density with pole orientation for a specified set of crystal planes is called pole figure. We have determined the pole figure of YBCO (103) for sample 5. To obtain the pole figure, the sample was mounted in the same way as for the normal θ-2θ scan. The detector was fixed at the 2θ position corresponding to the maximum intensity of (103) diffraction. The sample was then rotated along the ϕ and χ axes simultaneously (Fig.3.1). The resultant pole figure is plotted with contour lines in Fig.3.4(a). Each contour represents angles with equal diffraction intensity. As we will prove in the next section, this sample contains only (103) and (013) orientations. Therefore the two peaks appearing in the figure are due to (103) peak. This indicates the twinning of the (103) grains. In order to determine the angle between YBCO [103] and STO [110], the pole figure of STO (110) was also performed and is shown in Fig.3.4(b). From the ϕ and χ values of the poles, the angle between two sets of planes, denoted by δ, is given by

$$\cos \delta = \sin \chi_1 \sin \chi_2 + \cos \chi_1 \cos \chi_2 \cos (\phi_1 - \phi_2).$$

The angles between the two YBCO [103] poles and STO [110] pole are both about 0.8° and that between two YBCO [103] poles is 1.6°. In other words, STO [110] is situated at the middle of two YBCO [103] directions in the twin structure. This shows that the two YBCO (103) domains tilt at the same angle with respect to the substrate STO (110) planes. The tilting of YBCO [103] can be understood in terms of the difference of a and c/3. As shown in Fig.3.5, the angle σ tilted is given by

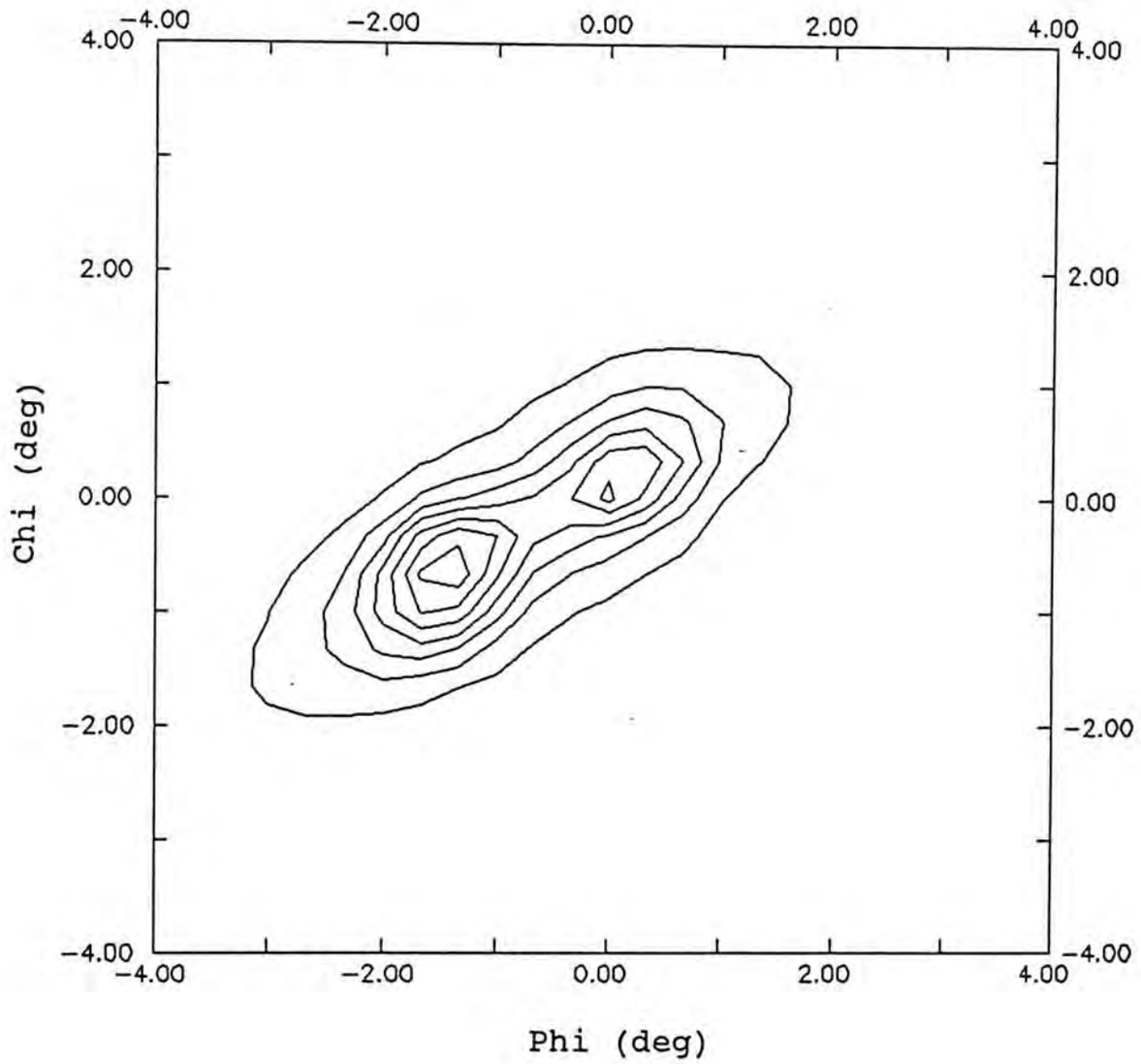

Fig. 3.4(a) Pole figure of YBCO (103) diffraction of sample 5.

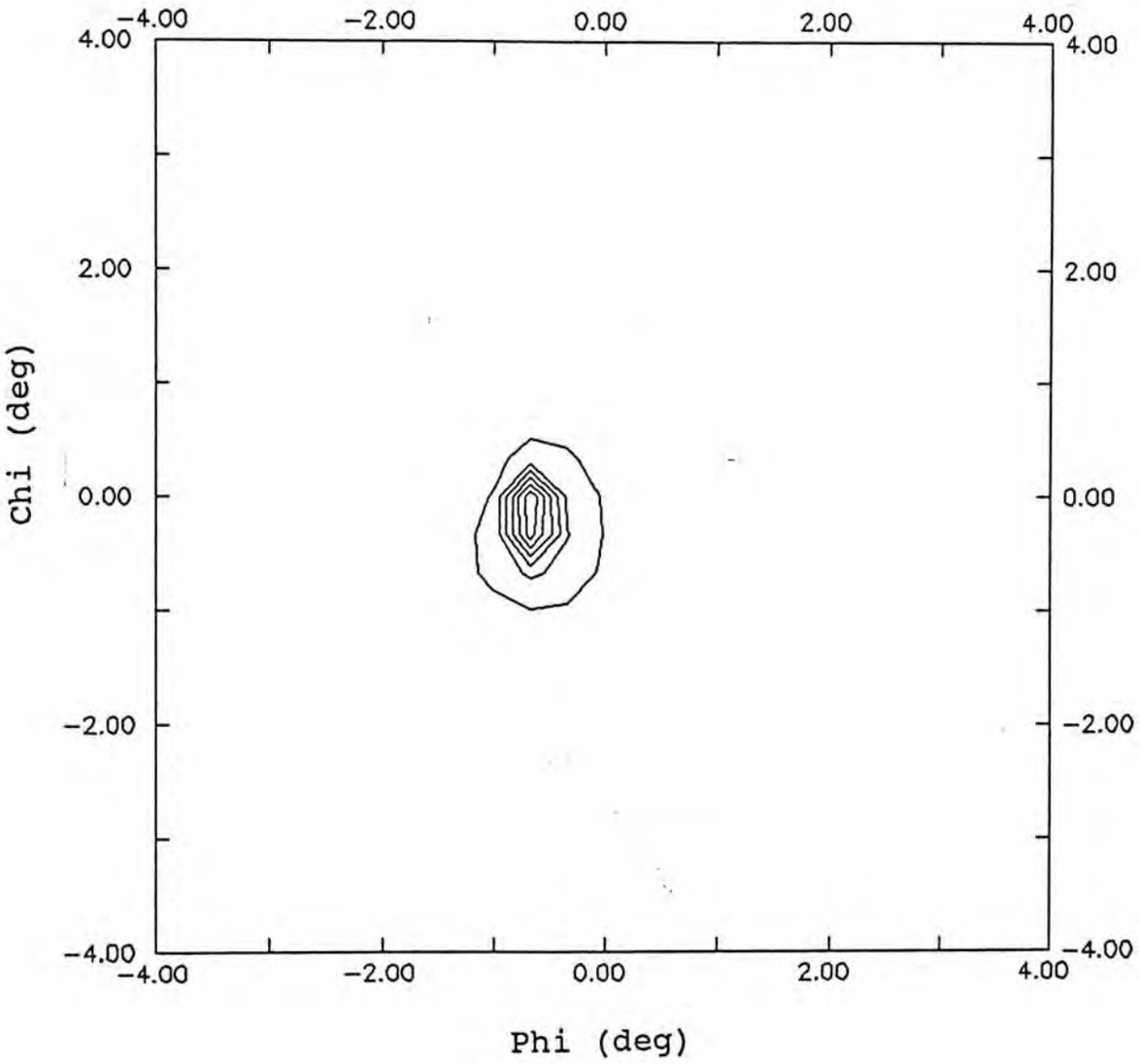

Fig. 3.4(b) Pole figure of STO (110) diffraction of sample 5.

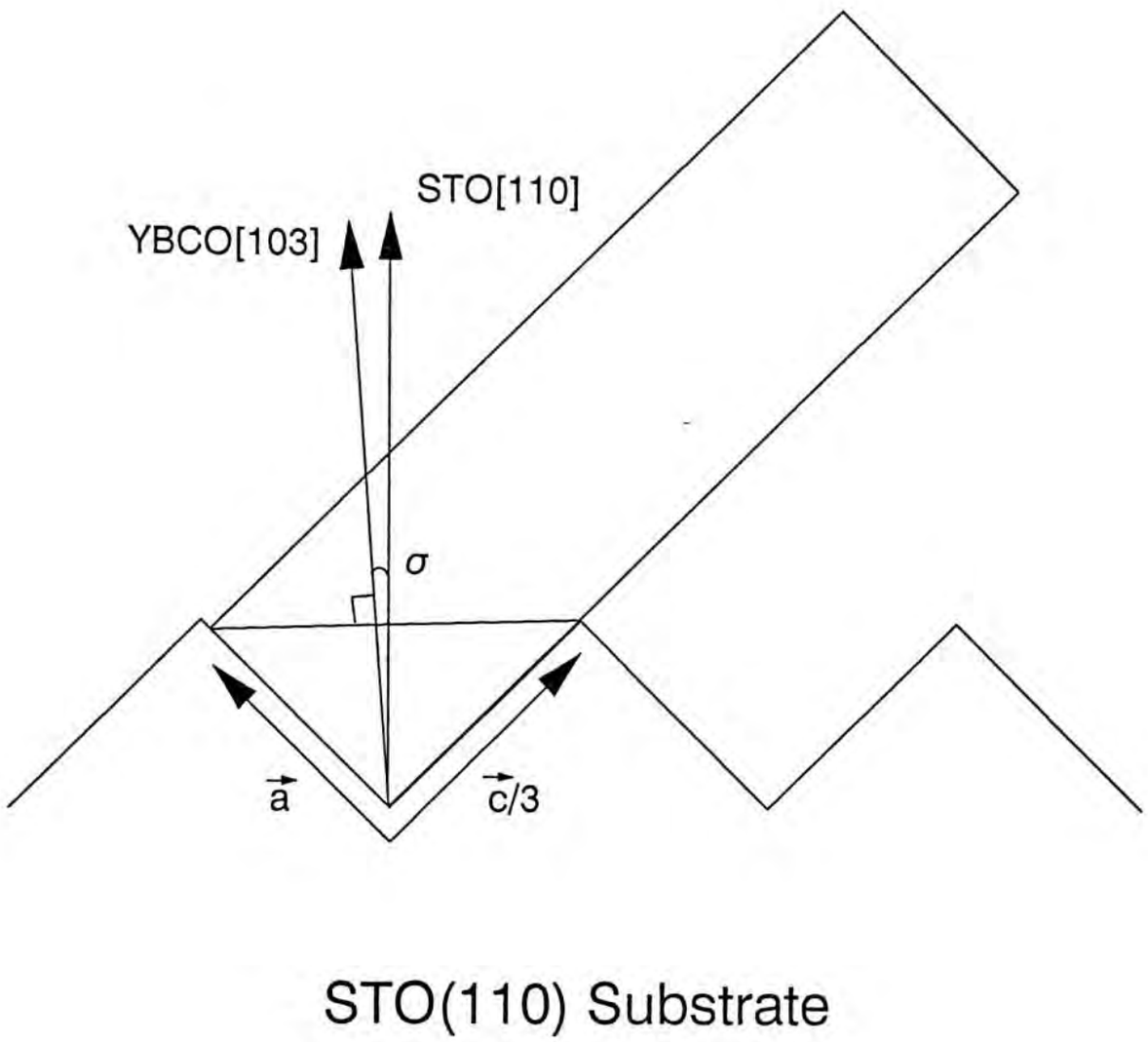

Fig. 3.5 Diagram showing the tilting of YBCO [103] from STO [110].

$$\tan(45^\circ-\sigma) = \frac{a}{c/3}$$

For this sample, a = 3.82 Å and c = 11.70 Å (see section 3.8), this gives σ = 0.6° which agrees fairly with our experimental result.

This sample contains also YBCO (013) phase and the corresponding 2θ value is very similar to STO (110). However, only one peak shows up in Fig.3.4(b). The tilting angle of the YBCO [013] pole with respect to the STO [110] should be less than 0.1°. Moreover the STO (110) diffraction has a much higher intensity than the YBCO (013) diffraction. That makes the measurement much more difficult than in the (103) pole-figure study.

3.5 OFF-SCAN

In order to find out whether the growth is epitaxial and to determine the texture of the samples, we need to perform off-axis scans. In this experiment, the sample was mounted on the goniometer in such a way that the ϕ axis of the diffractometer was normal to the substrate surface. Fig.3.6 is a schematic diagram of this arrangement.

To check quickly whether the film contains (103)/(013) grains, we study the diffraction vectors along either STO [100] or STO [010] direction. Here we assume the substrate has a (110) surface. As shown in Fig.1.2, the c-axis of a (103) or (013) film points along STO [100] or STO [010] direction (at 45° from the

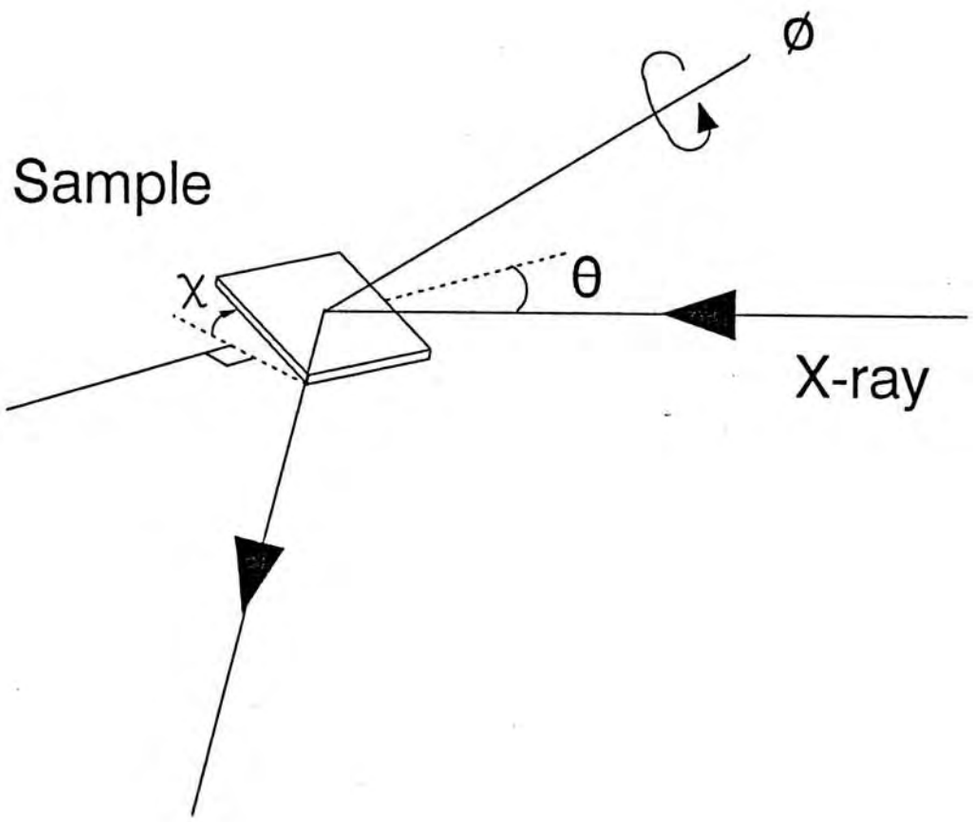

Fig. 3.6 Sample arrangement of x-ray diffraction off-scan.

substrate surface) while the c axis of a (110) film lies along the STO [001] direction (on the substrate surface). Hence the existence of (103) and/or (013) grains can be established if we observe (00ℓ) diffraction peaks for the scans along either STO [100] or STO [010] direction. But this experiment cannot distinguish (103) from (013) grains.

To perform the experiment, we first tilted the sample by 45° (i.e. χ = 45°) and set the diffractometer at 2θ = 46.472°. Then a ϕ scan from 0° to 360° was performed. Two peaks were observed which was 180° apart. This is expected because STO is cubic and the peaks are due to STO (200) or (020) diffractions. At these two ϕ values (called ϕ_1 and ϕ_2 for convenience of future discussion), the STO (100) and (010) planes are aligned with the diffractometer. At these ϕ/χ settings, we performed the θ-2θ scans. Fig.3.7(a)-(d) show the diffraction patterns for the films grown at 500°C, 525°C, 600°C and 720°C (samples 1, 2, 4, and 6) respectively. These diffraction patterns at ϕ_1 and ϕ_2 are similar because there are twinnings in all these three phases (the proof will be given below). In Fig.3.7(c) and (d), the YBCO (00ℓ) peaks, ℓ = 1 to 7, are clearly seen. This indicates that samples 4 and 6 contain (103)/(013) grains. Sample 6 has a higher YBCO (005) peak intensity than sample 4. This reflects that sample 6 has a higher percentage of (103)/(013) grains than sample 4. The situation is similar for samples 3 and 5. There is a tendency that the YBCO (005) diffraction intensity increases with increasing substrate temperature. We may conclude that the percentage of (110) grains in the sample decreases at higher substrate temperature, in

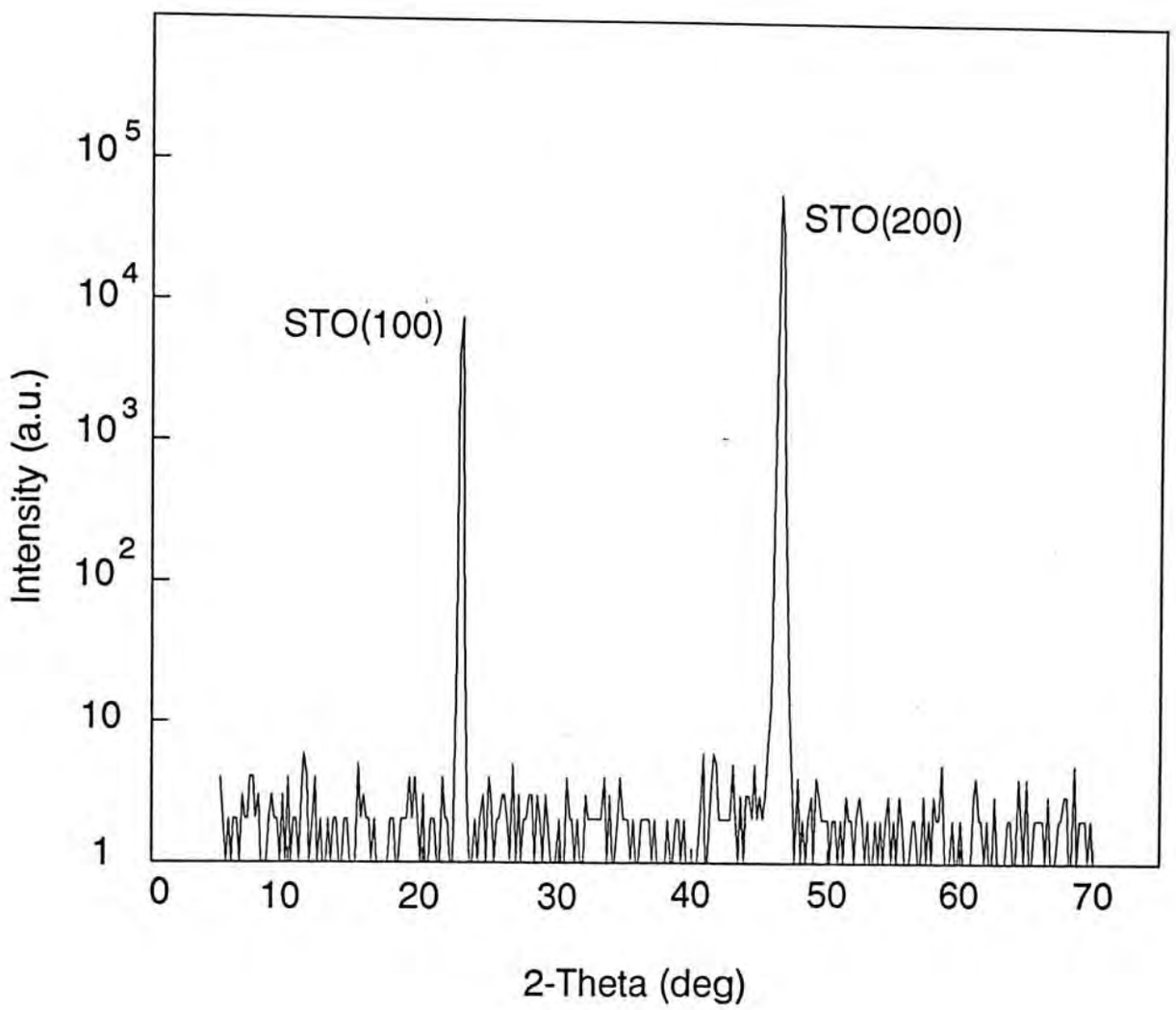

Fig.3.7(a) X-ray diffraction θ-2θ scan of sample 1 at $\chi = 45^{\circ}$.

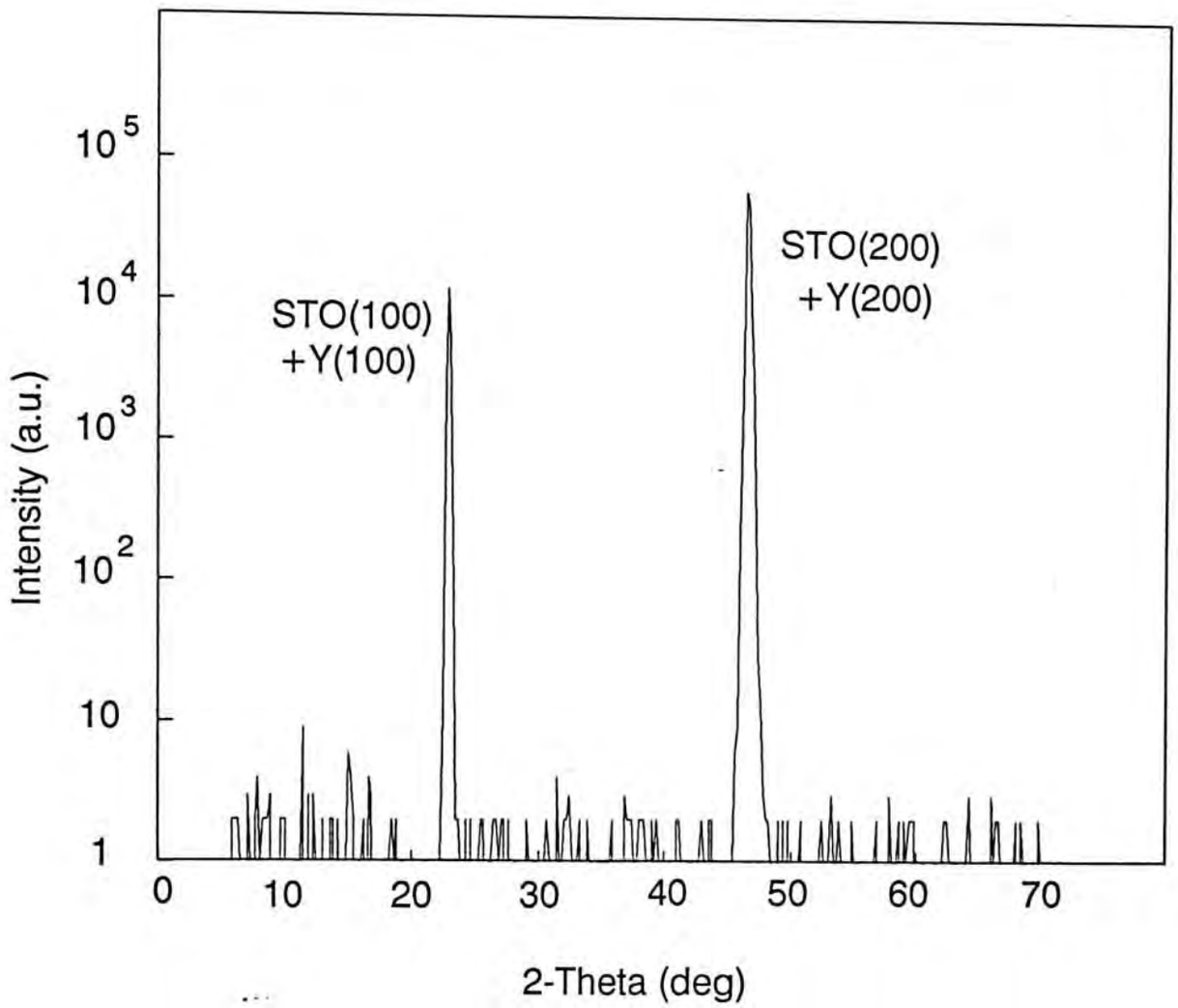

Fig.3.7(b) X-ray diffraction θ-2θ scan of sample 2 at $\chi = 45^{\circ}$.

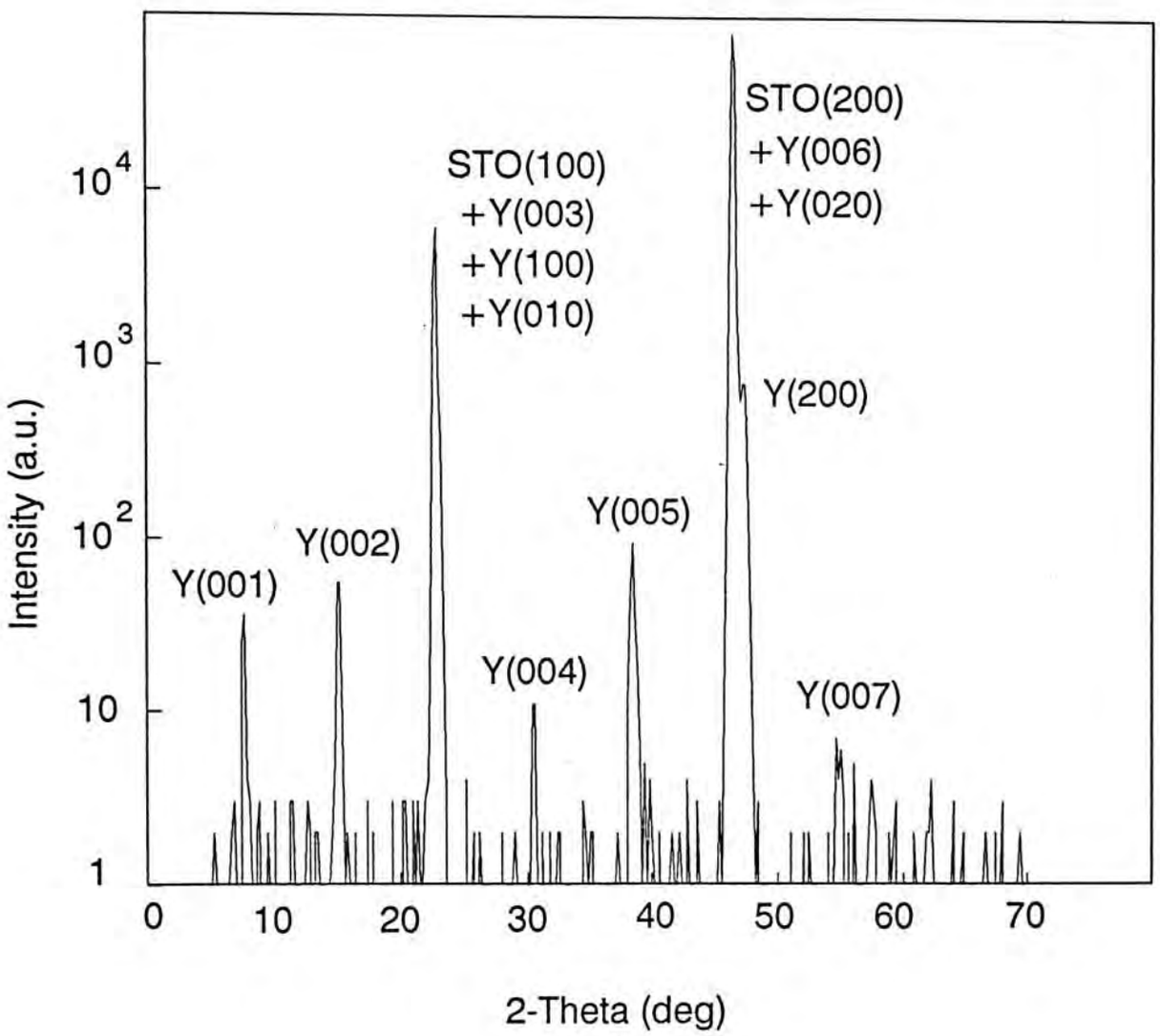

Fig.3.7(c) X-ray diffraction θ-2θ scan of sample 4 at $\chi = 45^{\circ}$.

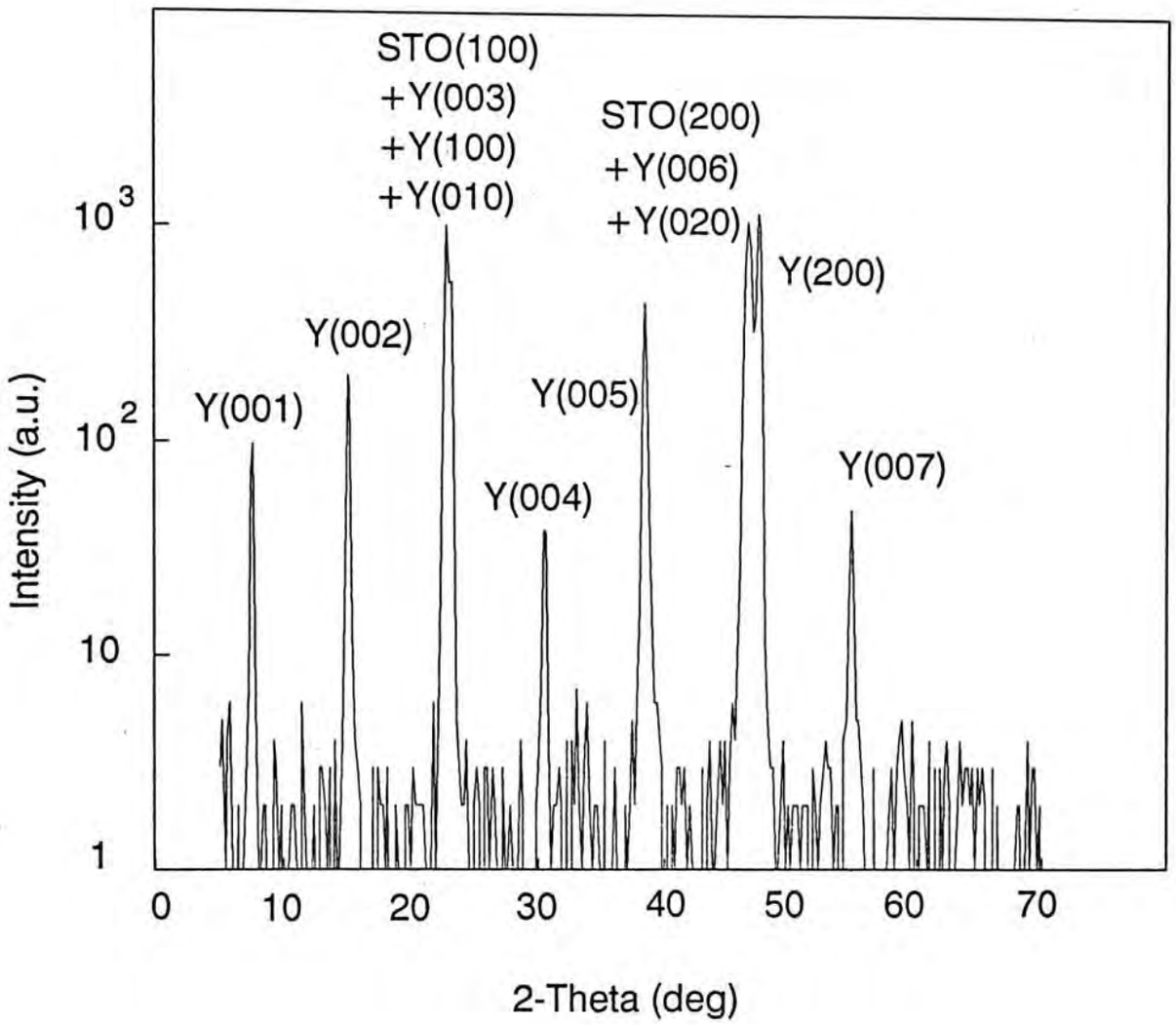

Fig.3.7(d) X-ray diffraction θ-2θ scan of sample 5 at $\chi = 45^{\circ}$.

agreement with our findings described in Section 3.2.

In Fig.3.7(c) and (d), we also observed YBCO (200) peak in the diffraction patterns. But in Fig.3.7(b), the peaks of STO (200) and YBCO (200) are very close and as shown in Fig.3.8, they can only be resolved by a finer scan. In this case, the YBCO (200) peak is shifted to a lower 2θ value because of the lengthening in the a-axis. This problem will be discussed in more detail below.

In these figures, no YBCO (020) peak was observed. This is expected because (020) peak is masked by the strong STO (200) peak. The 2θ values for YBCO (020) and STO (200) are 46.725°[20] and 46.47° respectively. For the sample 1, no YBCO (00ℓ) nor (200) peak is observed as shown in Fig.3.7(a). It indicates that the film does not contain (110), (103) or (013) grains. This result was also verified by the ϕ scan of (102) diffraction (see below). As we have proved in section 3.2, there is no other phases in this sample. Therefore we conclude that this sample is amorphous.

The existence of (110), (103) and (013) grains was confirmed by the ϕ scan of the YBCO (102) diffraction. We first calculate the angles between $\vec{K}_{102}$ and $\vec{K}_{hkl}$ for (hkℓ) = (110), (103) and (013) where $\vec{K}_{hkl}$ is the reciprocal lattice vector normal to the (hkℓ) planes. Let $\hat{x}$, $\hat{y}$ and $\hat{z}$ be the unit vectors along the a, b and c-axes respectively. Since YBCO is orthorhombic, the primitive vectors of reciprocal lattice are

$$a^* = \frac{1}{a}\hat{x} \quad , \quad b^* = \frac{1}{b}\hat{y} \quad \text{and} \quad c^* = \frac{1}{c}\hat{z} \ .$$

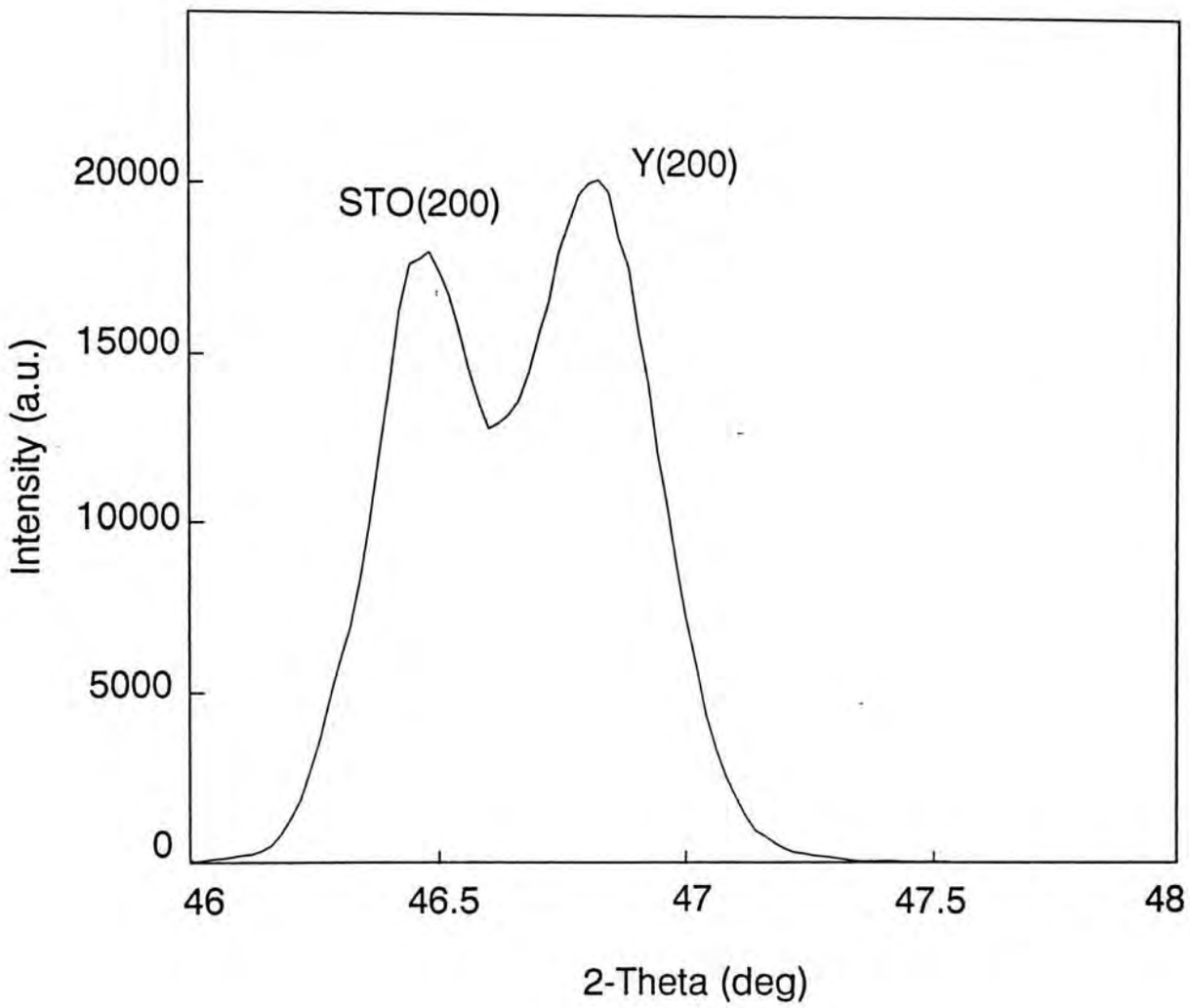

Fig. 3.8 Section of x-ray diffraction θ-2θ scan of sample 2 at $\chi = 45^{\circ}$.

The angle φ between (102) and (hkℓ) planes is given by

$$\cos\varphi = \frac{\vec{K}_{102} \cdot \vec{K}_{hkl}}{|\vec{K}_{102}| \cdot |\vec{K}_{hkl}|}$$

$$= \frac{(a^* + 2c^*) \cdot (ha^* + kb^* + lc^*)}{|a^* + 2c^*| \cdot |ha^* + kb^* + lc^*|}$$

$$= \frac{\frac{h}{a^2} + \frac{2l}{c^2}}{\left(\frac{1}{a^2} + \frac{4}{c^2}\right)^{1/2} \cdot \left(\frac{h^2}{a^2} + \frac{k^2}{b^2} + \frac{l^2}{c^2}\right)^{1/2}}$$

Assuming a = 3.82 Å, b = 3.89 Å and c = 11.68 Å, we get

$\varphi = 53.3^\circ$ for (110),

$\varphi = 11.3^\circ$ for (103),

and $\varphi = 67.2^\circ$ for (013).

To observe the (102) diffraction, we set the diffractometer around $2\theta = 27.89^\circ$, tilted the sample by a χ value given by $\chi = 90^\circ - \varphi$ and then performed a ϕ scan. For (110), (103) and (013) grains, $\chi = 36.7^\circ$, 78.7° and 22.8° respectively. The ϕ scan patterns of the (102) diffraction for samples 2 to 6 are shown in Fig.3.9(a)-(e). From the graphs, we see that (110) grains are present in samples 2, 3 and 4. Sample 2 has a pure (110) orientation. Sample 3 also has a (110) orientation but a trace amount of (013) grains exists. Sample 4 contains all (110), (103) and (013) grains. No (110) grains were observed in samples 5 and 6. These indicate that increasing the substrate temperature enhances the growth of (103) and (013) grains at the expense of smaller amount of (110) grains. The FWHM of the peaks in the ϕ

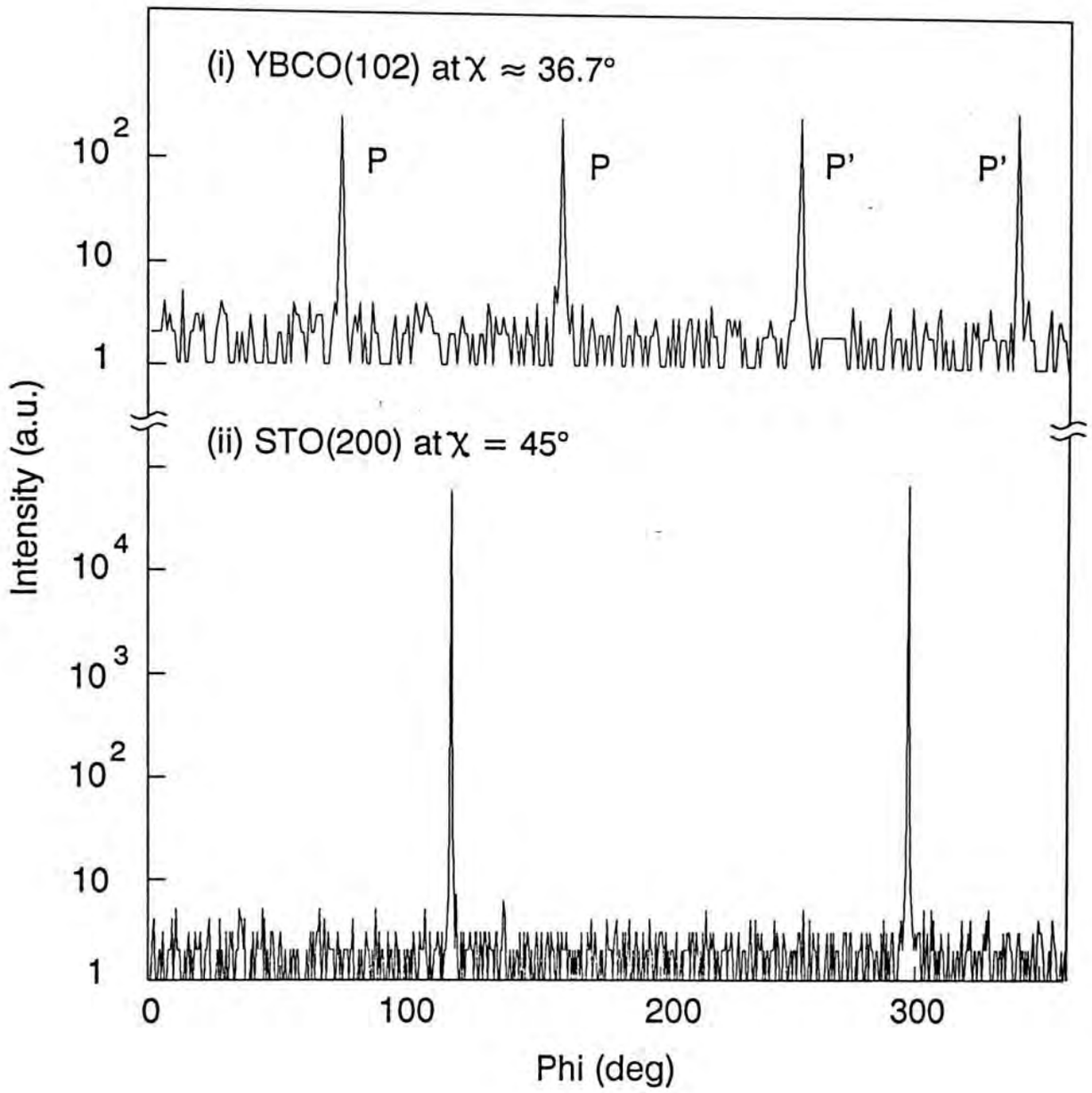

Fig.3.9(a) (i) ϕ scan of YBCO (102) diffraction on sample 2 at $\chi \simeq 36.7^{\circ}$. (ii) ϕ scan of STO (200).

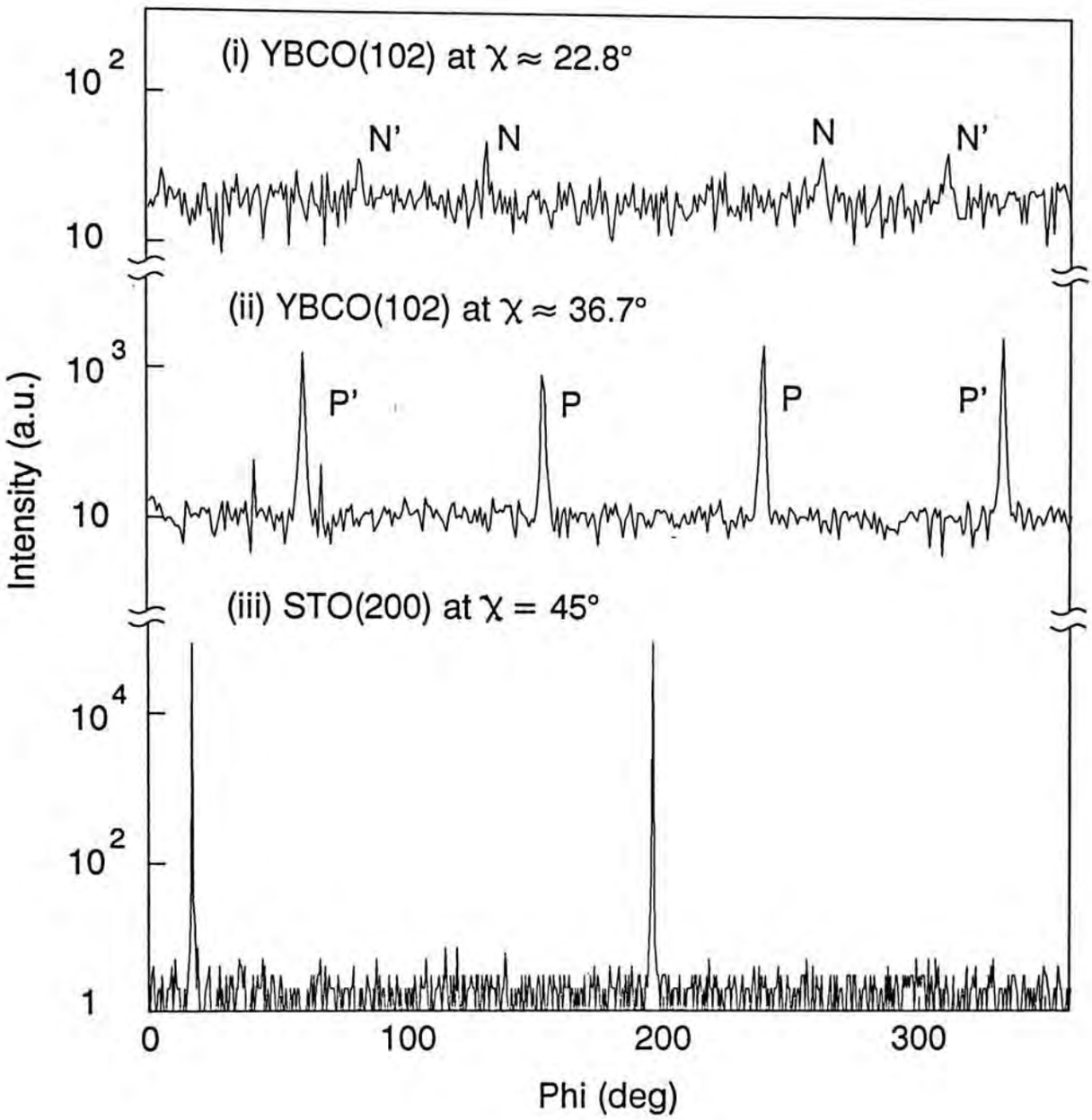

Fig.3.9(b) ϕ scans of YBCO (102) diffraction on sample 3 at (i) $\chi \simeq 22.8^{\circ}$, and (ii) $\chi \simeq 36.7^{\circ}$. (iii) ϕ scan of STO (200).

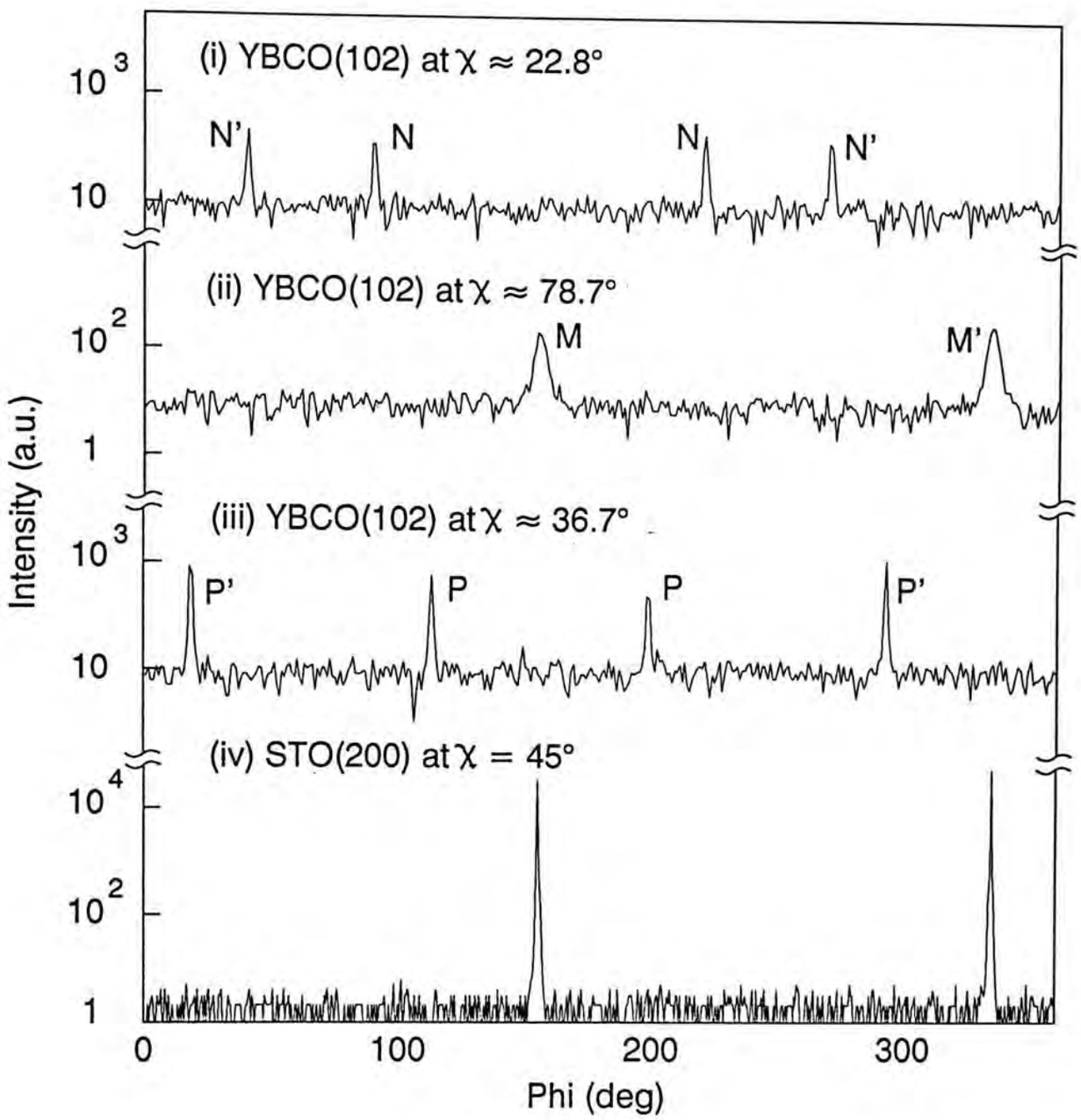

Fig.3.9(c) ϕ scans of YBCO (102) diffraction on sample 4 at (i) $\chi \simeq 22.8^{\circ}$, (ii) $\chi \simeq 78.7^{\circ}$, and (iii) $\chi \simeq 36.7^{\circ}$. (iv) ϕ scan of STO (200).

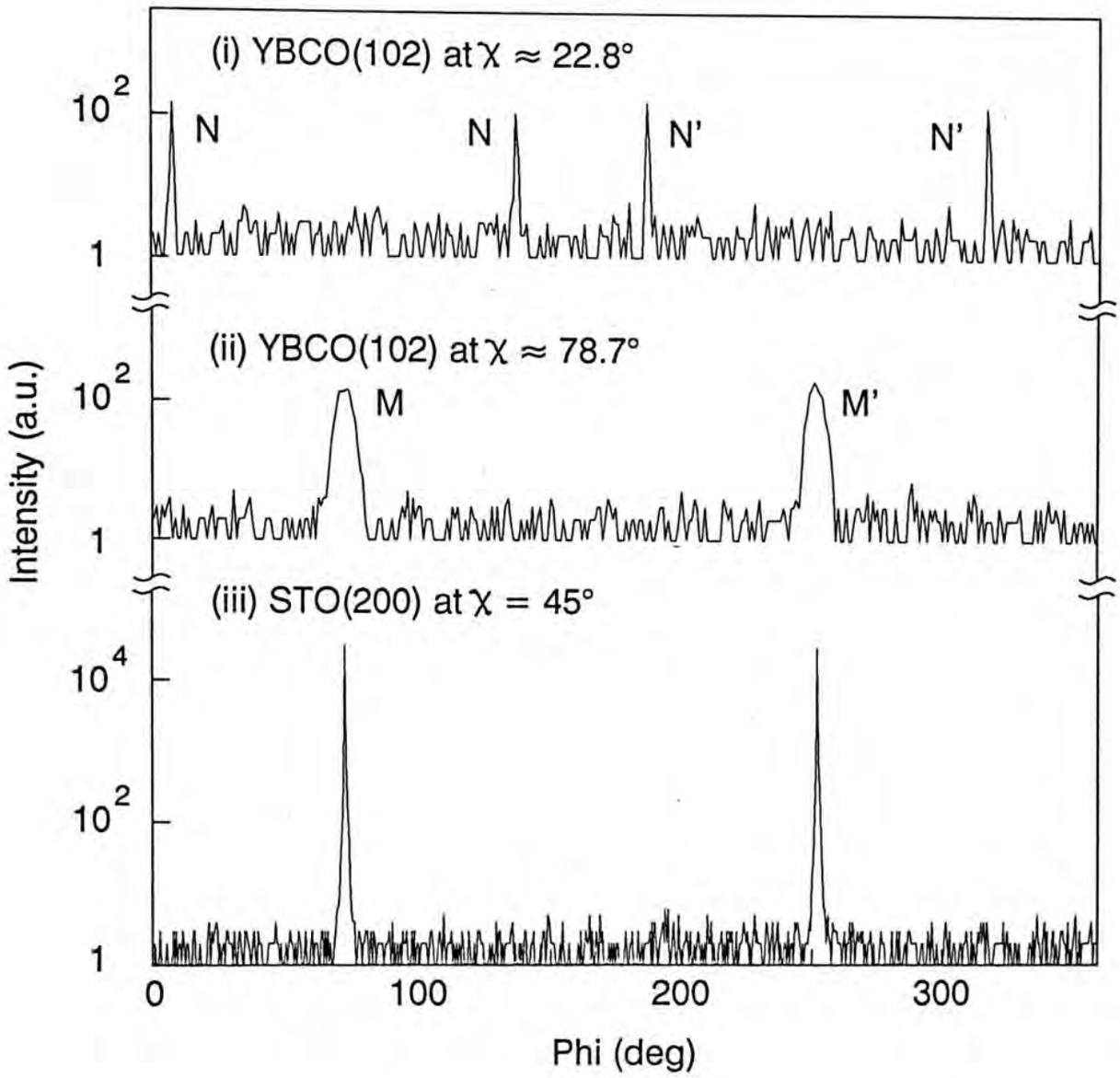

Fig.3.9(d) ϕ scans of YBCO (102) diffraction on sample 5 at (i) $\chi \simeq 22.8^{\circ}$, and (ii) $\chi \simeq 78.7^{\circ}$. (iii) ϕ scan of STO (200).

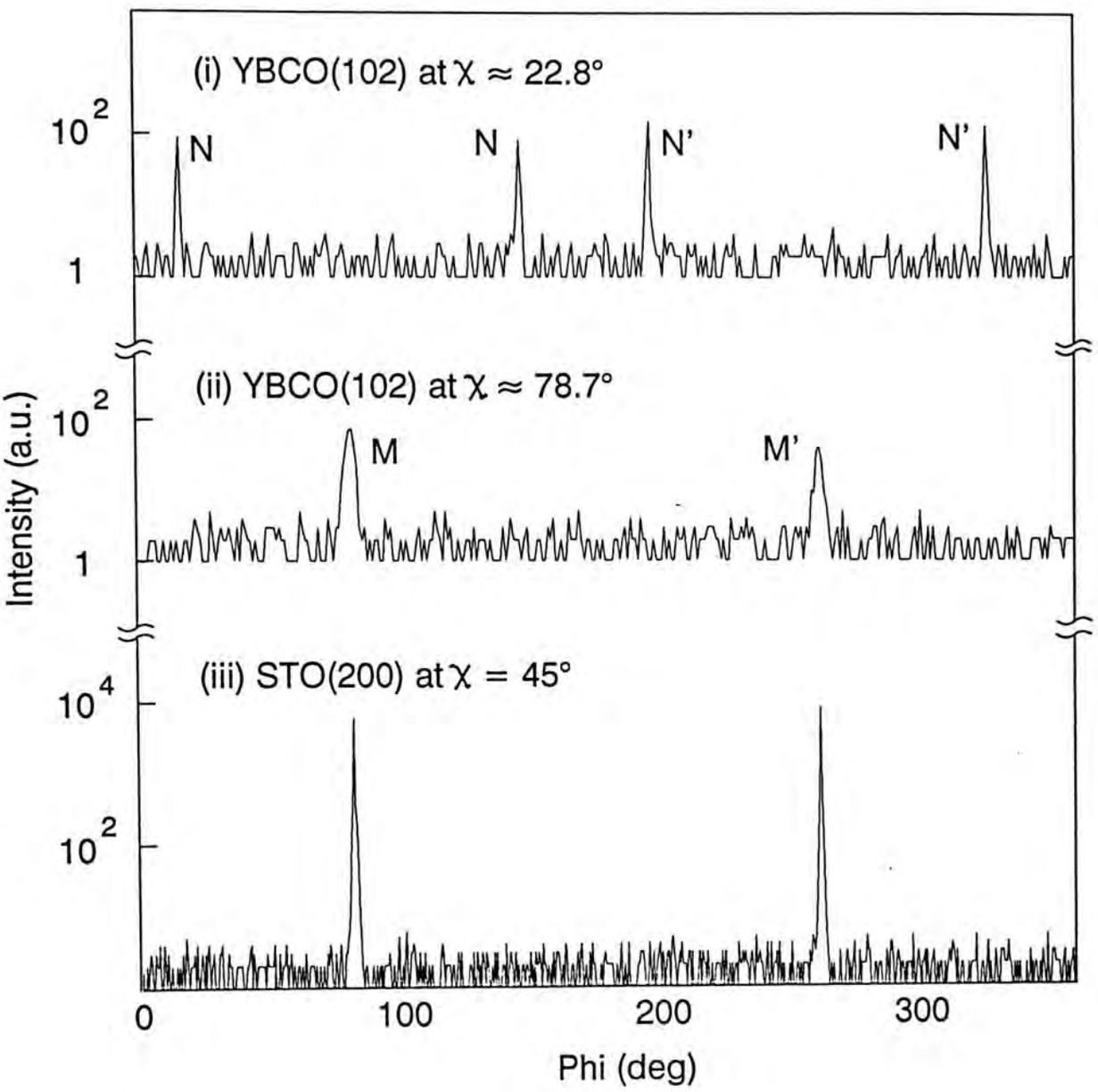

Fig.3.9(e) ϕ scans of YBCO (102) diffraction on sample 6 at (i) $\chi \simeq 22.8^{\circ}$, and (ii) $\chi \simeq 78.7^{\circ}$. (iii) ϕ scan of STO (200).

scan for (110) grains increases with substrate temperature from ~ 0.6° for sample 2 to ~ 1° for sample 4. This indicates that the growth of (110) is better at lower substrate temperature. For sample 1, these ϕ scans were also performed but no peaks were observed for all three χ values. This confirms the non-existence of the (110), (103) and (013) grains. The texture of the samples is summarized in Table 3.2.

In Fig.3.9, there are four peaks in the (102) ϕ scan patterns for (013) and (110) grains ($\chi \simeq 22.8°$, $36.7°$) while there are only two peaks for the (103) grains ($\chi \simeq 78.7°$). For example, in Fig.3.9(c), there are two pairs of peaks marked by P and P' separated by 180°; the peaks in each pair are separated by about 85.5°. These angles can be calculated by crystallography. Fig.3.10 shows the situation of the ϕ scan of (102) diffraction for grains with various orientations. Fig.3.10(a) is a schematic of the experiment in which the x-ray source and the detector are positioned such that to detect a peak, the normal of the (102) planes must lie in the diffraction plane and makes equal angles with the incident and diffracted beams.

We first consider the ϕ scan for the (110) grains. The schematic diagram is shown in Fig.3.10(b). Here the axis of rotation (i.e. the ϕ axis) is along $\vec{K}_{110}$. Note that $\vec{K}_{\bar{1}02}$ and $\vec{K}_{\bar{1}0\bar{2}}$ are always pointing downwards during the ϕ scan. Therefore the $(\bar{1}02)$ and $(\bar{1}0\bar{2})$ diffractions cannot be observed. We next show that the peaks marked by P are due to the (102) and $(10\bar{2})$ diffractions. Their reciprocal lattice vectors are

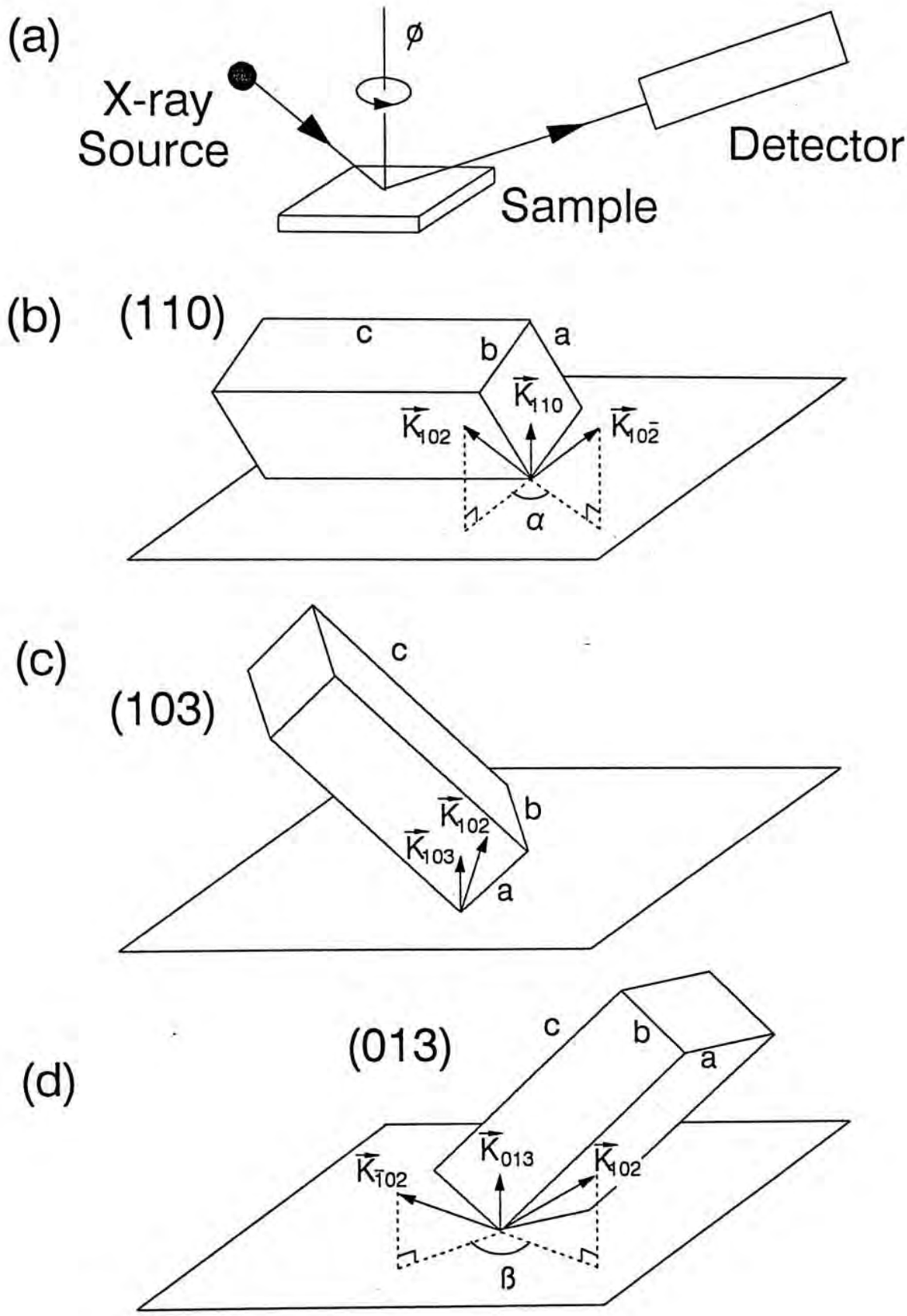

Fig. 3.10 Diagrams showing (a) the ϕ-scan experiment and reciprocal lattice vectors of {102} planes for (b) (110), (c) (103), and (d) (013) films.

$$\vec{K}_{102} = a^* + 2c^* \qquad \text{and} \qquad \vec{K}_{10\bar{2}} = a^* - 2c^*$$

Since the rotational axis is along $\vec{K}_{110}$, we project $\vec{K}_{102}$ and $\vec{K}_{10\bar{2}}$ on the (110) plane. Let $\hat{u}_{110}$ be the unit vector of $\vec{K}_{110}$. Then

$$\hat{u}_{110} = \frac{1}{\left(\frac{1}{a^2} + \frac{1}{b^2} \right)^{1/2}} \left(\frac{1}{a} \hat{x} + \frac{1}{b} \hat{y} \right)$$

$$= \frac{1}{(a^2 + b^2)^{1/2}} (b\hat{x} + a\hat{y})$$

$$\vec{K}_{102} \cdot \hat{u}_{110} = \left(\frac{1}{a} \hat{x} + \frac{2}{c} \hat{z} \right) \cdot \frac{1}{(a^2 + b^2)^{1/2}} (b\hat{x} + a\hat{y})$$

$$= \frac{b}{a(a^2 + b^2)^{1/2}}$$

Denote the components of $\vec{K}_{102}$ and $\vec{K}_{10\bar{2}}$ on (110) plane as ${}_{110}\vec{K}_{102}$ and ${}_{110}\vec{K}_{10\bar{2}}$ respectively. Then

$${}_{110}\vec{K}_{102} = \vec{K}_{102} - \frac{b}{a(a^2 + b^2)^{1/2}} \hat{u}_{110}$$

$$= \left(\frac{1}{a} \hat{x} + \frac{2}{c} \hat{z} \right) - \frac{b}{a(a^2 + b^2)} (b\hat{x} + a\hat{y})$$

$$= \frac{a}{(a^2 + b^2)} \hat{x} - \frac{b}{(a^2 + b^2)} \hat{y} + \frac{2}{c} \hat{z}$$

and

$${}_{110}\vec{K}_{10\bar{2}} = \frac{a}{(a^2 + b^2)} \hat{x} - \frac{b}{(a^2 + b^2)} \hat{y} - \frac{2}{c} \hat{z}$$

The angle α between ${}_{110}\vec{K}_{102}$ and ${}_{110}\vec{K}_{10\bar{2}}$ (defined in Fig.3.10(b)) is then given by

$$\cos\alpha = \frac{{}_{110}\vec{K}_{102} \cdot {}_{110}\vec{K}_{10\bar{2}}}{|{}_{110}\vec{K}_{102}| \cdot |{}_{110}\vec{K}_{10\bar{2}}|}$$

$$= \frac{\frac{1}{a^2 + b^2} - \frac{4}{c^2}}{\frac{1}{a^2 + b^2} + \frac{4}{c^2}}$$

The value of α can be determined from the angular separation of the peaks marked by P in Fig.3.9(c). For this sample (sample 4), the measured lattice parameters are a = 3.83 Å , b = 3.90 Å and c = 11.71 Å, then $\alpha = 86.07^\circ$. This agrees fairly with the experimental result ($\sim 85.5^\circ$). The other pair of peaks is 180° separated from this pair indicating that twinning exists in these (110) grains. This is expected because the lattice constants of YBCO $a \simeq b \simeq c/3$. According to the phase diagram of YBCO[27], our deposition conditions (substrate temperature and oxygen partial pressure) favour the tetragonal phase of YBCO ($YBa_2Cu_3O_6$). To become the superconducting orthorhombic phase ($YBa_2Cu_3O_7$), O_2 must be intaken during the cooling process. There is equal probability for oxygen atom to enter into the equivalent a and b-axes and hence twinning occurs. In order to study the epitaxial relationship of the films, the ϕ scan of the STO (200) diffraction for each sample was also performed and also shown in Fig.3.9(a)-(e). The STO (200) diffraction peak is situated in middle of the P peaks. This implies that YBCO [100] lies along STO [100] and [010].

(103) grains exists in samples 4, 5 and 6. The FWHM of the peaks in the (102) ϕ scan patterns is about 4° in all three

samples. This large FWHM is due to the large χ value (~ 78.7°), i.e. the ϕ axis makes a relatively small angle (~ 11.3°) with the scattering plane (i.e. the diffraction plane). The two peaks in the ϕ scan pattern are at the same ϕ positions of the STO (200) diffraction peaks. This can be easily understood in Fig.3.10(c). Of the four planes in {102}, only (102) plane makes 11.3° with (103) plane. Therefore the two peaks observed are also due to (103) plane, i.e. twinning exists. It is because a ≃ c/3, and thus both a and c-axes lie along STO [100]. This is shown in Fig.1.2. From this, it concluded that (103) phase grows with YBCO [010] ∥ STO [001] or [00$\bar{1}$].

Now we turn to the case for (013) grains. Similar to the (110) grains, only (102) and ($\bar{1}$02) contribute in the ϕ scan of (102) diffraction as shown in Fig.3.10(d). However four peaks are observed, the pair marked by N is 180° apart from the other pair marked by N'. The angle β between the peaks N can be calculated by a similar procedure as we have done for the (110) grains. In this case, the axis of rotation is $\vec{K}_{013}$. Let $\hat{u}_{013}$ be the unit vector of $\vec{K}_{013}$. Then

$$\hat{u}_{013} = \frac{1}{\left(\frac{1}{b^2} + \frac{9}{c^2} \right)^{1/2}} \left(\frac{1}{b} \hat{x} + \frac{3}{c} \hat{z} \right)$$

$$= \frac{1}{(9b^2 + c^2)^{1/2}} (c\hat{y} + 3b\hat{z})$$

$$\vec{K}_{102} \cdot \hat{u}_{013} = \frac{b}{c(9b^2 + c^2)^{1/2}}$$

The component of $\vec{K}_{102}$ on (013) plane is

$$_{013}\vec{K}_{102} = \vec{K}_{102} - \frac{b}{c(\,9b^2 + c^2\,)^{1/2}}\,\hat{u}_{013}$$

$$= \left(\frac{1}{a}\hat{x} + \frac{2}{c}\hat{z}\right) - \frac{b}{c(\,9b^2 + c^2\,)}\,(\,c\hat{y} + 3b\hat{z}\,)$$

$$= \frac{1}{a}\hat{x} - \frac{6b}{9b^2 + c^2}\hat{y} + \frac{2c}{9b^2 + c^2}\hat{z}$$

Similarly, $_{013}\vec{K}_{\bar{1}02} = \frac{-1}{a}\hat{x} - \frac{6b}{9b^2 + c^2}\hat{y} + \frac{2c}{9b^2 + c^2}\hat{z}$

Therefore $\cos\beta = \dfrac{_{013}\vec{K}_{102} \cdot {}_{013}\vec{K}_{\bar{1}02}}{|\,_{013}\vec{K}_{102}| \cdot |\,_{013}\vec{K}_{\bar{1}02}|}$

$$= \frac{\dfrac{-1}{a^2} + \dfrac{36b^2 + 4c^2}{(9b^2 + c^2)^2}}{\dfrac{1}{a^2} + \dfrac{36b^2 + 4c^2}{(9b^2 + c^2)^2}}$$

For this sample, a = 3.83 Å , b = 3.90 Å and c = 11.71 Å. Hence $\beta = 130.3^\circ$ which agrees well with the experimental result ($\sim 130.2^\circ$). As expected, twinning also exists. The reason is the same as in the case for (103) grains except that b ≃ c/3 instead of a ≃ c/3. The situation is shown in Fig.1.2. By the ϕ position of STO (200), we conclude that (013) grains grow with YBCO [100] ∥ STO [001] or [00$\bar{1}$].

3.6 GRAZING INCIDENCE X-RAY DIFFRACTION

In conventional XRD, the planes parallel to or tilted at an angle with the film surface are examined. But the in-plane

structure cannot be measured directly. Recently, a powerful technique called the grazing incidence x-ray diffraction (GID), has been developed that allows one to examine the surface structure of a film. In GID, the x-ray beam is incident on the film at a glancing angle (< 1°). At this angle, total reflection occurs and at the same time the beam is diffracted by crystal planes perpendicular to the surface if the Bragg equation is satisfied. The lattice parameters parallel to the surface can be found from the θ-2θ scan. Matsubara et al[28] had applied this method to characterize YBCO films on STO (110).

The in-plane structure of samples 2 and 5 were studied by GID. The experimental arrangement is the same as for the texture analysis. χ was set at a very small value, usually ≤ 1°. θ-2θ scans were performed at ϕ_1 and (ϕ_1 + 90°). Fig.3.11(a) and (b) show the GID patterns for sample 2 at ϕ_1 and (ϕ_1 + 90°). As proved above, sample 2 has a pure (110) orientation. In Fig.3.11(a), two peaks are observed, which corresponding to the expected $(1\bar{1}0)$ and $(2\bar{2}0)$ diffractions. The d spacings calculated from these peaks are nearly equal to that measured in previous texture analysis where the planes parallel to the film surface are studied. This indicates that the film may be free of strain in the volume irradiated in GID. (00ℓ) peaks are seen in Fig.3.11(b), from which c may be found out. For sample 5 ((103)/(013) oriented), GID were also performed at ϕ_1 and (ϕ_1 + 90°) and the results were shown in Fig.3.12(a)/(b). As marked in Fig.12(a), $(10\bar{3})/(01\bar{3})$ and $(20\bar{6})/(02\bar{6})$ peaks are observed. Similar to sample 2, the d spacings are almost the same as those obtained in previous texture

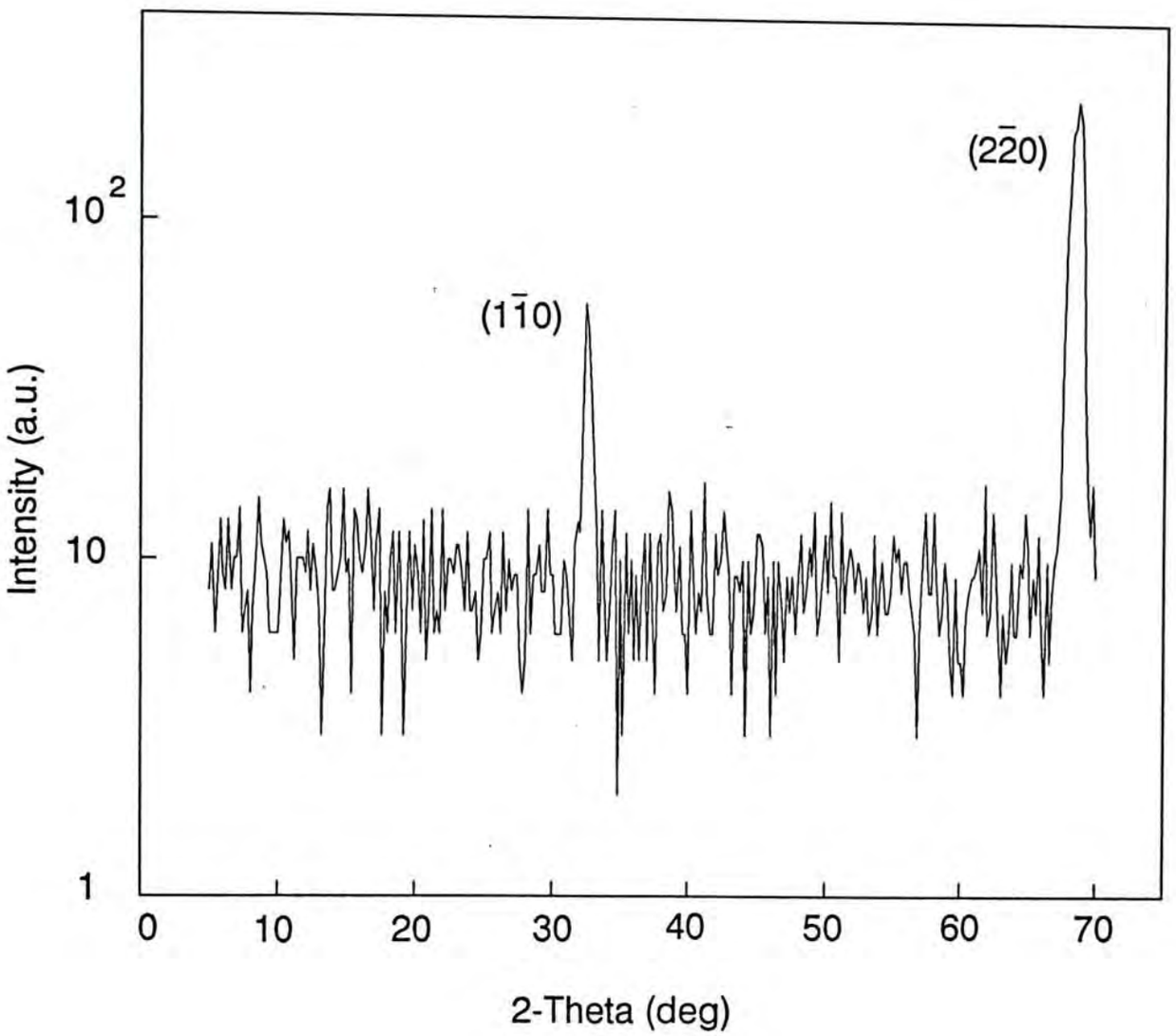

Fig.3.11(a) GID pattern on sample 2 at $\phi = \phi_1$.

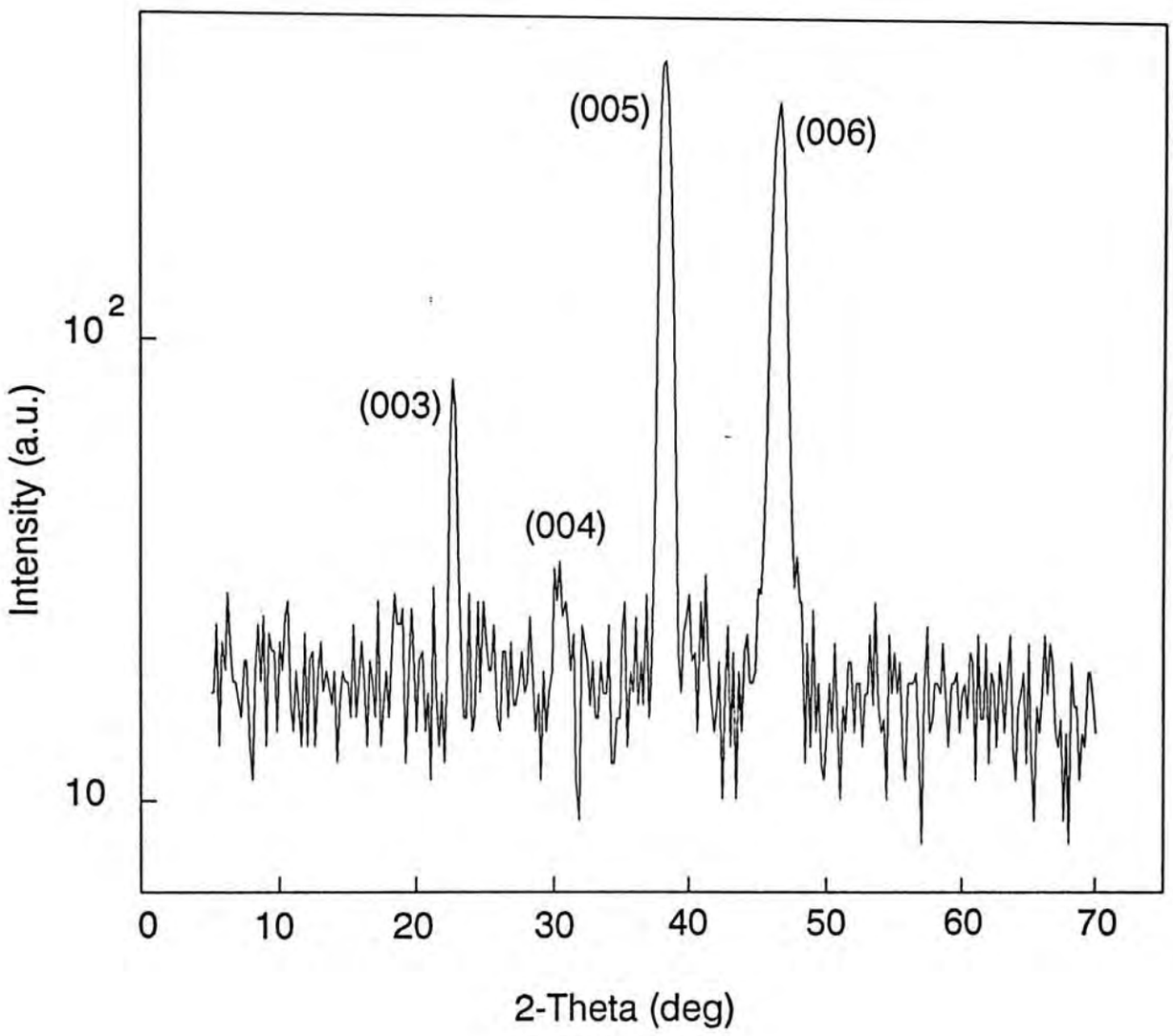

Fig. 3.11(b) GID pattern on sample 2 at $\phi = \phi_1 + 90^\circ$.

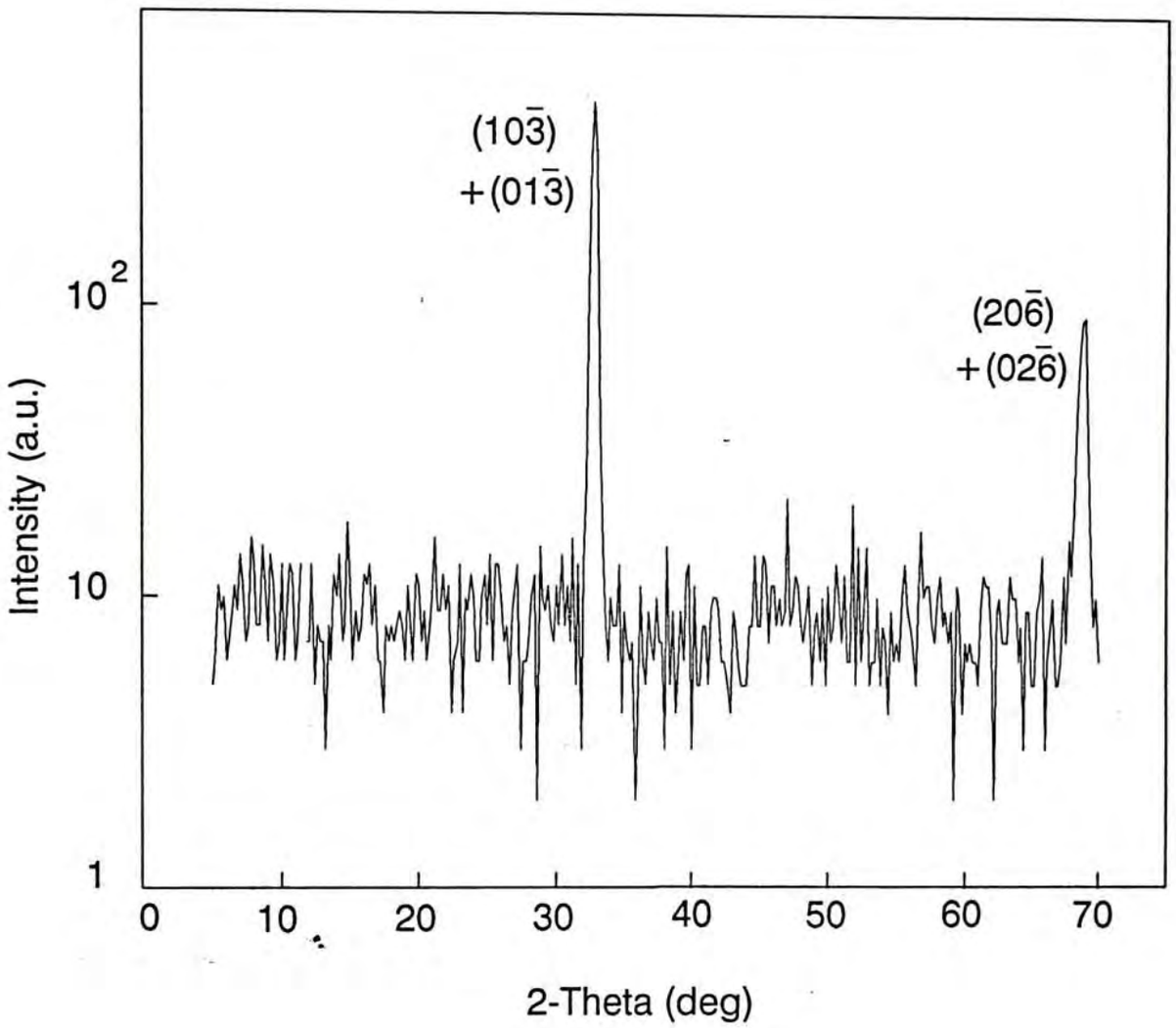

Fig.3.12(a) GID pattern on sample 5 at $\phi = \phi_1$.

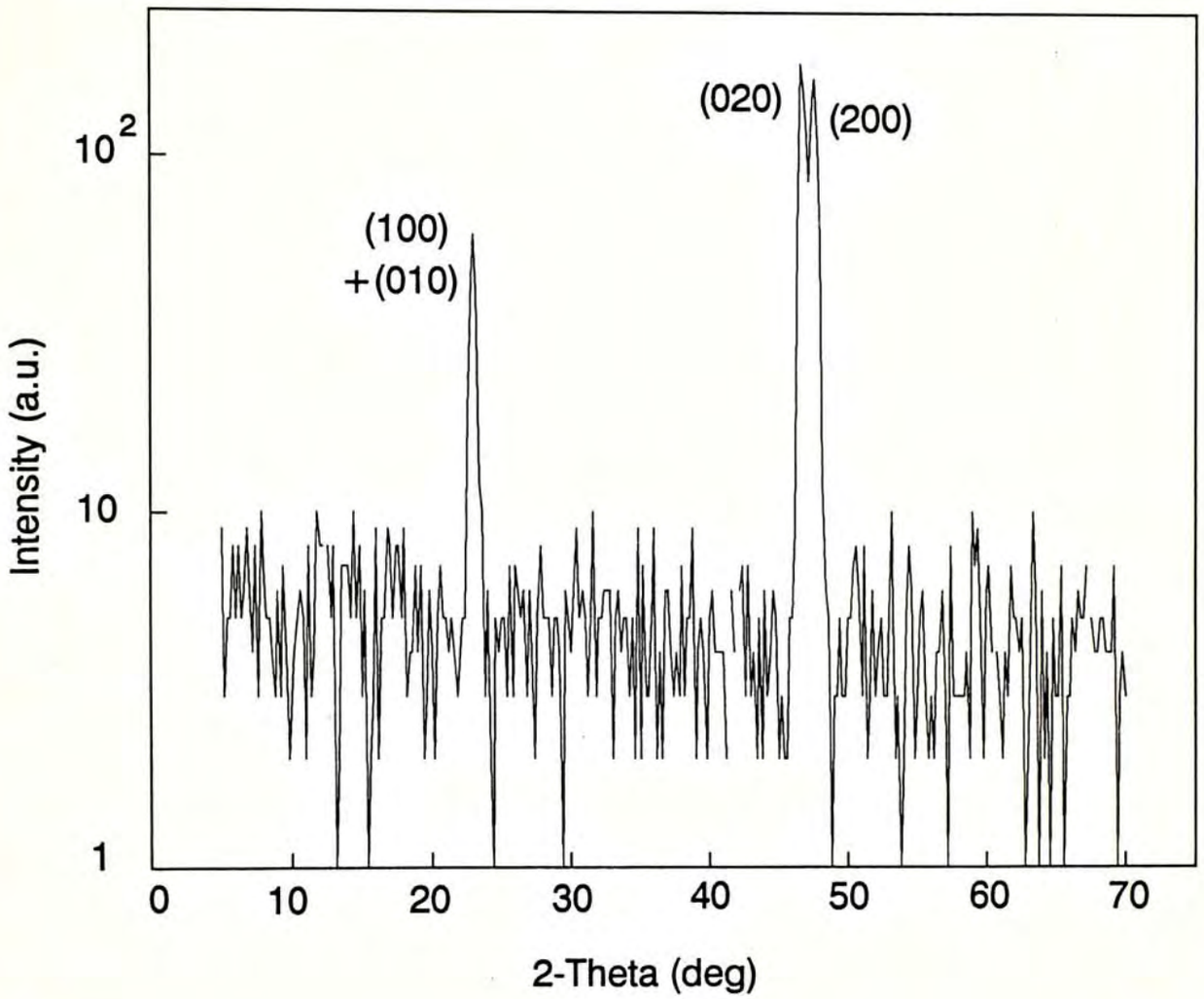

Fig. 3.12(b) GID pattern on sample 5 at $\phi = \phi_1 + 90^\circ$.

analysis. In Fig.12(b), the (200) and (020) peaks are observed and thus a and b may be calculated. As discussed in previous section, b is difficult to find because the (020) peak is always masked by the strong STO (200) peak. However in GID, x-ray can only penetrate the surface layer (about several hundred angstrom thick) and thus no substrate signal could be detected. Hence we may measure b directly from the (020) peak.

3.7 PERCENTAGE OF (110) PHASE

The amount of (110) grains in the samples were found from the (102) diffraction intensities of (110), (103) and (013) grains. For a quantitative study, we need to find the χ angle correcting factors for these diffractions. These include the defocusing and absorption factors. The defocusing effect is arisen from the tilting of the sample, i.e. the surface plane of the sample is not perpendicular to the diffraction plane. This results in broadening of the diffracted beam. Because of the fixed receiving slits, the measured intensity (at $\chi \neq 90^\circ$) is smaller than that measured at $\chi = 90^\circ$. Gale et al.[29] derived a calibration function $C(\theta,\varphi)$ for the intensity ratio $I(\varphi)/I(0)$ when the sample is tilted by an angle φ. The function is given by

$$C(\theta,\varphi) = \frac{I(\varphi)}{I(0)} = \frac{\tau\sqrt{2}}{2a\cdot\mathrm{erf}\left(\dfrac{W}{2\tau\sqrt{2}}\right)} \left\{ \alpha_1\cdot\mathrm{erf}(\alpha_1) - \alpha_2\cdot\mathrm{erf}(\alpha_2) + \frac{1}{\sqrt{\pi}} \left[\exp(-\alpha_1^2) - \exp(-\alpha_2^2) \right] \right\}$$

where $C(\theta,\varphi)$ = value of the calibration function at Bragg angle θ and tilting angle φ,

$\tau = \frac{\omega}{\sqrt{2\pi}}$ in which ω is the integral width of the diffraction line profile at $\varphi = 0$,

$$\alpha_1 = \frac{a + \frac{1}{2}W}{\tau\sqrt{2}} ,$$

$$\alpha_2 = \frac{a - \frac{1}{2}W}{\tau\sqrt{2}} ,$$

W = height of the receiving slit,

$a = \cos\theta \cdot \tan\varphi \cdot \frac{E}{R}$,

E = width of the incident x-ray beam at the center of the goniometer,

R = distance from the center of the goniometer to the receiving slits, and

$$\mathrm{erf}(x) = \frac{2}{\sqrt{\pi}} \int_0^x \exp(-y^2)\, dy .$$

In our setup, W = 2 mm, R = 304.8 mm, and the angle $\chi = 90^\circ - \varphi$. The parameter E was found by fitting the function $C(\theta,\varphi)$ to the experimental data obtained using Si wafers. (100) and (111)-oriented Si wafers were used and the intensities of Si (311) diffraction peak at different χ angles were recorded. The Bragg angle 2θ is 56.13° and ω is about 0.25°. The best fitted value of E is approximately 1 mm. For the YBCO (102) diffraction peak, the Bragg angle θ and the corresponding ω is about 13.9° and 0.25° respectively. From now on, the calibration function $C(\theta,\varphi)$ is written as $C(\chi)$ for simplicity.

The calibration function $C(\chi)$ was derived under the assumption that the sample was infinitely thick. For our films, the absorption effect must be considered. Wu et al.[24] obtained the χ angle correcting factor by performing experiments on Si and taking it the same as for their YBCO films. They ignored the absorption effect. The absorption factor A is given by

$$A = \frac{1 - \exp\left(\frac{-2\mu t}{\sin \gamma}\right)}{1 - \exp\left(\frac{-2\mu t}{\sin \theta}\right)}$$

where $\cos \gamma = \sqrt{\sin^2\theta \cdot \cos^2\chi + \cos^2\theta}$,

γ = the angle of the incident x-ray beam with the surface plane of the sample,

μ = the linear absorption coefficient of the specimen,

and t = the thickness of the specimen.

The denominator is to normalize the factor to 1 at $\chi = 90^\circ$. For $YBa_2Cu_3O_7$, the mass absorption coefficient $\mu/\rho = 69.32$ cm^2/g where ρ is the density. For our films, we treat the density as 80% of the value of the bulk material (6.35 g/cm^3). The thickness of the film is taken as 2000 Å. The measured intensity at χ, $I(\chi)$, is given by

$$I(\chi) = F(\chi) \cdot I(\chi=90^\circ).$$

where $F(\chi) = C(\chi) \cdot A$. The graph of $F(\chi)$ against χ is shown in Fig. 3.13. Table 3.3 shows some of the values of $F(\chi)$.

The percentages of the three grains in a sample is calculated by

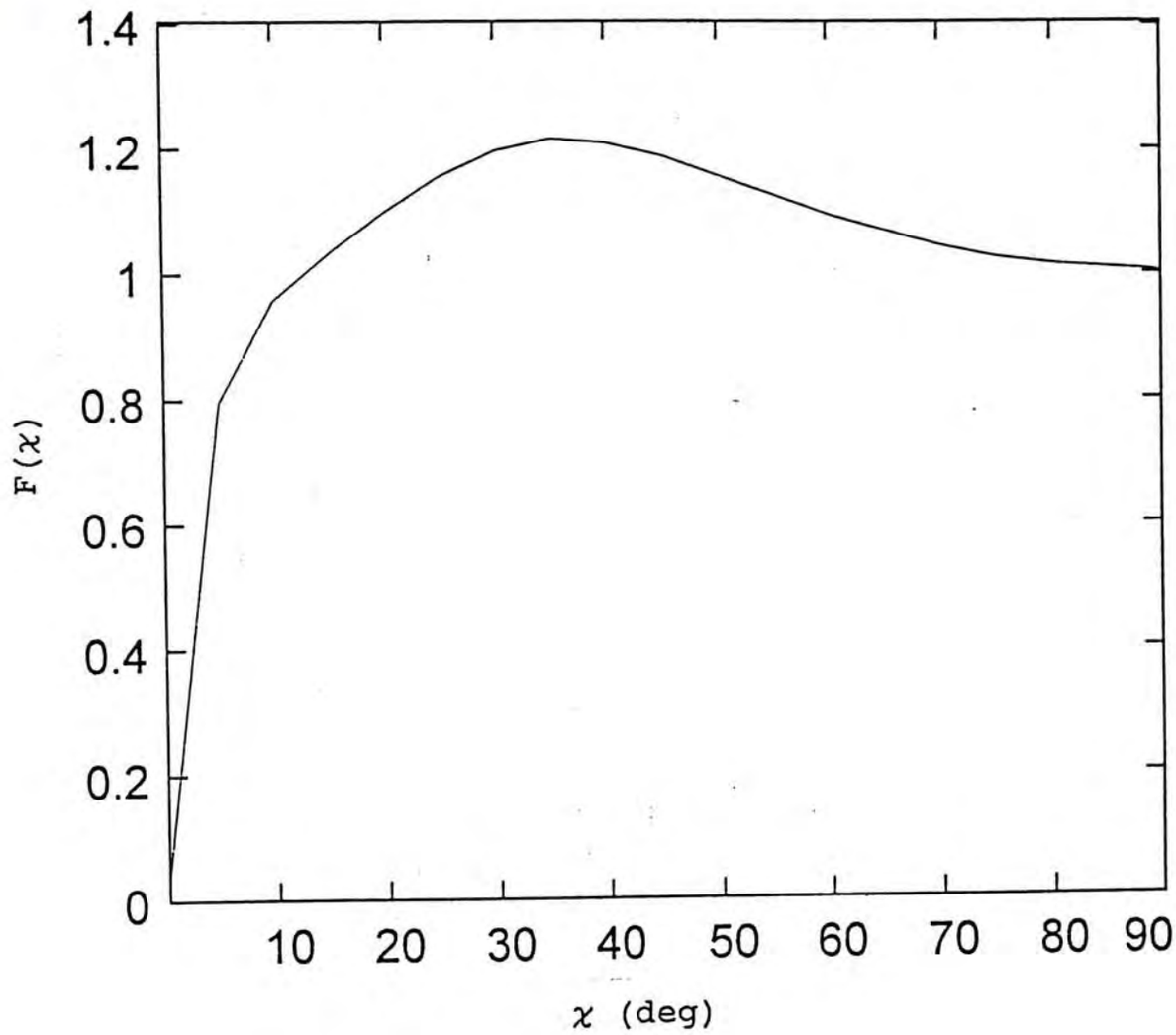

Fig. 3.13 Variation of intensity ratio factor $F(\chi)$ with angle χ.

$$(013)\% = \frac{I^{(102)}_{(013)} / 1.13}{I^{(102)}_{(013)} / 1.13 + I^{(102)}_{(110)} / 1.21 + I^{(102)}_{(103)} / 1.01} \times 100\%$$

$$(110)\% = \frac{I^{(102)}_{(110)} / 1.21}{I^{(102)}_{(013)} / 1.13 + I^{(102)}_{(110)} / 1.21 + I^{(102)}_{(103)} / 1.01} \times 100\%$$

$$(103)\% = \frac{I^{(102)}_{(110)} / 1.01}{I^{(102)}_{(013)} / 1.13 + I^{(102)}_{(110)} / 1.21 + I^{(102)}_{(103)} / 1.01} \times 100\%$$

where $I^{(102)}_{(hkl)}$ is the intensity of (102) diffraction from (hkℓ) grains, (hkℓ) denotes (013), (110) and (103). Fig.3.14 shows the variation of the percentages of the three grains with the substrate temperature. It can be seen that the (110) orientation dominates at substrate temperatures below about 630°C.

Table 3.3 Some values of $F(\chi)$.

χ	$F(\chi)$	Corresponding grain orientation
22.8°	1.13	(013)
36.7°	1.21	(110)
78.7°	1.01	(103)

3.8 Lattice Parameters

The centers of the diffraction peaks were found by fitting

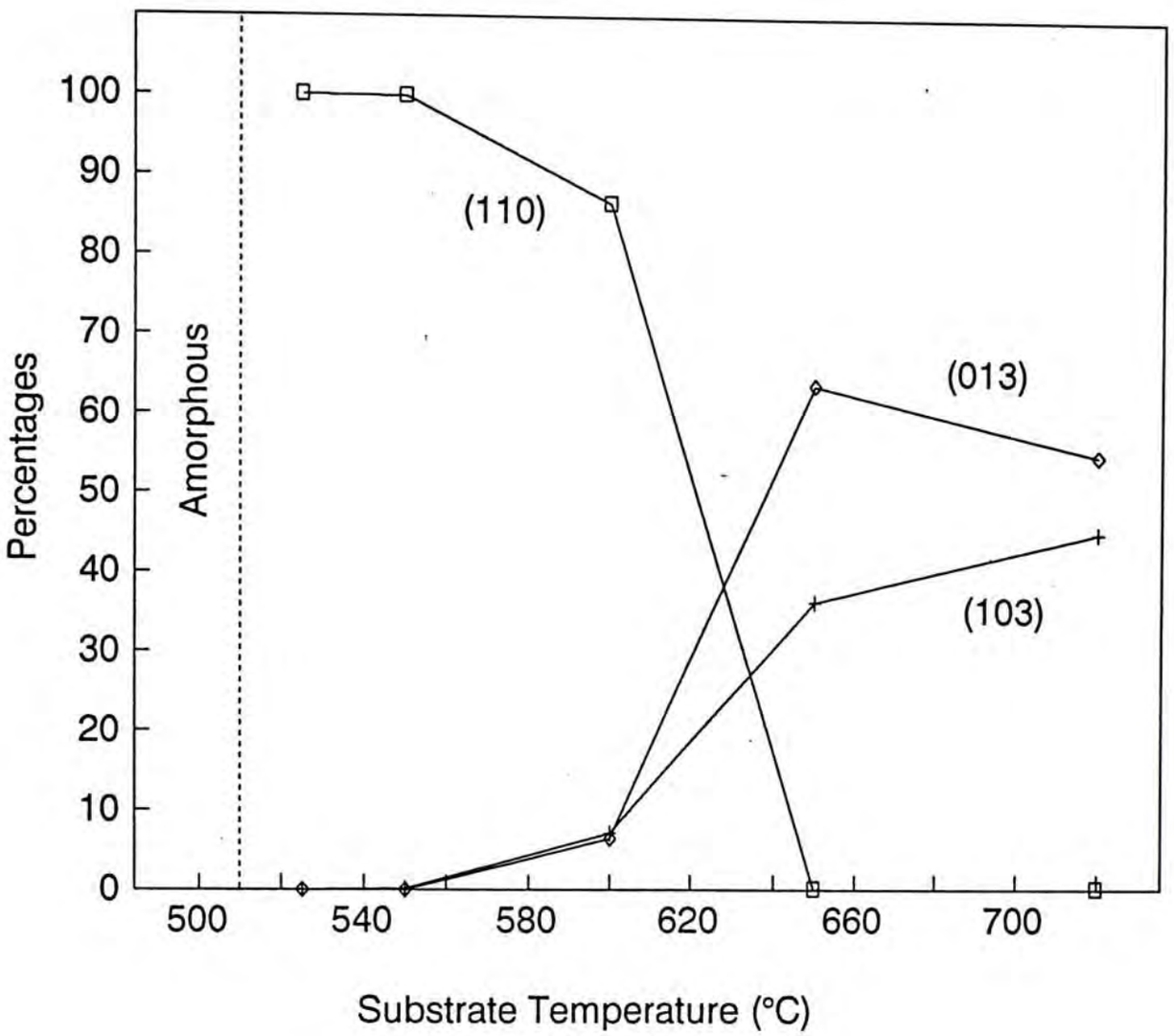

Fig. 3.14 Variation of percentages of (110), (103) and (013) grains with substrate temperature.

the data with a software called 'Peakfit' (Jandel Scientific Peakfit, AISN Software, 1990 Version 2.01). The peaks and the background were assumed to be in Gaussian and quadratic/linear forms respectively. By tilting the sample to different χ values, diffraction peaks (005), (200), (102) and (220)/(206) were used to find the lattice parameters of the samples. (020) diffraction peak was observed in some samples by GID from which b could be directly measured. Moreover, by the optimal χ positions in the ϕ scans of the (102) diffraction in finding (110), (103) and (013) orientations, more informations could be obtained. The results are summarized in Table 3.4.

Table 3.4 Lattice parameters of the samples at different substrate temperatures.

Sample	a (Å)	b (Å)	c (Å)
2	3.87	3.87	11.74
3	3.85	3.88	11.76
4	3.83	3.90	11.71
5	3.82	3.89	11.70
6	3.83	3.89	11.71

CHAPTER 4

TRANSPORT PROPERTIES

4.1 EXPERIMENTAL

The resistance of our films was measured with a closed cycle refrigerator (Air Products Inc., Model DE202). The refrigerator has a copper block which can be cooled to any temperature > 11 K. Each sample was mounted on the copper block by varnish. A gold-iron thermocouple and a heater were mounted at one end of the copper block. The temperature was measured and controlled with a digital temperature controller (Air Products Inc., APD-E). Prior to cooling, the refrigerator was evacuated to a pressure below 10^{-2} Torr using a rotary pump.

The critical temperatures of our films were found by a four-lead resistance measurement. Our films were square in shape with length of each side = 6.5 mm. The four corners of the films were coated with silver layer by evaporation at pressure lower than 10^{-4} Torr. Four wires were fixed on the silver layers by varnish and silver paste was used for the electrical contact. Two leads were for the current and other two leads were for the voltage measurement. A schematic diagram of the measurement method is shown in Fig.4.1. A constant d.c. current source (Hewlett·Packard, Model 6181B) was used to supply a small current to the sample. This current was monitored by a resistor in series with the sample. This was done to verify that the current did not change during the course of the measurement. The potential difference of the sample and the resistor was measured by digital

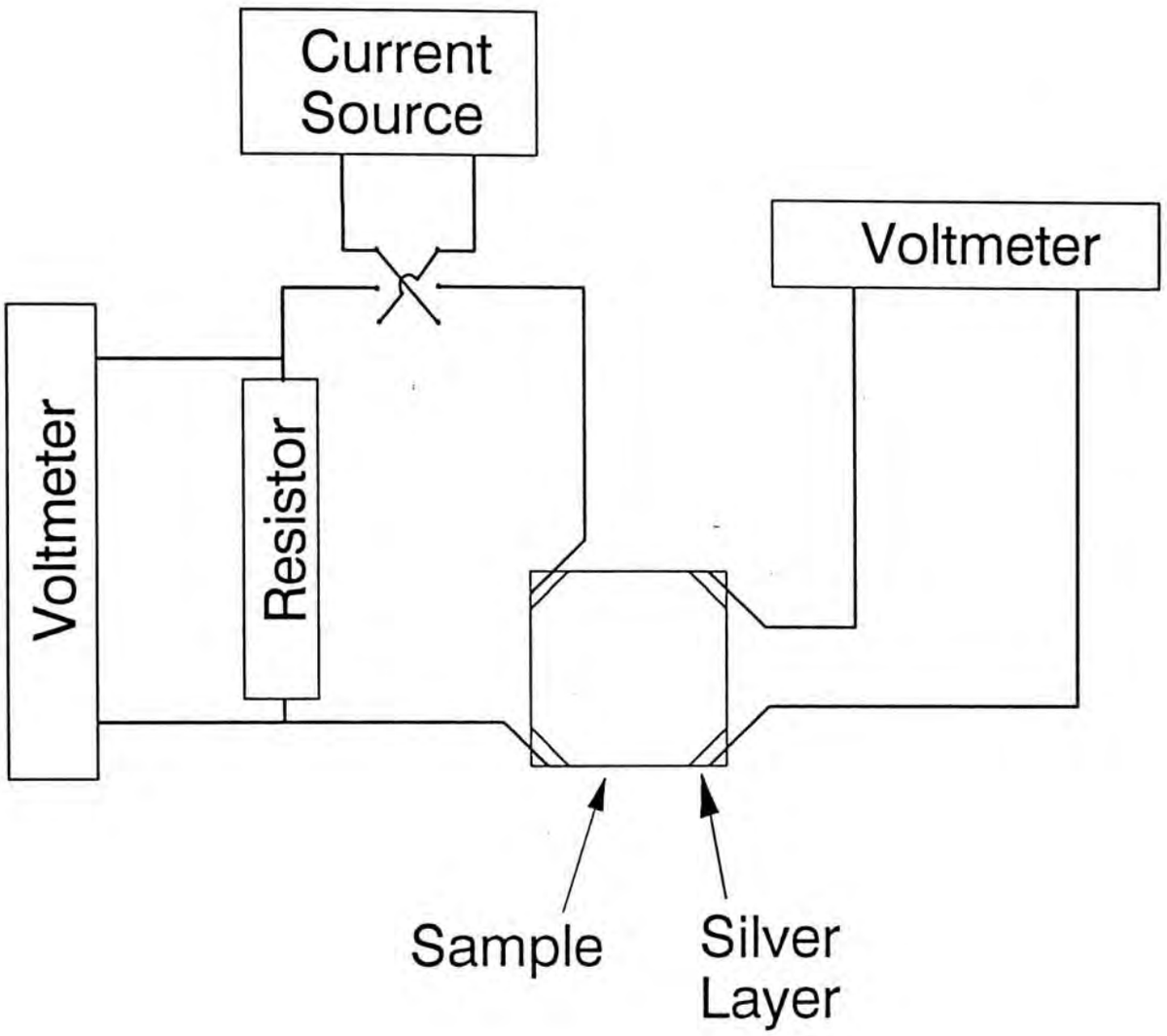

Fig. 4.1 Schematic diagram of four-lead resistance measurement.

multimeters (with 1μV sensitivity). A switch was used to alter the direction of the current. The resistance of the sample was taken as the average of the resistance measured with the current flowing in opposite directions.

4.2 RESULT

Fig. 4.2(a)-(e) show the normalized resistivity curves for our samples as a function of temperature. Resistance is plotted as a ratio = R(T)/R(300) where R(T) and R(300) are the resistances at temperature T and 300 K respectively. The T_c of the films are summarized in Table 4.1. T_c is defined as the temperature at which the resistance drops to one-half of its normal state value at the onset of the transition. Sample 2 shows a semiconductor-like behavior and no transition to superconducting state was observed down to 12.8 K (Fig. 4.2(a)). Like sample 2, sample 3 also shows a semiconductor-like behavior, but the resistance begins to drop at bout 40 K (Fig. 4.2(b)). However, it does not drop to zero even the temperature is 12 K. From Table 3.3, we know that there is an increase in the length of a-axis for samples 2 and 3. Sample 2 may probably be tetragonal. This may be due to the lower growth temperature (525°C for sample 2 and 550°C for sample 3). Films grown at higher temperatures (650°C and 720°C) show a sharp transition and the T_c recorded are as high as 90.0 K and 87.8 K. At moderate growth temperature, sample 4 is also superconducting but T_c is lower (79.3 K).

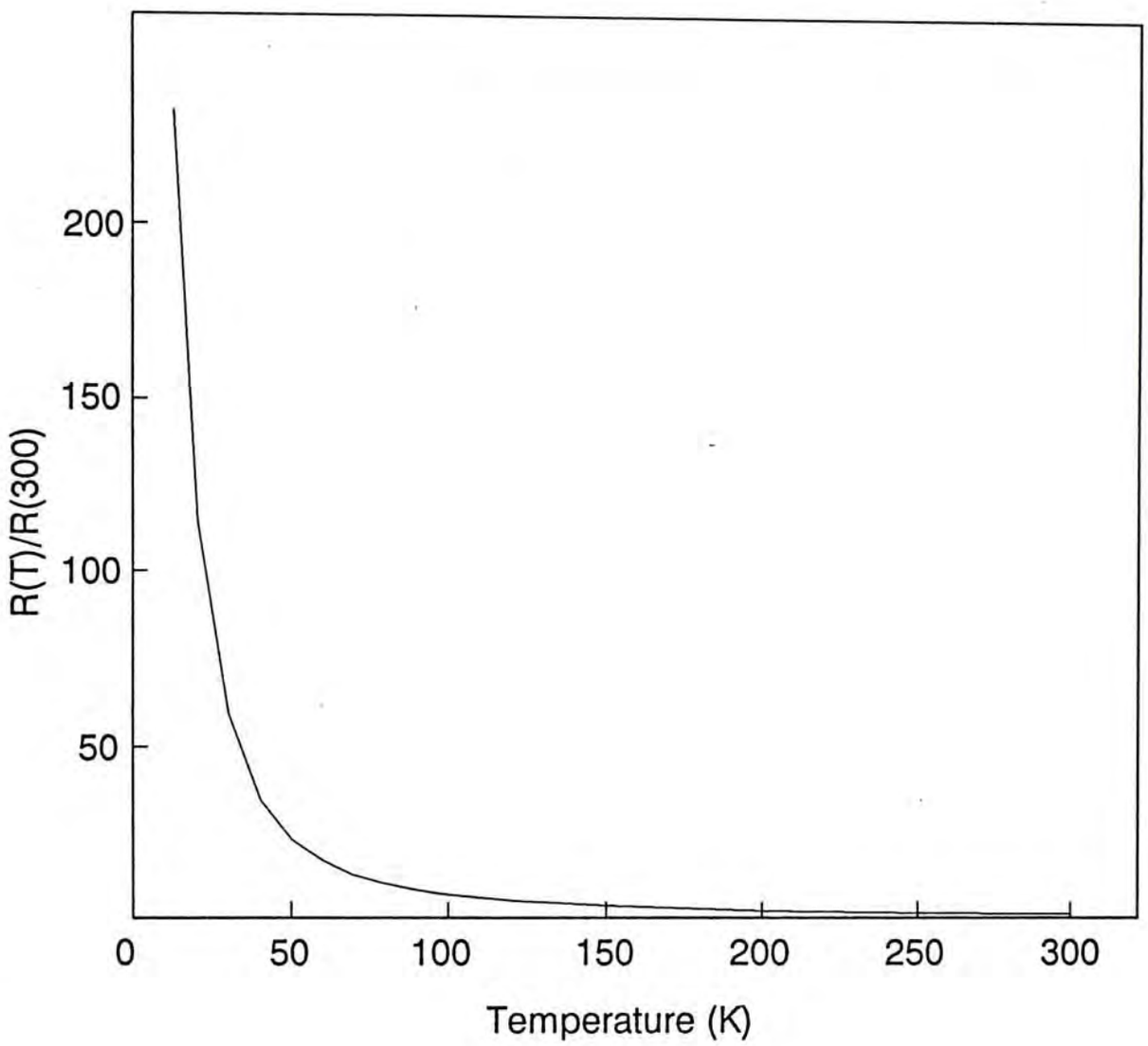

Fig. 4.2(a) Normalized temperature dependent resistivity curve of sample 2.

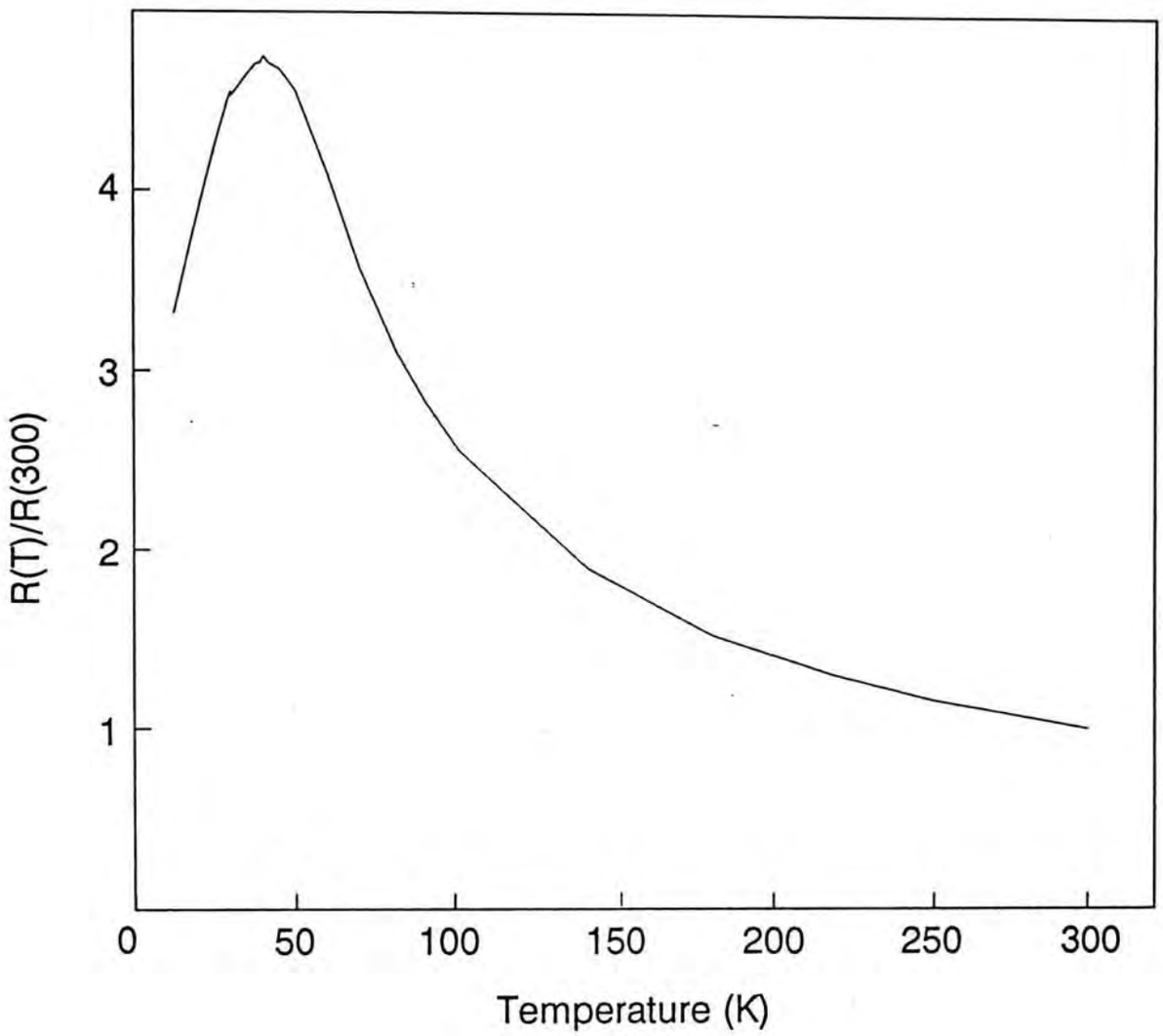

Fig. 4.2(b) Normalized temperature dependent resistivity curve of sample 3.

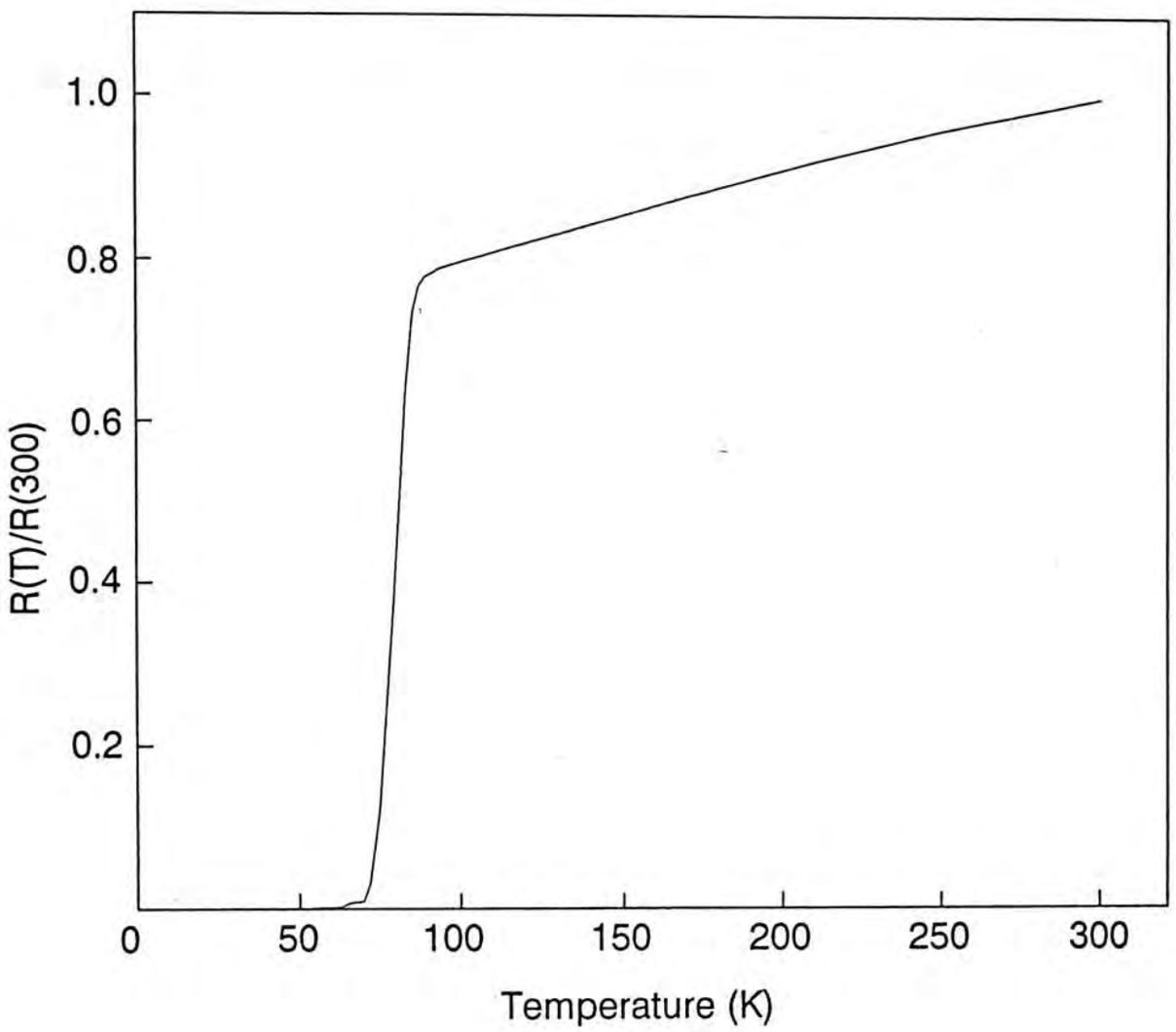

Fig. 4.2(c) Normalized temperature dependent resistivity curve of sample 4.

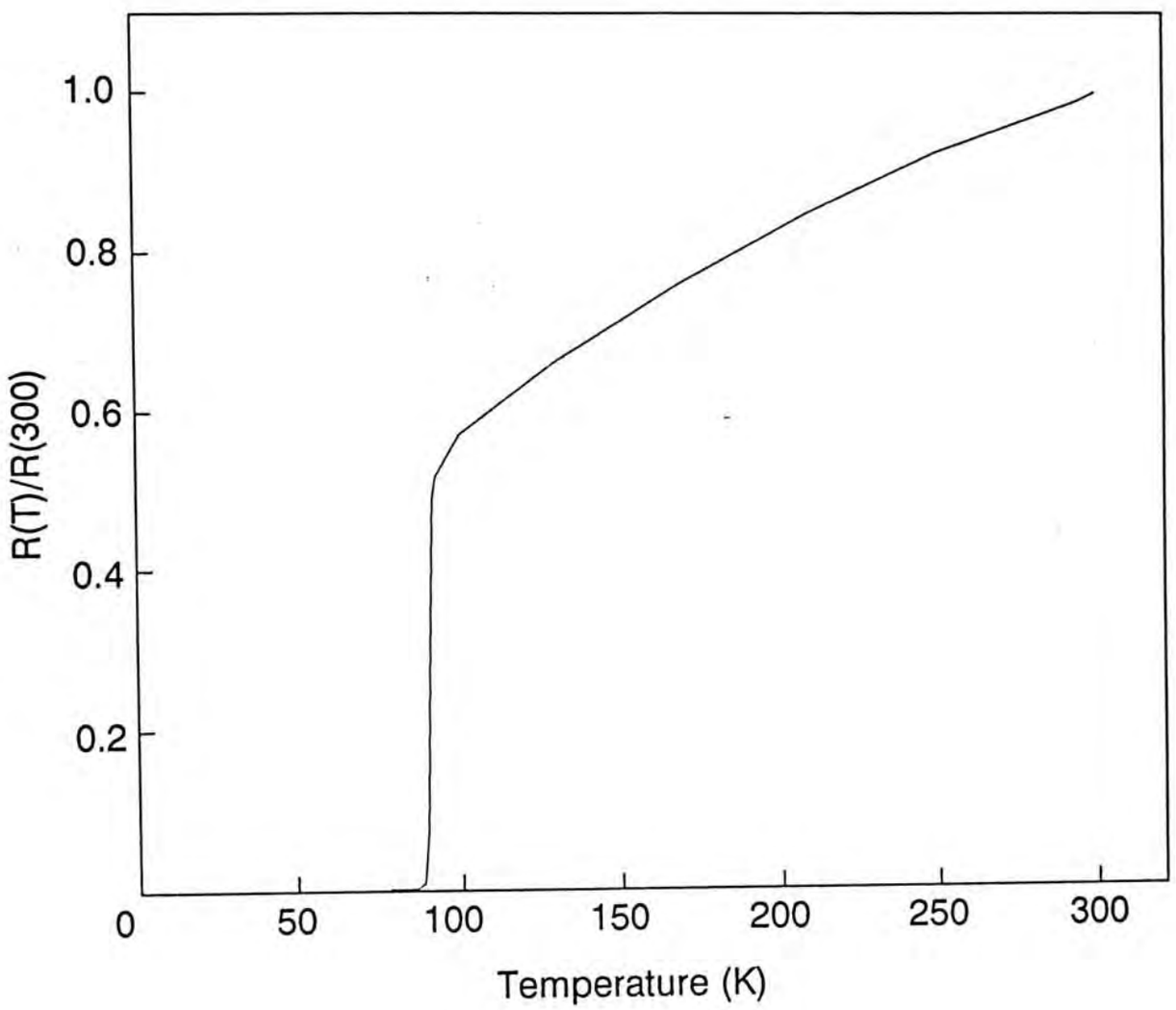

Fig. 4.2(d) Normalized temperature dependent resistivity curve of sample 5.

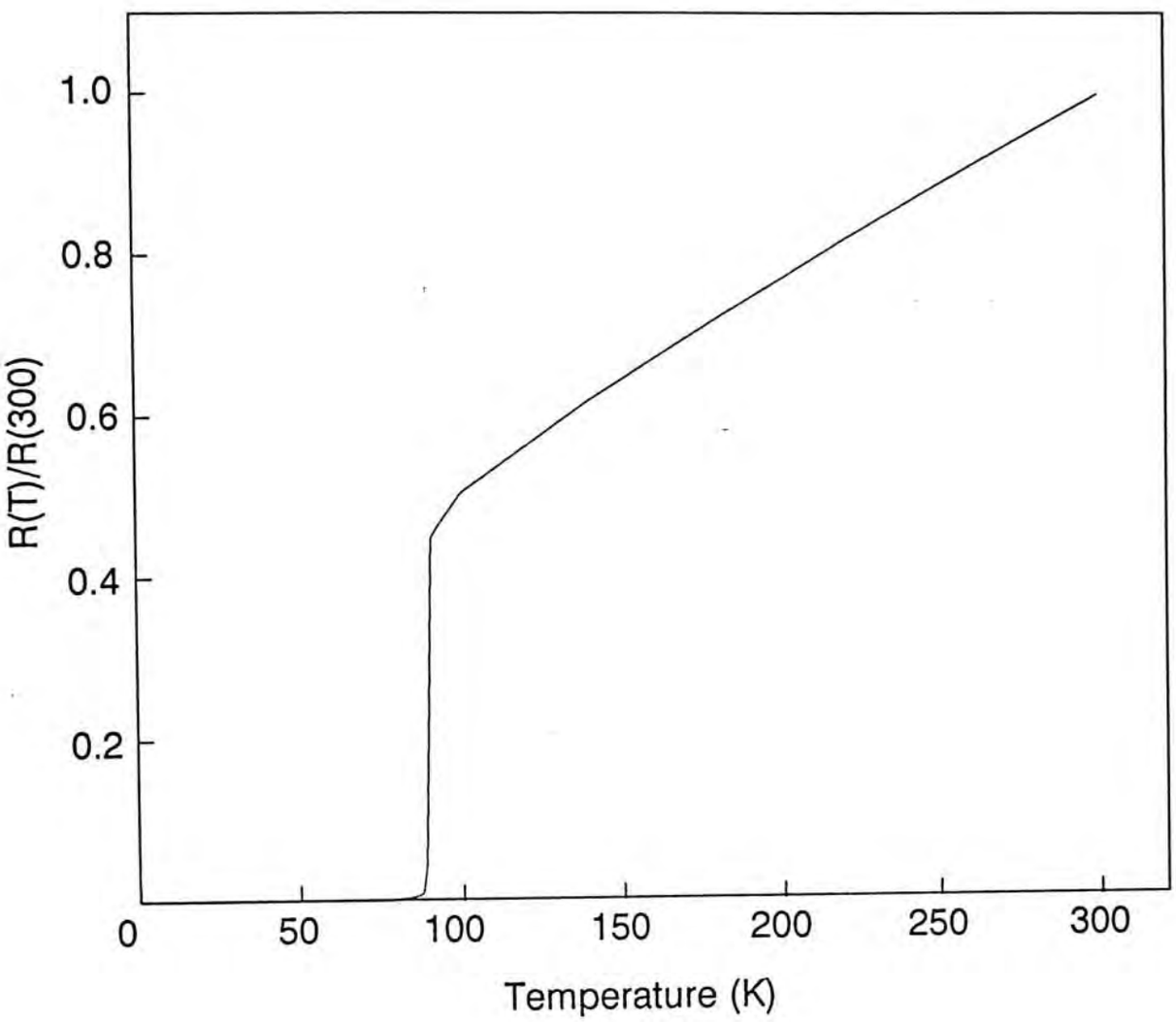

Fig. 4.2(e) Normalized temperature dependent resistivity curve of sample 6.

Table 4.1 T_c of the films grown at different temperatures.

Sample	Substrate Temperature (°C)	T_c (K)
2	525	- - -
3	550	- - -
4	600	79.3
5	650	90.0
6	720	87.8

CHAPTER 5

SURFACE MORPHOLOGY

Scanning electron microscopy (SEM) (JSM-35CF) was used to examine the surface morphology of our films. The SEM photographs are shown in Fig.5.1(a)-(e). These pictures indicate that the films have tiny droplets (diameter $\simeq$ 1 μm) on an otherwise smooth surface. This is a common problem for films deposited by excimer laser ablation. This drawback can be overcome by using plasma-assisted deposition[30] or by using an off-axis deposition geometry[31].

The scanning electron micrographs of the films can be divided into two groups: Fig.5.1(a)-(c) and (d)-(e). Despite the laser droplets, samples 2 to 4 have smooth surface while the others have rough surface. This difference is due to the orientation of the films. Cracks along YBCO [1$\bar{1}$0], with about 4 μm separation, are observed in sample 2 which is a pure (110) film. Recently Olsson et al.[32] observed the same cracks in (110) films and explained the cracks in terms of the different thermal expansion coefficients of YBCO c-axis and STO. In Fig.5.1(d), the grains are in rectangular shape with the longer sides all lie in the same direction. As it is (103)/(013) oriented, the c-axis points 45° to the surface plane. Since [100] and [010] are fast growing directions for YBCO, the elongated side of the grains is in direction of a and/or b-axis. Hence the shorter side is along [$\bar{3}$01] and/or [0$\bar{3}$1]. When the film grows, the grains start to coalesce and rough surface results since two grains ((103) and

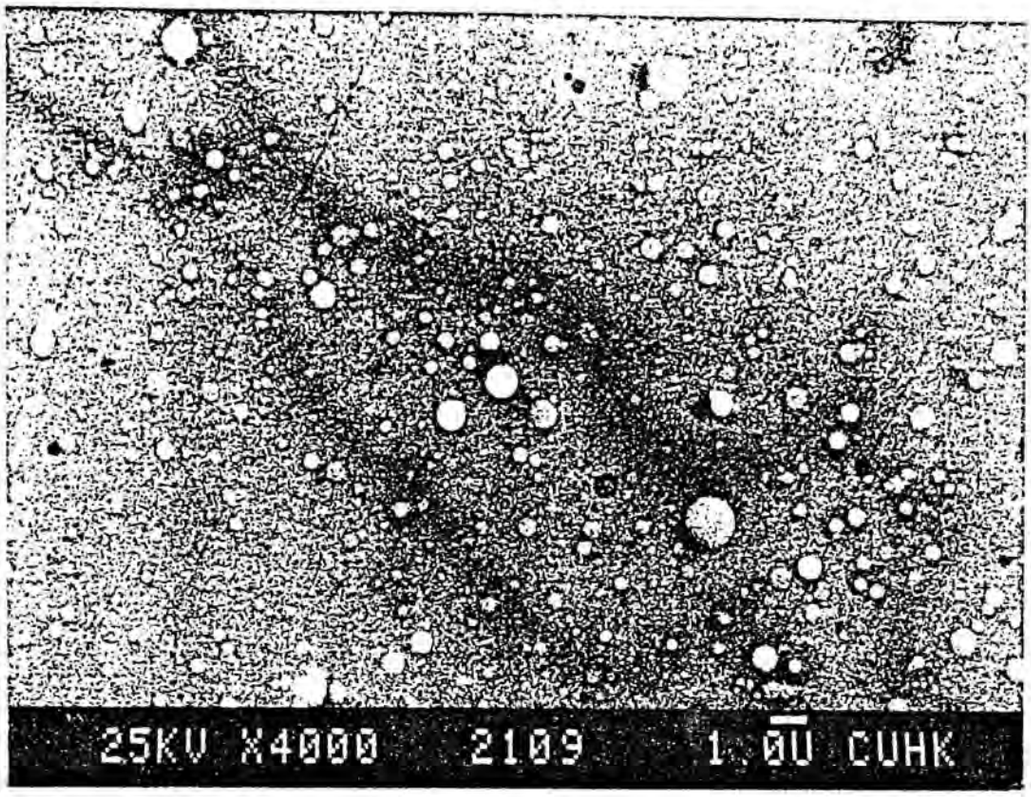

Fig.5.1(a) SEM photograph of sample 2.

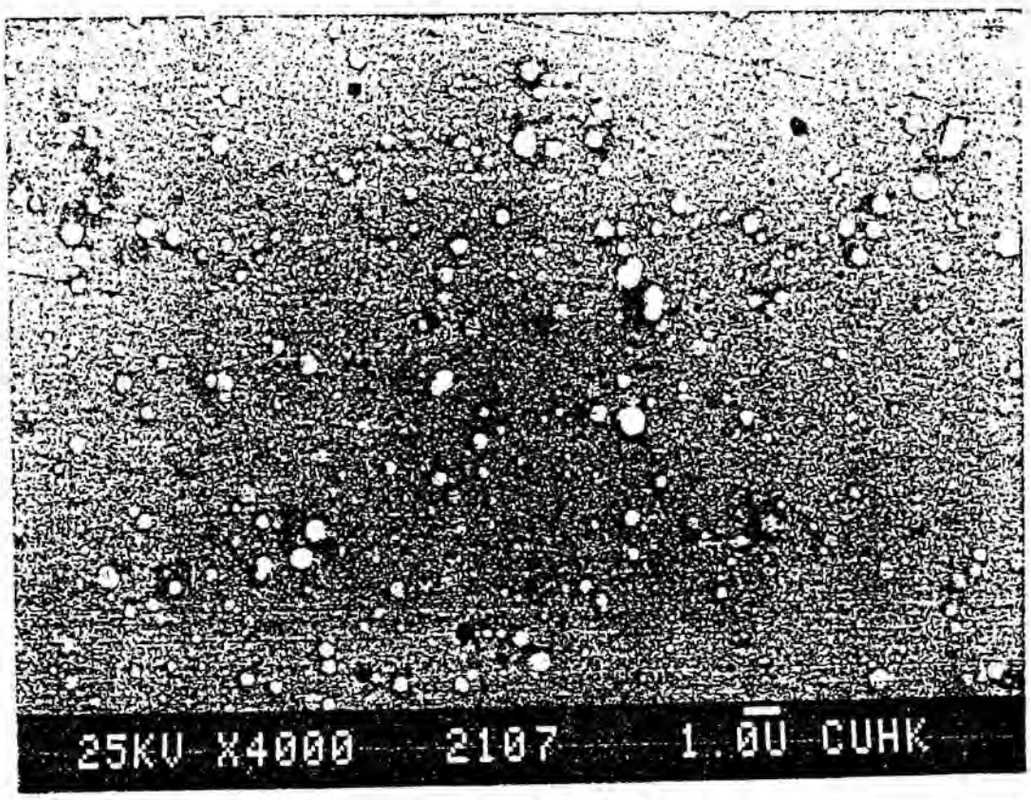

Fig.5.1(b) SEM photograph of sample 3.

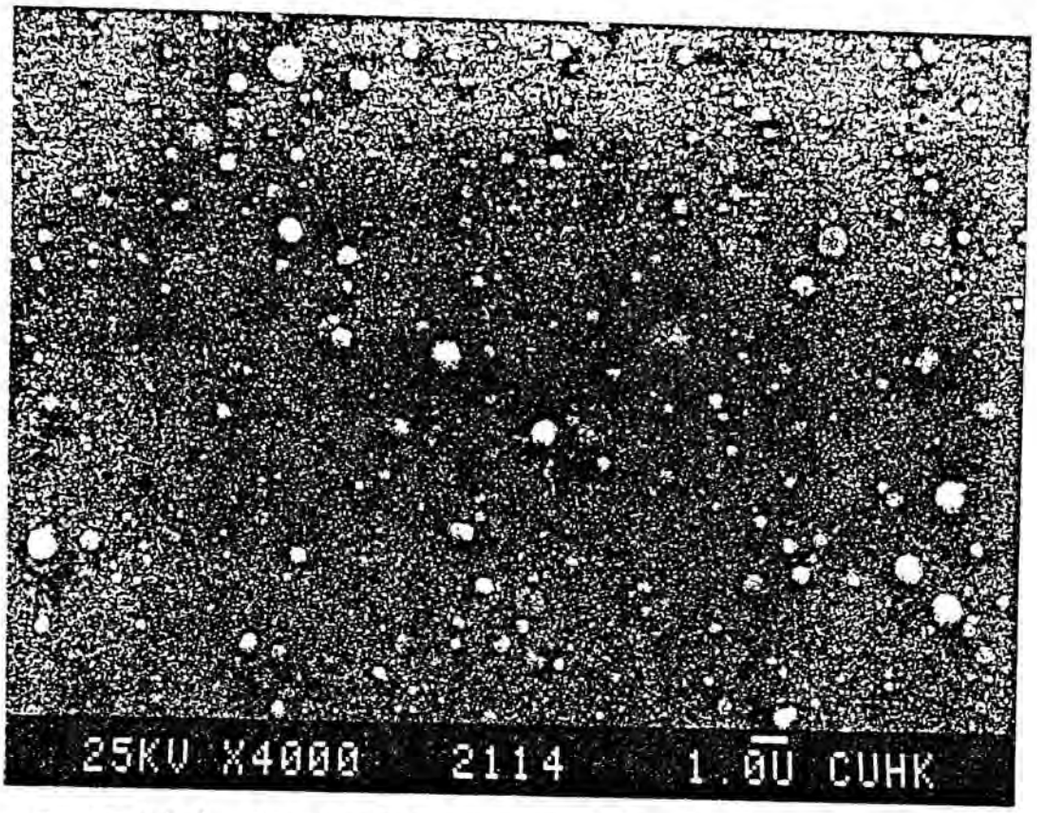

Fig.5.1(c) SEM photograph of sample 4.

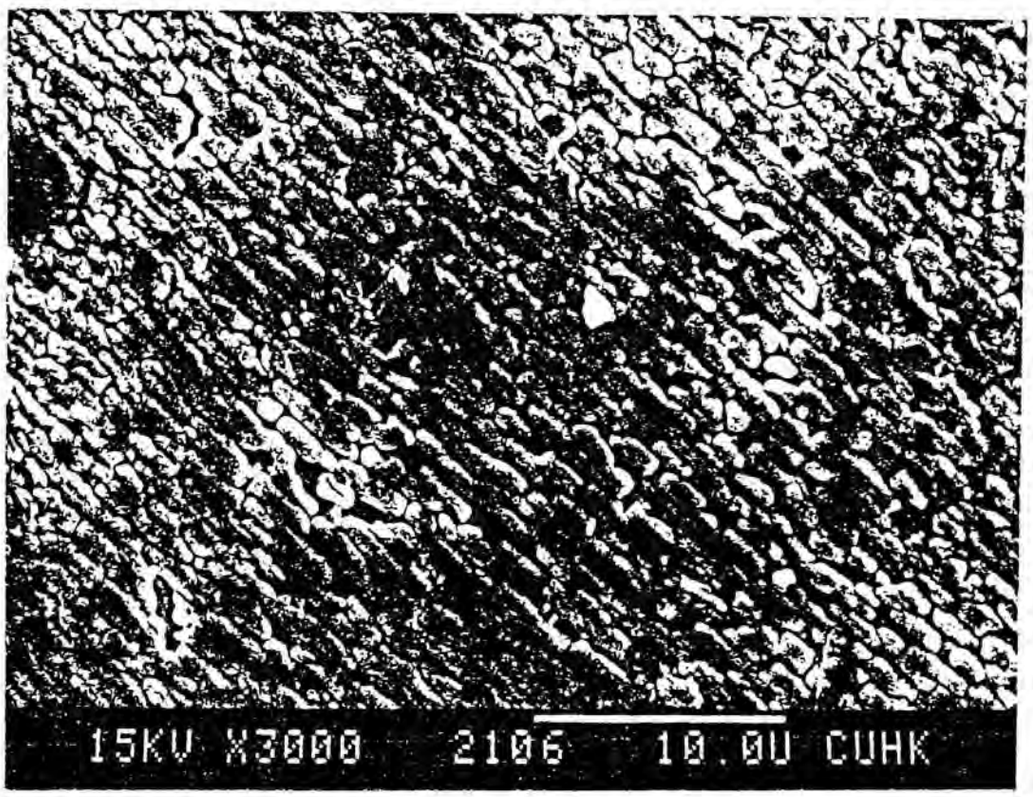

Fig.5.1(d) SEM photograph of sample 5.

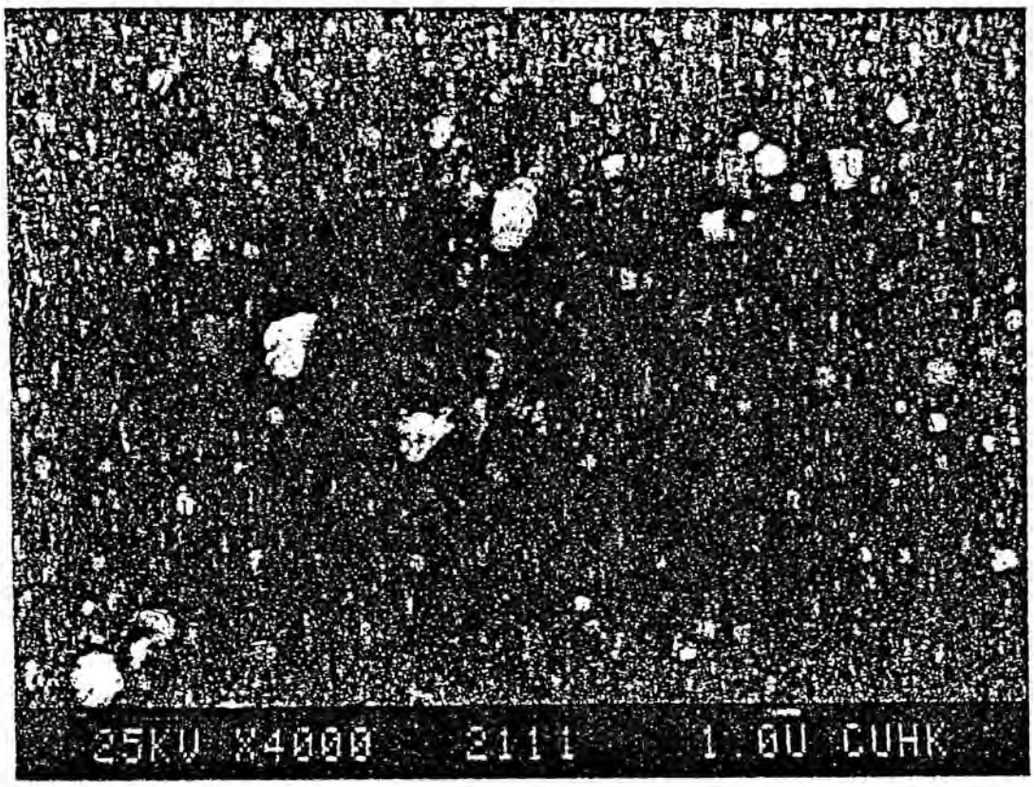

Fig.5.1(e) SEM photograph of sample 6.

(013)) exist in the film and there are twinning in both orientations.

CHAPTER 6

DISCUSSION

Our films were grown in 200 mTorr oxygen and at substrate temperatures higher than about 450°C. From the phase diagram[27], we know that the as-deposited samples are in a tetragonal phase. These samples took up oxygen to form the superconducting orthorhombic phase in cooling process during which we backfilled the chamber with 1 atm. O_2. At substrate temperature about 550°C or above, tetragonal phase is formed with (103) orientation. In oxidation, oxygen atom may enter into the same a and b-axes of YBCO. If it enters into the axis along STO [001], then orthorhombic YBCO (103) phase will be formed. Otherwise, (013) will be resulted. Since the formation of (103) and (013) grainsdepend on which axis the oxygen atoms are absorbed during oxidation, it is likely that both phases will exist. This seems impossible to have pure (103) or (013) oriented film. It is of interest to note most authors have neglected this (013) phase simply because they did not perform detailed texture analysis.

We have grown a number of YBCO films with pure (110) orientation at substrate temperature 525°C. But these films are not superconducting. Zheng et al.[18] obtained similar result. They grew a nearly pure (110) oriented film at 580°C by laser ablation, and the transition temperature was below 10 K. The temperature range for growing YBCO films with pure (110) orientation is very narrow (less than 50°C). AT lower temperature (500°C), the as-deposited films are amorphous. And (013) grains

appear in films grown at 550°C. The higher the substrate temperature, the less the percentage of the (110) grains presents. Grains with all three orientations ((110), (103) and (013)) coexist in films grown at 600°C. At higher substrate temperature (≥ 650°C), only (103) and (013) grains were present in the films. Terashima et al.[22] observed similar trend and explained it by the different thermal expansion coefficients of YBCO along a and c-axes. They argued that at temperature less than 570°C, the lattice misfit between YBCO and STO along the c-axis is smaller and thus the c-axis of the film should lie on the substrate surface resulting in a (110) orientation. For temperature higher than 570°C, lattice misfit between YBCO and STO along the a-axis becomes smaller and thus (103) orientation is preferred. Our results show the same thing except with a temperature shift from 570°C to about 630°C. This discrepancy may be due to the different methods of the temperature measurement. Another important factor is the growth technique : they grew the films by activated reactive evaporation at an oxygen pressure of 10^{-2} Torr, and our films were deposited by pulsed laser ablation at an oxygen pressure of 0.2 Torr. The difference in pressure also changes the thermal expansion coefficients of YBCO and thus affects the orientation of the films.

We have also used the bi-layer method to grow YBCO films on STO (110). The first layer was grown at temperatures ranging from 450°C to 625°C and then the second layer was grown at 720°C. The oxygen pressure was kept constant at 200 mTorr during the whole deposition process. Surprisingly, (00ℓ) diffraction peaks were

observed besides the peaks for (110), (103) and (013) grains. Witanachchi et al.[30] had also reported the existence of (00ℓ) phase of YBCO on STO (110) produced by plasma-assisted pulsed laser ablation.

To understand why the bi-layer method failed to improve the film quality, we annealed some (110) films for about 10 minutes under the following condition : oxygen pressure = 200 mTorr and annealing temperature = 600°C - 720°C. After the annealing, the chamber was back-filled with 1 atm. oxygen and the sample was cooled to room temperature. After annealing, XRD shows (00ℓ) diffraction peaks in addition of the (110)/(103) and (220)/(206) peaks. This indicates the change in structure during annealing. The result is consistent with our bi-layer results. In addition, some (110) films were also annealed for about 13 hours under a condition of temperature = 525°C and oxygen pressure = 1 atm O_2. These samples were slowly cooled to room temperature at a rate of -30°C/hr. But there was no observable change in structure and superconductivity. Similar results were obtained for rapid thermal annealing (RTA) treatment on the (110) films. Here the annealing temperature was varied from 600°C to 900°C and the typical annealing time was 20 s. Since no improvement in superconductivity of (110) films by different annealing methods, we believe that the low T_c of our (110) films is not because of insufficient oxygen content. It may be due to the oxygen disordering in the basal copper oxide planes.

Recently, Agostinelli et al.[33] reported the growth of cubic

phase YBCO (with lattice parameter of 3.897 Å) thin films on MgO (100) and STO (100) substrates by pulsed laser ablation. The stoichiometry of their films was Y:Ba:Cu:O = 1.18:1.97:3.05:6.95 which is very close to the 1:2:3 phase. They found that the cubic phase formed at heater block temperature near 560°C. Above 600°C, c-axis orthorhombic 1:2:3 phase was obtained while insulating amorphous films were produced at temperature below about 540°C. The temperature-dependent resistivity measurement of the cubic phase film showed no transition to superconductivity down to 10 K and that the resistivity increases with decreasing temperature. This is similar to what we found for our pure (110) films. The deposition temperature window of our (110) films is also similar to that of their cubic phase film — both are higher than the temperature for amorphous films by about 20°C. The main difference is that our films are in tetragonal form.

To the best of our knowledge, no superconducting YBCO (110) films could be grown at low substrate temperatures using the pulsed laser deposition technique. The only exception is the report of Elkin et al.[34]. They successfully grew superconducting (110) films (with zero resistance at 83 - 87 K) using the bi-layer approach. In this method, a thin layer of YBCO was first grown at a low substrate temperature which favours the formation of (110) orientation and then the substrate temperature was increased to a higher value without interruption of the growth process. Several research groups[17,34] have fabricated (110) films by sputtering and high T_c were recorded. Elkin et al.[34] explained this as the growing film increases the absorption of radiation and thus

substrate temperature rises during the growth. So the temperature regime is like the one used for their pulsed laser deposition. We have also tried this method. We deposited YBCO film of about 400 Å at 525°C and then the substrate temperature was increased to 650°C at a rate of about 28°C/min without interrupting the deposition process. All other deposition parameters were kept the same as before. After deposition, the chamber was filled with 1 atm. oxygen and the heater current was switched off immediately. The sample was furnace-cooled to room temperature. The texture of the film was characterized by XRD. Very interestingly, the film contains no (00ℓ) orientation which is in sharp contrast with the result of the (110) films annealed at 650°C. This seems that the (00ℓ) phase is formed during prolonged annealing. By the ϕ scan of (102) diffraction, the sample was confirmed to be nearly pure (110) oriented (> 99%). There are a small amount of (103) grains and no signal for (013) grains was detected. In order to find the T_c of the sample, we followed the procedures described in chapter 4. The resistance started to drop at temperature about 92.2 K and zero resistance was obtained at 81.8 K. The mid-transition point was about 90.3 K. This is as high as our (103)/(013) oriented films.

CHAPTER 7

CONCLUSIONS

There are three possible orientations for YBCO grown on STO (110) substrate — (110), (103) and (013). We have successfully grown epitaxial YBCO (110) and YBCO (103)/(013) thin films on STO (110) by pulsed laser deposition. Our films were characterized using a conventional 4 circle x-ray diffractometer. Due to the similar 2θ positions of the (110), (103) and (013) diffractions, ϕ scans of (102) diffraction were performed to distinguish the three types of grains. The diffraction intensities, after corrected by considering the defocusing and absorption effect, were used to find the percentage of the (110) grains in the samples. The orientation of the films depends on the substrate temperature. YBCO grows in (110) orientation at low temperatures, and in (103) and (013) orientations at high temperatures. At moderate growth temperatures, three phases coexist in the sample.

YBCO films with a pure (110) orientation were obtained at substrate temperatures within a small window around 525°C. The films grew epitaxilly with YBCO (110) ∥ STO (110) and YBCO [001] ∥ STO [001]. The structure of the films is very good as reflected by the small FWHM of the (220) rocking curves. However, these films are not superconducting. In fact they are semiconductor-like. No improvement in superconductivity was observed even after various annealing processes. We believe that this is probably attributed to the oxygen disordering but not due to insufficient oxygen content.

A superconducting YBCO film with (110) orientation was fabricated by means of a modified bi-layer deposition method in which a thin (110) layer was first grown at low substrate temperature and then the substrate temperature was increased without interrupting the deposition process. Zero resistance was obtained at 81.8 K.

REFERENCE

[1] J.G.Bednorz, and K.A.Müller, Z. Phys. B46, 149 (1986).

[2] S.Jin, T.H.Tiefel, R.C.Sherwood, M.E.Davis, R.B.van Dover, G.W.Kammlott, R.A.Fastnacht, and H.D.Keith, Appl. Phys. Lett., 52, 2074 (1988).

[3] I.D.RAistrick, D.W.Cooke, J.G.Beery, F.H.Garzon, H.Javadi, M.P.Maley, A.D.Rollett, T.Roy, D.N.Sinha, and D.K.Wilde, Mat. Res. Soc. Symp. Proc. Vol 169, 695 (1990).

[4] D.K.Christen, C.E.Klabunde, R.Feenstra, D.H.Lowndnes, D.norton, H.R.Kerchner, J.R.Thompson, S.T.Sekula, J.D.Budai, L.A.Boatner, J.Narayan, and R.Singh, Mat. Res. Soc. Symp. Proc. Vol 169, 883 (1990).

[5] T.L.Hylton, A.Kapitulnik, M.R.Beasley, J.P.Carini, L.Drabeck, and G.Gruner, Appl. Phys. Lett., 53, 1343 (1988).

[6] J.W.Ekin, A.I.Braginski, A.J.Panson, M.A.Janocko, D.W.Capon II, N.J.Zaluzec, B.Flandermeyer, O.F. de Lima, M.Hong, J.Kwo, and S.H.Lion, J. Appl. Phys., 62, 4821 (1987).

[7] D.H.Shin, J.Silcox, S.E.Russek, D.K.Lathrop, and R.A.Buhrman, Mat. Res. Soc. Symp. Proc. Vol 169, 773 (1990).

[8] B.Roas, L.Schultz, and G.Endres, Appl. Phys. Lett. 53, 1557 (1988).

[9] G.C.Xiong, and S.Z.Wang, Appl. Phys. Lett. 55, 902 (1989).

[10] C.T.Blue, C.A.Blue, and P.Boolchard, J. Appl. Phys. 72, 1021 (1992).

[11] J.R.Gavaler, J.Talvacchio, T.T.Braggins, M.G.Forrester, and J.Greggi, J. Appl. Phys. 70, 4383 (1991).

[12] J.A.Alarco, G.Brorsson, Z.G.Ivanov, P.-Å.Nillson, E.Ollsson, and M.Löfgren, Appl. Phys. Lett. 61, 723 (1992).

[13] R.W.Simon, C.E.Platt, A.E.Lee, G.S.Lee, K.P.Daly, M.S.Wire, J.A.Luine, and M.Urbanik, Appl. Phys. Lett. 53, 2677 (1988).

[14] J.Q.Zheng, X.K.Wang, M.C.Shik, S.Williams, J.So, S.J.Lee, P.Dutta, R.P.H.Chang, and J.B.Ketterson, Appl. Phys. Lett. 58, 2303 (1991).

[15] A.Inam, C.T.Rogers, R.Ramesh, K.Remschning, L.Farrow, D.Hart, T.Venkatesan, and B.Wilkens, Appl. Phys. Lett. 57, 2484 (1990).

[16] F.Heidelback, H-R.Wenk, R.E.Muenchausen, S.Foltyn, N.Nogar, and A.D.Rollett, J. Mate. Res. Vol 7,549 (1992).

[17] Y.Enomoto, T.Murakami, M.Suzuki, and K.Moriwarki, Jpn. J. Appl. Phys. 26, L1248 (1987).

[18] J.P.Zheng, S.Y.Dong, D.Bhattacharya, and H.S.Kwok, J. Appl. Phys. 70, 7167 (1991).

[19] J.K.Wu, and W.K.Chu, Preprint.

[20] Wong-Ng, W.Roth, R.S.Swartzendruber, L.J.Bennett, L.H.Chiang, C.K., Beech, F., and Hubbard, C.R., Advanced Ceramic Materials, Vol. 2, No. 3B, Special issue, 1987 P.569.

[21] X.K.Wang, D.X.Li, D.Q.Li, Y.P.Lu, S.N.Song, Y.H.Shen, J.Q.Zheng, R.P.H.Chang, J.B.Ketterson, J.M.Chabala, D.Hansley, and R.Levi-Setti, J. Appl. Phys. 67, 4217 (1990).

[22] T.Terashima, Y.Bando, K.Iijima, K.Yamamoto, and K.Hirata, Appl. Phys. Lett. 53, 2232 (1988).

[23] H.-U.Habermeier, A.A.C.S.Lourenço, B.Friedl, J.Kircher, and J.Köhler, Solid State Commun. 77, 683 (1991).

[24] J.Z.Wu, P.Y.Hsieh, A.V.McGuire, P.L.Schmidt, L.T.Wood, Y.Shen, and W.K.Chu, Phys. Rev. B 44, 12643 (1991).

[25] G.Linker, X.X.Xi, O.Meyer, Q.Li, and J.Geerk, Solid State Commun. 69, 249 (1989).

[26] C.B.Eom, A.F.Marshall, Y.Suzuki, T.H.Geballe, B.Boyer, R.F.W.Pease, R.B.van Dover, and Julia M.Plillips, Phy. Rev. B 46, 11902 (1992).

[27] H.Shaked, J.D.Jorgensen, P.G.Hirks, R.L.Hitterman, and B.Dabrowski, Physica C 205, P.225 (1993).

[28] E.Matsubara, Y.Waseda, and K.T.Jacob, J. Mater. Science Letters 10, 677, (1991).

[29] B.Gale, and D.Griggiths, Brit. J. Appl. Phys. 11, 96 (1960).

[30] S.Witanachchi, H.S.Kwok, X.W.Wang, and D.T.Shaw, Appl. Phys. Lett. 53, 234 (1988).

[31] B.Holzapfel, B.Roas, L.Schultz, P.Bauer, and G.Saemann-Ischenko, Appl. Phys. Lett. 61, 3178 (1992).

[32] E.Olsson, A.Gupta, M.D.Thoules, A.Segmuller, and D.R.Clarke, Appl. Phys. Lett. 58, 1682 (1991).

[33] John A.Agostinelli, Samuel Chen, and G.Braunstein, Phys. Rev. B 43, 11396 (1991).

[34] B.Elkin, H.-U.Habermeier, B.Leibold, and D.Shen, Preprint.

Appendix A

Powder Diffraction Pattern of YBCO system [20]

Powder Diffraction Patterns for $YBa_2Cu_3O_7$, Annealed in Oxygen at 780°C

d(Å)	I^{rel}	h k ℓ	2θ(°)	d(Å)	I^{rel}	h k ℓ	2θ(°)
11.69	1L	0 0 1	7.557	1.2566	1	2 0 7	75.615
5.836	4	0 0 2	15.169	1.2341	1L	2 2 4	77.247
3.891	10	0 0 3, 0 1 0	22.835	1.2309	4	0 1 9	77.480
3.819	4	1 0 0	23.274	1.2286	6	1 0 9, 0 3 3	77.654
3.235	3	0 1 2	27.554	1.2263	5	1 3 0	77.827
3.196	5	1 0 2	27.893	1.2099	5	3 0 3, 3 1 0	79.088
2.918	1L	0 0 4	30.618	1.2015	3	1 2 7	79.749
2.750	55	0 1 3	32.538	1.1844	1	3 1 2	81.141
2.725	100	1 1 0, 1 0 3	32.842	1.1763	2	2 2 5	81.812
2.653	2	1 1 1	33.757	1.1702	1L	1 3 3	82.335
2.468	3	1 1 2	36.370	1.1683	1	0 0 10	82.498
2.336	13	0 0 5, 0 1 4	38.512	1.1551	1	3 1 3	83.650
2.319	5	1 0 4	38.799	1.1188	3	0 1 10	87.028
2.2317	14	1 1 3	40.384	1.1161	6	1 2 8, 2 2 6	87.287
1.9909	2	1 1 4, 1 0 5	45.524	1.1114	4	2 1 8	87.748
1.9461	22	0 0 6	46.633	1.0861	1	1 3 5	90.351
1.9425	21	0 2 0	46.725	1.0792	1	0 2 9	91.089
1.9096	12	2 0 0	47.580	1.0734	1	2 0 9	91.722
1.7732	4	1 1 5	51.495	1.0617	1	0 0 11	93.027
1.7408	3	0 1 6	52.526	1.0551	1	2 2 7	93.786
1.7345	4	1 0 6	52.733	1.0377	4	1 3 6	95.853
1.7144	2	2 0 3, 2 1 0	53.400	1.0333	4	2 3 3	96.394
1.6683	2	0 0 7	54.997	1.0273	4	3 1 6	97.145
1.6595	1	1 2 2	55.313				
1.5837	26	1 1 6, 1 2 3	58.207				
1.5685	13	2 1 3	58.826				
1.5334	1L	0 1 7	60.309				
1.5292	1	1 0 7	60.494				
1.4939	2	0 2 5	62.080				
1.4899	2	1 2 4	62.262				
1.4783	3	2 0 5, 2 1 4	62.809				
1.4225	2	1 1 7	65.571				
1.3751	5	0 2 6	68.134				
1.3666	5	0 1 8	68.618				
1.3635	13	1 0 8, 2 0 6	68.797				
1.3619	12	2 2 0	68.888				
1.2978	1	0 0 9	72.820				
1.2951	1L	0 3 0	72.995				
1.2865	2	2 1 6, 1 1 8	73.561				
1.2657	1L	0 2 7, 3 0 1	74.977				

Crystal Data
Orthorhombic
Pmmm
a = 3.8185(3)
b = 3.8856(3)
c = 11.6804(6)

Powder Diffraction Pattern for $YBa_2Cu_3O_{6.8}$, Air Slow Cool

d(Å)	I^{rel}	h	k	ℓ	2θ(°)
11.72	1L	0	0	1	7.535
5.85	4	0	0	2	15.131
3.894	10	0	0	3, 0 1 0	22.820
3.818	4	1	0	0	23.279
3.237	5	0	1	2	27.531
3.203	5	1	0	2	27.832
2.924	1L	0	0	4	30.548
2.752	58	0	1	3	32.508
2.728	100	1	0	3, 1 1 0	32.808
2.654	1L	1	1	1	33.741
2.471	3	1	1	2	36.327
2.339	11	0	0	5	38.452
2.320	5	1	0	4	38.779
2.233	17	1	1	3	40.351
1.994	1L	1	0	5, 1 1 4	45.448
1.950	13	0	0	6	46.542
1.943	20	0	2	0	46.708
1.910	13	2	0	0	47.578
1.774	4	1	1	5	51.466
1.7394	3	0	2	3	52.573
1.7336	2	1	2	0	52.761
1.7160	2	2	0	3, 2 1 0	53.346
1.7140	2	1	2	1	53.414
1.6707	2	0	0	7	54.913
1.6617	1	1	2	2	55.236
1.5834	29	1	2	3	58.221
1.5697	13	2	1	3	58.778
1.5342	1L	0	1	7	60.277
1.5300	1L	1	0	7	60.459
1.4951	2	0	2	5	62.024
1.4904	3	1	2	4	62.240
1.4791	3	2	1	4, 2 0 5	62.771
1.4239	3	1	1	7	65.498
1.3758	5	0	2	6	68.097
1.3679	5	0	1	8	68.546
1.3658	8	1	0	8	68.666
1.3633	11	2	2	0	68.808
1.2958	1L	0	3	0	72.949
1.2872	1	2	1	6	73.514
1.2669	1L	0	2	7	74.890
1.2576	1	2	0	7	75.541
1.2349	1L	2	2	4	77.188
1.2322	1	0	1	9	77.382
1.2298	3	0	3	3, 1 0 9	77.566
1.2268	6	1	3	0	77.786
1.2108	5	3	0	3, 3 1 0	79.013
1.2026	1L	1	2	7	79.664
1.1850	1L	0	3	4, 3 1 2	81.088
1.1778	2	2	2	5	81.688
1.1707	2	1	3	3	82.295
1.1675	2	3	0	4	82.570
1.1563	2	3	1	3	83.548
1.1196	3	0	1	10	86.948
1.1175	6	1	2	8	87.146
1.1164	6	2	2	6	87.258

<u>Crystal Data</u>
Orthorhombic
Pmmm
a = 3.8214(7)
b = 3.8877(6)
c = 11.693(2)

Powder Diffraction Pattern for $YBa_2Cu_3O_6$, Annealed in Argon

d(Å)	I^{rel}	h	k	ℓ	2θ(°)	d(Å)	I^{rel}	h	k	ℓ	2θ(°)
11.85	3	0	0	1	7.453	1.2074	3	2	1	7	79.282
5.992	5	0	0	2	14.947	1.1948	1	3	1	2	80.284
3.947	6	0	0	3	22.507	1.1841	1	0	0	10	81.167
3.860	10	1	0	0	23.022	1.1819	4	2	2	5	81.349
3.232	15	1	0	2	27.574	1.1794	3	3	0	4	81.555
2.759	100	1	0	3	32.429	1.1654	2	3	1	3	82.746
2.729	52	1	1	0	32.793	1.1317	6	1	0	10	85.794
2.658	1	1	1	1	33.696	1.1279	3	3	1	4	86.153
2.478	3	1	1	2	36.216	1.1234	4	2	1	8	86.575
2.3690	9	0	0	5	37.951	1.0868	2	2	0	9	90.270
2.3484	16	1	0	4	38.296	1.0844	4	3	1	5	90.531
2.2441	13	1	1	3	40.151	1.0700	1L	3	2	0	92.091
2.0180	2	1	0	5	44.879	1.0618	2	2	2	7	93.012
2.0066	5	1	1	4	45.148	1.0530	1	3	2	2	94.033
1.9731	5	0	0	6	45.959	1.0375	4	3	1	6	95.883
1.9295	34	2	0	0	47.059	1.0328	5	3	2	3	96.467
1.8338	1	2	0	2	49.677	1.0237	1L	3	0	7	97.615
1.7881	6	1	1	5	51.036	1.0090	2	2	0	10	99.536
1.7566	1	1	0	6	52.019	1.0062	3	3	2	4	99.908
1.7330	2	2	0	3	52.782						
1.7252	3	2	1	0	53.039						
1.6915	3	0	0	7	54.181						
1.6565	5	2	1	2	55.422						
1.5988	8	1	1	6	57.607						
1.5808	26	2	1	3	58.326						
1.5486	4	1	0	7	59.659						
1.4954	5	2	0	5	62.012						
1.4906	8	2	1	4	62.231						
1.4375	3	1	1	7	64.805						
1.3945	1L	2	1	5	67.064						
1.3820	5	1	0	8	67.752						
1.3788	9	2	0	6	67.929						
1.3638	8	2	2	0	68.779						
1.2985	2	2	1	6	72.769						
1.2891	2	2	2	3	73.387						
1.2862	1	3	0	0	73.584						
1.2718	4	2	0	7	74.556						
1.2566	1L	3	0	2	75.611						
1.2230	6	3	0	3	78.075						
1.2198	10	3	1	0	78.324						

<u>Crystal Data</u>
Tetragonal
P4/mmm
a = 3.8578(2)
b = 11.8391(7)